Cognitive Radar Network Design and Applications

Yogesh A. Nijsure

Newcastle University

Newcastle upon Tyne, U.K.

A thesis submitted for the degree of

Doctor of Philosophy

May 2012

Acknowledgements

I would like to express my deepest gratitude towards my advisor, Dr. Yifan Chen, for his excellent guidance, patience, and support throughout my academic career as a M.Sc. and a Ph.D. student. I am deeply indebted to him for accepting me as his Ph.D. student and providing me with all the academic support over the course of five years that I have worked under his guidance and supervision. Dr. Yifan Chen has been a persistent source of motivation and inspiration for me. He has always stood behind me, pushing me to aim higher, work harder, and achieve more. I thank him profoundly for being patient, tolerating my weaknesses and for all the painstaking efforts he has put in to improve my technical and presentation skills. I would also like to thank my co-supervisors Dr. Zhiguo Ding an Prof. Said Boussakta for their guidance and support.

I take this opportunity to thank University of Newcastle upon Tyne and University of Greenwich for providing me with all the financial support and funding, without which undertaking this research programme would not have been possible for me. I would like to thank Institute for Infocomm Research, Singapore for providing me the research internship opportunity. I wish to thank Prof. Predrag Rapajic, Prof. Chew Yong Huat and Dr. Chau Yuen who have collaborated with me on research ideas and provided constructive criticism and enriched my understanding and knowledge of this research domain.

I would like to thank my parents, my brother and my wife for their constant support and motivation which allowed me to undertake this research programme. I thank my parents from the bottom of my heart for having the faith in me and providing me with the best up-bringing. Above all, I thank God Almighty, for all the blessings He has bestowed upon me.

Abstract

In recent years, several emerging technologies in modern radar system design are attracting the attention of radar researchers and practitioners alike, noteworthy among which are multiple-input multiple-output (MIMO), ultra wideband (UWB) and joint communication-radar technologies. This thesis, in particular focuses upon a cognitive approach to design these modern radars. In the existing literature, these technologies have been implemented on a traditional platform in which the transmitter and receiver subsystems are discrete and do not exchange vital radar scene information. Although such radar architectures benefit from these mentioned technological advances, their performance remains sub-optimal due to the lack of exchange of dynamic radar scene information between the subsystems. Consequently, such systems are not capable to adapt their operational parameters "on the fly", which is in accordance with the dynamic radar environment. This thesis explores the research gap of evaluating cognitive mechanisms, which could enable modern radars to adapt their operational parameters like waveform, power and spectrum by continually learning about the radar scene through constant interactions with the environment and exchanging this information between the radar transmitter and receiver. The cognitive feedback between the receiver and transmitter subsystems is the facilitator of intelligence for this type of architecture.

In this thesis, the cognitive architecture is fused together with modern radar systems like MIMO, UWB and joint communication-radar designs to achieve significant performance improvement in terms of target parameter extraction. Specifically, in the context of MIMO radar, a novel cognitive waveform optimization approach has been developed which facilitates enhanced target signature extraction. In terms of UWB radar system design, a novel cognitive illumination and target tracking algo-

rithm for target parameter extraction in indoor scenarios has been developed. A cognitive system architecture and waveform design algorithm has been proposed for joint communication-radar systems. This thesis also explores the development of cognitive dynamic systems that allows the fusion of cognitive radar and cognitive radio paradigms for optimal resources allocation in wireless networks. In summary, the thesis provides a theoretical framework for implementing cognitive mechanisms in modern radar system design. Through such a novel approach, intelligent illumination strategies could be devised, which enable the adaptation of radar operational modes in accordance with the target scene variations in real time. This leads to the development of radar systems which are better aware of their surroundings and are able to quickly adapt to the target scene variations in real time.

Contents

List of Symbols

u(t)	Gaussian monocycle at time instant t
T	Pulse width or observation sequence length or training length sequence
M	Total number of transmit antennas or number of radar units or total number of point to point communication links
N	Total number of receiver antennas
$\mathbf{y}_n$	Received signal at n^{th} antenna
K	Length of the PR sequence generated or RSS levels or number of samples
$\mathbf{x}_{m,n}$	Transmission signal or position vector
$h_{m,n}$	Channel response between the m^{th} transmit and the n^{th} receive antennas
$\mathbf{Y}$	Ensemble of received signals
$\mathbf{X}$	Ensemble of transmission sequences or target trajectory
$\mathbf{H}$	Scattering matrix
$\mathbf{\Theta}$	Noise matrix or RSS/TOA profile
ξ_{av}	Average radar cross section
$\mathcal{I}(\cdot)$	Mutual Information
$\mathcal{H}(\cdot)$	Entropy
$\mathbf{R}$	Covariance matrix
P	Transmission/Received power or RSS at a distance d
$\mathbf{\Psi}$	Radar location vector or optimal power allocation
τ	Received signal delay or propagation delay or inter-pulse (PPM) delay or number of predictions
υ	Received signal Doppler shift or motion perturbation
$\chi(\tau, \upsilon)$	Ambiguity function
Q	Total number of Gaussian UWB pulses
f	Spatial frequency
P_{fa}	Probability of false alarm
ε	Received signal threshold
σ^2	noise variance or variance of step size
d	Propagation distance

α	One way path-loss exponent or channel gain
$\mathbf{A}$	State transition matrix
$\mathbf{B}$	Observation matrix
λ	HMM parameter set or SNR or estimated entropy
π	Initial probability distribution
a_{mn}	State transition probability
b_{mk}	Observation probability
$\mathbf{Z}_T$	RSS/TOA observation sequence
$\mathbf{Q}_T$	Target trajectory state sequence
μ	Mean vector of received signal
$\mathbf{\Sigma}$	Covariance matrix
o	Observation level
ρ	Signal to noise ratio
C	Capacity of CRR network
$X(t)$	Hidden stochastic process
$Y(t)$	Observation stochastic process
$S(t)$	HMM state of channel occupancy
P_e	Probability of error

List of Acronyms

PRF Pulse Repetition Frequency

GCA Ground Control Approach

ATC Air Traffic Control

FM Frequency Modulation

CW Continuous Wave

HF High Frequency

MI Mutual Information

IID Independent and Identically Distributed

MIMO Multiple Input Multiple Output

UWB Ultra-Wideband

PRF Pulse Repetition Frequency

LFM Linear Frequency Modulation

GPS Global Positioning System

NLOS Non Line-of-Sight

pdf Probability Density Function

HMM Hidden Markov Model

OFDM Orthogonal Frequency Division Multiplexing

CRR Cognitive Radar Radio

CRN Cognitive Radar Network

PCRB Posterior Cramer-Rao Bound

PCL Passive Coherent Location

RMS Root Mean Square

RMSE Root Mean Squared Error

SAR Synthetic Aperture Radar

RCS Radar Cross Section

STAP Space Time Adaptive Processing

SIMO Single-Input Multiple-Output

SINR Signal to Interference and Noise Ratio

FCC Federal Communications Commission

RF Radio Frequency

RFID Radio-Frequency Identification

WPAN Wireless Personal Area Networks

WRSN Wireless Radar Sensor Network

WLS-MDS Weighted Least Square with Multidimensional Scaling

LS-DC Least Square with Distance Contraction

EKF Extended Kalman Filter

PF Particle Filter

SMACOF Scaling by Majorizing A Complicated Function

DSSS Direct-Sequence Spread Spectrum

PR Pseudo-Random

DSA Dynamic Spectrum Access

SU Secondary User

PU Primary User

LOS Line-Of-Sight

AWGN Additive White Gaussian Noise

SVD Singular Value Decomposition

AF Ambiguity Function

MSE Mean Squared Error

SCNR Signal-to-Clutter-plus-Noise Ratio

ROC Receiver Operating Characteristics

CFAR Constant False Alarm Rate

RSS Received Signal Strength

TOA Time Of Arrival

MLE Maximum Likelihood Estimation

TDOA Time Difference Of Arrival

AOA Angle Of Arrival

EM expectation-maximization

FIM Fisher Information Matrix

CRLB Cramer-Rao Lower Bound

UMTS Universal Mobile Telecommunications System

SNR Signal to Noise Ratio

PPM Pulse Position Modulation

BER Bit Error Rate

PRI Pulse Repetition Interval

ISI Inter Symbol Interference

CRU Cognitive Radio Users

CBS Cognitive Base Station

CMS Cognitive Mobile Station

CE Cognitive Engine

BWA Baum-Welsh algorithm

ANN Artificial Neural Network

USS Unknown State Sequence

KSS Known State Sequence

List of Figures

List of Tables

Chapter 1

Introduction

1.1 Background on Radar Systems

The word radar is an abbreviation for RAdio Detection And Ranging. In general, radar systems use modulated waveforms and directive antennas to transmit electromagnetic energy into a specific volume in space to search for targets [1]. Objects (targets) within a search volume will reflect portions of this energy (radar returns or echoes) back to the radar. These echoes are then processed by the radar receiver to extract target information such as range, velocity, angular position, and other target identifying characteristics [2]. Radars can be classified as ground based, airborne, spaceborne, or ship based radar systems [2]. They can also be classified into numerous categories based on the specific radar characteristics, such as the frequency band, antenna type, and waveforms utilized. Another classification is concerned with the mission and/or the functionality of the radar. This includes: weather, acquisition and search, tracking, track-while-scan, fire control, early warning, over the horizon, terrain following, and terrain avoidance radars [1].

Radars are most often classified by the types of waveforms they use, or by their operating frequency. Considering the waveforms first, radars can be continuous wave or pulsed radars [2]. Continuous wave radars are those that continuously emit electromagnetic energy, and use separate transmit and receive antennas. Unmodulated continuous wave radars can accurately measure target radial velocity (Doppler shift) and angular position. Target range information cannot be extracted without utilizing some form of modulation. The primary use of unmodulated continuous wave radars is in target velocity search and track, and in missile guidance [2]. Pulsed

radars use a train of pulsed waveforms (mainly with modulation). In this category, radar systems can be classified on the basis of the pulse repetition frequency (PRF) as low PRF, medium PRF, and high PRF radars. Low and medium PRF radars are primarily used for ranging where target velocity (Doppler shift) is not of interest. High PRF radars are mainly used to measure target velocity. Continuous wave as well as pulsed radars can measure both target range and radial velocity by utilizing different modulation schemes [2]. Radar has been employed on the ground, in the air, on the sea, and in space. Ground-based radar has been applied chiefly to the detection, location, and tracking of aircraft or space targets. Shipboard radar is used as a navigation aid and safety device to locate buoys, shore lines, and other ships, as well as for observing aircraft. Airborne radar may be used to detect other aircraft, ships, or land vehicles, or it may be used for mapping of land, storm avoidance, terrain avoidance, and navigation. In space, radar has assisted in the guidance of spacecraft and for the remote sensing of the land and sea.

The major user of radar, and contributor of the cost of almost all of its development, have been the military, although there have been increasingly important civil applications, chiefly for marine and air navigation [2]. As indicated in [2], the major areas of radar application, in no particular order of importance, are briefly described below.

- Air Traffic Control (ATC): Radars are employed throughout the world for the purpose of safely controlling air traffic en-route and in the vicinity of airports. Aircraft and ground vehicular traffic at large airports are monitored by means of high-resolution radar. Radar has been used with GCA (ground-control approach) systems to guide aircraft to a safe landing in bad weather. In addition, the microwave landing system and the widely used ATC radar-beacon system are based in large part on radar technology.

- Aircraft Navigation: The weather-avoidance radar used on aircraft to outline regions of precipitation to the pilot is a classical form of radar. Radar is also used for terrain avoidance and terrain following. Although they may not always be thought of as radars, the radio altimeter (either frequency modulation (FM)/continuous wave (CW) or pulse) and the Doppler navigator are also radars. Sometimes ground-mapping radars of moderately high resolution are used for aircraft navigation purposes.

- Ship Safety: Radar is used for enhancing the safety of ship travel by warning of potential collision with other ships, and for detecting navigation buoys, especially in poor visibility. In terms of numbers, this is one of the largest applications of radar, but in terms of physical size and cost it is one of the smallest. It has also proven to be one of the most reliable radar systems. Automatic detection and tracking equipments (also called plot extractors) are commercially available for use with such radars for the purpose of collision avoidance. Shore-based radar of moderately high resolution is also used for the surveillance of harbors as an aid to navigation.

- Remote Sensing: All radars are remote sensors; however, as this term is used it implies the sensing of geophysical objects, or the "environment." For some time, radar has been used as a remote sensor of the weather. It was also used in the past to probe the moon and the planets (radar astronomy). The ionospheric sounder, an important adjunct for high frequency (HF) (short wave) communications, is a radar. Remote sensing with radar is also concerned with Earth resources, which includes the measurement and mapping of sea conditions, water resources, ice cover, agriculture, forestry conditions, geological formations, and environmental pollution. The platforms for such radars include satellites as well as aircraft.

- Law Enforcement: In addition to the wide use of radar to measure the speed of automobile traffic by highway police, radar has also been employed as a means for the detection of intruders.

- Military: Many of the civilian applications of radar are also employed by the military. The traditional role of radar for military application has been for surveillance, navigation, and for the control and guidance of weapons. It represents, by far, the largest use of radar.

1.2 Recent Advances and Research Scope

As mentioned in the abstract, this thesis aims at developing cognitive mechanisms for designing modern radar systems. The purpose of this section is to introduce these modern technological advances and indicate the scope for improvement by

utilizing a cognitive architecture. Specifically, this thesis focuses on three domains of radar research,

1. Radar waveform design and optimization strategies for target discrimination in presence of clutter and non-stationary radar environments.

2. Target detection, tracking and target parameters extraction in indoor and outdoor radar applications.

3. Radars equipped with added functionalities like the joint communication-radars.

1.2.1 Radar Waveform Design and Optimization Strategies for Target Discrimination

Adaptive waveform design for radar applications has been a well investigated subject in the past. Some of the pioneering works like [3], have applied information-theoretic measures for the design of radar waveforms in order to facilitate improved target detection and classification. The basic difference between the application of information theory in communication and radar systems design has been shown in Fig. 1.1. In communication systems design, the source of uncertainty of information lies at the transmitter, since the receiver has no knowledge of the transmitted signal. Here we intend to make the received signal statistically more dependant on the transmitted signal in order to reduce the bit error rate. Hence the basic objective is to maximize the mutual information between the received signal and the transmitted signal in order to improve the overall information capacity of the communication system. However as seen from Fig. 1.1, the source of uncertainty or information in the radar system lies at the target. In this case, the receiver has an exact knowledge of the transmitted signal. Thus the distortion brought about by the target upon the transmitted signal is a matter of interest to us. In radar systems we want to ensure that the transmission waveforms would be designed with the sole objective of making the received signal more statistically dependant upon the target signature, and we intend to suppress the non-target contributions from noise and clutter. Thus, in this case we intend to maximize the mutual information between the received signal and the estimated target impulse response given the transmission signal. In this thesis we explore such a waveform optimization approach which allows us to

design optimum transmission waveforms which would "match" the target based on the information-theoretic measures.

In recent years, the research on the development of knowledge-aided waveform design has received great impetus. Some of the noteworthy works in this area include [4–8]. In these works the radar transmission parameters are modified in order to improve the target parameters estimation in a dynamic radar environment. Based on the prior knowledge about targets and environments, transmit signals can be adaptively optimized to improve system performance and efficiency. Inspired by this concept, many attempts have been focusing on target recognition using waveform-adaptation. In [9], Goodman proposed the integration of waveform design techniques with a sequential-hypothesis testing framework [10] that controls when hard decisions may be made with adequate confidence [6]. He also compared two different waveform design techniques for use with active sensors operating in a target recognition application. One is based on a maximization of the mutual information (MI) between a random target ensemble and the echo signal, while the other is based on maximizing the weighted average Euclidean distance or Mahalanobis distance (in additive colored noise) between the ideal echoes from different target hypotheses [8, 10], where known impulse responses are used to model the target scattering behaviors.

Multiple-input multiple-output (MIMO) radar has attracted more and more attention of researchers in recent times. The concept of MIMO has appeared in the field of communication system since the 1990s. However, it has not appeared in sensor and radar systems until recently [11]. Unlike the standard phased array radar transmitting a single waveform at a time, MIMO radar transmits multiple orthogonal waveforms by multiple antennas simultaneously. These waveforms are extracted by a bank of matched filters in the receiver. All the matched filter output are then combined to obtain the desired information [12]. Recent theoretical research has shown some advantages to operate a radar in MIMO mode, e.g., improved target detecting performance, better target model parameter estimation and target image creation [13]. However, from a system engineering viewpoint, there are serious tradeoffs of MIMO versus phased array radars relative to cost, system complexity and risk and it is not clear what advantages MIMO radar offers [13]. MIMO radars can be broadly classified into 2 categories, distributed and collocated MIMO architectures. In the distributed MIMO radar scene the MIMO transmitter and receiver

elements are spatially separated by a significant distance. This allows the different transceiver units to view the target from distinct aspect angles and thus the MIMO receiver can exploit the spatial diversity of the MIMO channel. In this thesis, we evaluate a distributed MIMO architecture in Chapter 3.

Research Scope

Most of the research pertaining to statistical characterization of radar scene, treats clutter as a wide sense stationary random process. Nevertheless, focusing on the scattering phenomena that give rise to the received signal, we observe that the received clutter depends on the radar scene in a certain temporal range. Thus, the clutter process cannot be stationary, particularly over long time intervals. Mitigation of Doppler spread clutter can be achieved by estimating the covariance matrix of slow-time data across the coherent processing interval. Typically, this covariance matrix is estimated by averaging snapshots of the slow-time clutter time series at neighboring range bins [14]. However in complex propagation conditions, the clutter return is often "***non-stationary***" in range which seriously limits the availability of independent, identically distributed (IID) signal-free training data [15].

For such radar scenarios, which are heavily cluttered and non-stationary, MIMO radars offer attractive solutions to enhance target detection and discrimination. MIMO radar empowered with a cognitive architecture can facilitate efficient target discrimination by exploiting the spatial diversity, waveform diversity and by adopting a cognitive approach through continual interactions with the radar environment. Consequently, such a radar would be able to adjust its operational parameters like the transmit power, waveform shape and frequency "on the fly" and in a completely autonomous manner. In this thesis, Chapter 3 extends the relevant works on information theoretic waveform design to waveform optimization in MIMO radars. In this Chapter, the concept of MI is used to design and select the MIMO waveforms. The objective of this algorithm is to extract the target impulse response from the radar scene which is heavily cluttered and non-stationary.

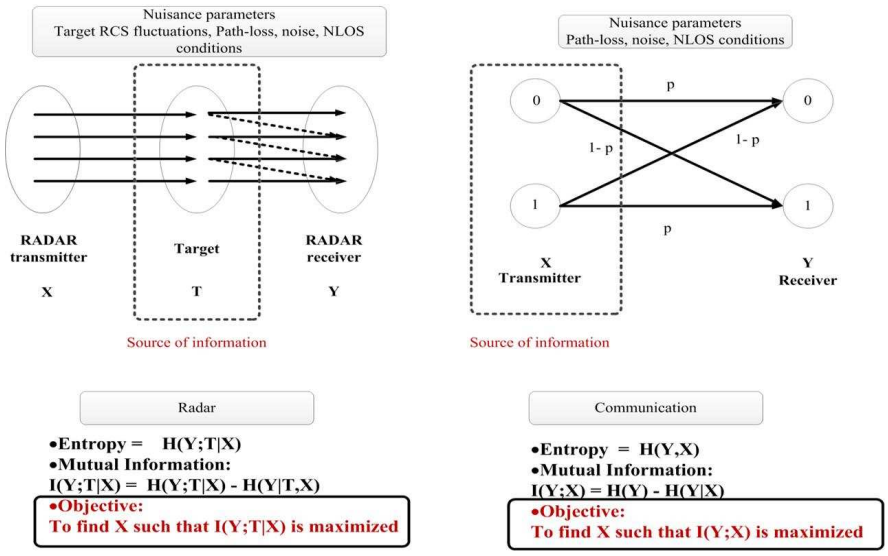

Figure 1.1: Differences in the application of information theory to radar system and communication system design

1.2.2 Target Detection, Tracking and Parameter Extraction in Indoor Radar Applications

Over past several decades there has been an extensive research on designing efficient radar illumination strategies for target detection and tracking applications. Wireless radar sensor network is emerging as an enabling technology for applications such as border surveillance, intrusion monitoring for unauthorized movement of targets around critical facilities. Surveillance applications, i.e., real-time detection, tracking and classification of intrusion, require mission critical networking capabilities in wireless sensor networks [16]. Generally, low power ultra-wideband (UWB) radar sensors are used in detection, tracking and localization of an intruder in sensor field [17, 18]. The proliferation of wireless localization technologies provides a promising future for serving human beings in indoor scenarios. Their applications include real-time tracking, activity recognition, health care, navigation, emergence detection, and target-of-interest monitoring, among others. Additionally, indoor localization technologies address the inefficiency of Global Positioning System (GPS) inside buildings [16]. However, due to the complex of indoor environments, the development of an indoor localization technique is always accompanied with a set of challenges, e.g. non line of sight (NLOS), multipath effect, and noise interference [19]. These challenges result

mainly from the influence of obstacles (e.g. walls, equipments, and human beings) on the propagation of electromagnetic waves. For instance, the mobility of people incurs changes in physical conditions of the environment, which might significantly affect the behavior of wireless radio propagation. Although these negative effects cannot be eliminated completely, in recent years researches are constantly going on to improve the performance of indoor (human/object) tracking.

The use of location and tracking information is an excellent tool to improve productivity and to optimize the resources management in a wide range of sectors [20]: industry, medicine, home-automation or military. An additional potentiality of the tracking problem that has not been explored enough is the mobility of the moving targets, especially for the complex surroundings [21]. The Kalman filter can get the optimal solution to the tracking problem in the assumption of linear Gaussian environment. However, in many situations of interest, the assumptions made above do not hold. The extended Kalman filter [22] utilizes the first term in a Taylor expansion of the nonlinear function, but the required probability density function (pdf) is still approximated by a Gaussian, which may be a gross distortion of the true underlying structure and may lead to filter divergence.

Research Scope

Design of indoor localization and tracking radar systems is a challenging research field. There is a need for employing a radar architecture which can adapt autonomously and effectively to the dynamic radar environment. The indoor wireless environment is rich in multipath and clutter sources, which can prove to be detrimental to target detection and tracking. These problems can be alleviated by adopting a cognitive architecture in the design of the indoor radar systems, which would constantly learn from the extracted target parameters information for the radar scene. In this way, intelligent illumination strategies could be devised which ensure effective target illumination in the indoor radar environment. This problem is dealt with in more detail in Chapter 4 of this thesis. In this Chapter, a cognitive illumination strategy for an indoor cognitive radar network is devised which learns from the target trajectory by utilizing a hidden Markov model (HMM) thus improving the target detection and tracking performance. By adopting this framework, the tracking algorithm is more robust to rapid target movements and alleviates some of the problems like the Gaussian approximations which are made in the contemporary tracking algorithms.

1.2.3 Joint Communication-Radar System Design

Wireless communications and radar have always been independent research entities in the past. Wireless communications focus upon achieving the best possible information capacity across a noisy wireless channel under power and complexity constraints. On the other hand, radar systems attempt to achieve better target resolution and parameter estimation in the presence of surrounding clutter and noise. In recent years, the research in integrating the communication and radar system designs under a common platform has gained significant momentum [23–29]. Such a joint radar and communication system would constitute a unique cost-efficient solution for future intelligent surveillance applications, for which both environmental sensing and establishment of *ad hoc* communication links is essential. This type of systems can be used in mission-critical and military operations to address the surveillance and communication issues simultaneously [24]. It is thus envisaged that future personal communication devices will have comprehensive radar-like functions such as spectrum sensing and localization, in addition to multi-mode and multi-band communication capability. Recent works such as [24] and [25] in particular focus upon the development of devices that have multiple radio functions and combine communication and radar in a small portable form with ultra low power consumption.

Communication information can be embedded in the radar system through waveform diversity [30,31]. Meanwhile, in the radar network, the communication message for instance the reports on the detected targets can be embedded into the orthogonal frequency division multiplexing (OFDM) radar waveform [32]. A unique covert opportunistic spectrum access solution to enable the coexistence of OFDM based data communication with UWB noise radar is presented in [33]. A multi-functional waveform has been designed, by embedding an OFDM signal within a spectrally notched UWB random noise waveform [33].

Research Scope

There is a significant research potential in the design of joint communication-radar systems. An interesting extension to this research problem is developing cognitive waveform design solution which would adapt to the dynamic radar scene while still maintaining the communication link between radar units. Another aspect of this research is the fusion of the cognitive radar and cognitive radio paradigms for wire-

less network applications. The research on cognitive radar and cognitive radio is beginning to gain momentum in recent years. Both of these models strive to impart intelligence to traditional wireless systems which utilize a static framework for resource management and hence are not able to cope up with the ever increasing demands of wireless devices being deployed.

In this thesis, Chapter 5 investigates such a joint communication-radar network by employing cognitive radar principles. In this Chapter, a novel system architecture and waveform design method has been illustrated for cognitive radar radio (CRR) networks. Chapter 6 further extends this idea and utilizes the superior target parameter extraction capability of cognitive radars to allocate crucial resources like power, spectrum over the wireless network. This Chapter also illustrates the fusion of cognitive radar and cognitive radio paradigms for exploring opportunistic spectrum access methods for improving the channel sensing abilities of the wireless devices in a network.

1.3 Motivation for Cognitive Radar System Design

According to the *Oxford English Dictionary*, cognition is "knowing, perceiving, or conceiving as an act". Cognitive radar network (CRN) is an innovative paradigm for optimizing radar surveillance within non-stationary environments, where the radar scene can be highly time-variant [34–37]. As mentioned in [35], the three ingredients are basic to the constitution of a cognitive radar:

1. Intelligent signal processing, which builds on learning through interactions of the radar with the surrounding environment;

2. Feedback from the receiver to the transmitter, which is a facilitator of intelligence;

3. Preservation of the information content of radar returns, which is realized by the Bayesian approach to target detection through tracking.

This cognitive approach to radar design is possible because of the three distinct capabilities of modern radars [35]:

1. The inherent ability of radar to sense its environment on a continuous basis

2. The ability of phased-array antennas to electronically scan the environment in a fast manner

3. The ever-increasing power of computers to digitally process signals

From the moment a surveillance radar system is switched on, the system becomes electromagnetically linked to its surrounding environment in the sense that the environment has a strong and continuous influence on the radar returns (i.e., echoes). In so doing, the radar builds up its knowledge of the environment from one scan to the next and makes decisions of interest on possible targets at unknown locations in the environment; the locations are not known before the radar is switched on, but they become determined by the radar receiver once the targets under surveillance are declared. From signal processing and control theory perspective, we know that it is not necessary for the radar to keep the entire record of past data [35]. Rather, by adopting a state-space model of the environment and recursively updating the state vector representing an estimate of certain parameters pertaining to the environment, the need for storing the entire history of radar data on the environment is eliminated [34, 35]. The requirement to update estimation of the environmental state is necessitated by the fact that the radar environment is non-stationary.

Recursive updating of a state is synonymous with adaptivity, which is the natural method for dealing with non-stationarity. In current designs of radar systems, however, adaptivity is usually confined to the receiver [36]. For a radar to be cognitive, adaptivity has to be extended to the transmitter too. Moreover, the radar has to learn from experience on how to deal with different targets, large and small, and at widely varying ranges, all in an effective and robust manner.

This way of thinking leads us to the block diagram of Figure 1.2, which depicts the picture of a cognitive cycle performed by a cognitive radar system. The cycle begins with the transmitter illuminating the environment. The radar returns produced by the environment are fed into two functional blocks: radar-scene analyzer and Bayesian target-tracker. The tracker makes decisions on the possible presence of targets on a continuing time basis, in light of information on the environment provided to it by the radar-scene analyzer. The transmitter, in turn, illuminates the environment in light of the decisions made on possible targets, which are fed back to it by the receiver. The cycle is then repeated over and over again. Note also that although the process of target detection is not explicitly shown in the cog-

nitive cycle of Fig. 1.2, it is part and parcel of the Bayesian target-tracker, which performs detection through tracking [34]. All the three cognitive ingredients are featured in the echo-location system of a bat as shown in Fig. 1.3 as found in [35], which may be viewed as a physical realization (albeit in neurobiological terms) of cognitive radar [34]. Transmission pattern of four species of bat are represented in Fig. 1.3. As seen from the corresponding frequency against time plot, all the bat species adapt their frequency of transmission as they approach the target. The bats also decrease the time duration between the subsequent bursts of transmission as they approach the target. This enables the bats to efficiently track the flying insects and other stationary targets in the surroundings. This cognitive ability of adjusting the frequency and time operation in order to better track the flying insect is in-built in bat's brain. Based on Fig. 1.2 and 1.3, a cognitive radar distinguishes itself from an adaptive radar in three important respects,

- The radar continuously learns about the environment through experience gained from interactions with the environment and, in a corresponding way, continually updates the receiver with relevant information on the environment.
- The transmitter adjusts its illumination of the environment in an intelligent manner, taking into account such practical matters as the size of the target and its range, and consequently, making adjustments to the transmitted signal in an effective and robust manner.
- The whole radar system constitutes a dynamic closed feedback loop encompassing the transmitter, environment, and receiver.

In summary, cognitive radar is a significant improvement over traditional adaptive radar systems. In a typical traditional adaptive radar system, the receiver gathers radar scene information and adopts intelligent reception strategies [35] to facilitate target discrimination. These include receiver-side beamforming, angular filtering and other adaptive techniques which facilitate in mitigation of clutter and non-target scatterer responses. However in cognitive radar system design, the intelligence is extended to the transmitter side through a cognitive feedback link from the radar receiver. This allows the transmitter to implement cognitive optimization

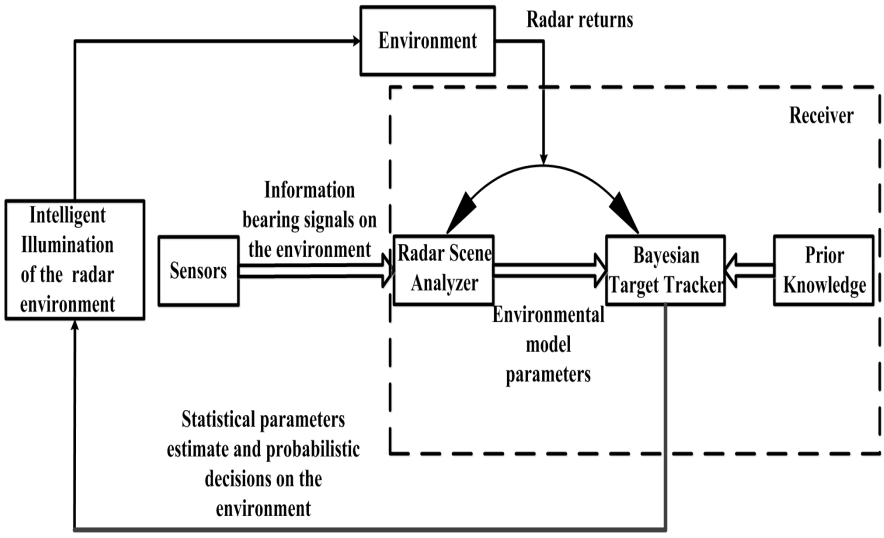

Figure 1.2: Cognitive Radar Architecture as shown in [33]

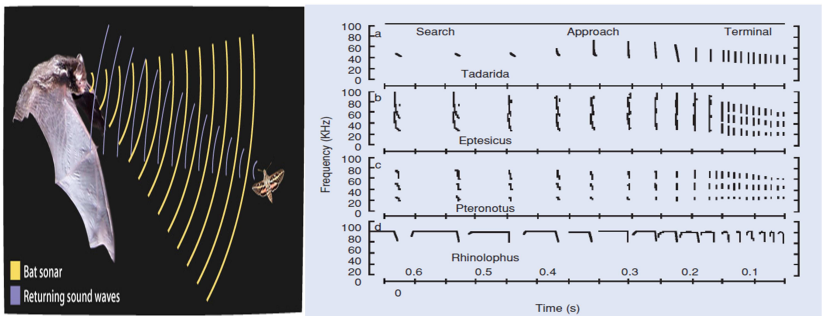

Figure 1.3: Bat using cognitive echo-location as shown in [33]

strategies to enhance target parameters extraction. Cognitive radar systems show improvement in target discrimination by adopting a multiple iterative approach to adapt and learn about the radar scene in real time.

A CRN [38] incorporates several radars working together to achieve the task of enhanced remote sensing capability. The network can operate in two modes, distributed cognition and central cognition. In a distributed cognitive network, each radar is capable of cognitive processing, whereas in a central cognitive network, a single radar acts as the brain of the entire network. With several radars operating in parallel, the system performance is considerably improved over a single radar. Several problems have been addressed in the past under the closed-loop cognitive

framework. In this thesis, both of these central and distributed cognitive architectures have been explored. Specifically, in Chapters 3 and 4, a central cognitive architecture is adopted, in the rest of the Chapters a more distributed cognitive approach is investigated.

The cognitive framework is illustrated in Fig. 1.4. As shown in Fig. 1.4, the cognitive framework consists of a closed loop involving the adaptive control over operational parameters of the radar system, the radar environment, the perception of the environment gained through constant interactions with it and the feedback channel that allows the adaptive control. Also the fundamental building blocks for the cognitive radar system which differentiate it from the traditional radar systems are shown in Fig. 1.4. The authors of [9] integrate waveform design, based on the maximization of MI, with sequential hypothesis testing. In [39], the authors use a cognitive radar for single-target tracking and propose a waveform optimization based on the minimization of the posterior Cramer-Rao bound (PCRB). In [40], the authors employ dynamic programming to select optimal waveforms from a prescribed library using PCRB as an optimization criterion. In [41], the authors use a CRN for extended target recognition, and in [42], the authors propose an adaptive waveform design for a cognitive radar for target recognition. Finally, in [43], the authors describe time resource allocation techniques for a cognitive radar system.

In [44] the author proposes a cognitive version of passive coherent location (PCL) which has much in common with the broad cognitive radar concept, but adapts only to the waveforms it senses in the environment, and exploits those that are most useful to it for target detection. In addition, it would model the terrain to improve coverage and provide countermeasures against direct signal saturation. By its name, PCL does not transmit, but relies on emissions from other radiating systems, such as broadcast services, other radars, cellular radio, WiFi, and so on. It is clear that such a cognitive system, consisting of multiple, cooperating receivers, can achieve excellent performance in the presence of deliberate jamming, difficult terrain, and attempts at target stealth.

When the targets are moving in a dense urban environment, this problem becomes much more challenging [45]. The propagation path in such an environment consists of multiple scatterers, which can be in relative motion with respect to the sensors. This introduces both delay and Doppler shift in the received signals. To exploit this inherent delay-Doppler diversity and to obtain better performance, ac-

curate prior information about the multipath channel state is required. When no prior information is available, the channel state has to be estimated along with the target state. When multiple sensors are employed, the channel state between each pair of sensors has to be estimated. Hence, the problem of tracking multiple targets in complex scenarios, such as an urban environment, poses a computational challenge due to the high-dimensionality of the state space.

For an active sensor network, such as a radar network, it is also important to consider the constraints on the signal power to be transmitted, and the sensor locations while formulating the optimization problem. Few works in the past have addressed the problem of sensor scheduling for active sensor networks like a distributed MIMO radar network. In [46], the authors propose a subset selection algorithm for the task of estimating the position of a single stationary target. They assume that there is no multipath and the signals transmitted from each radar are orthogonal to each other. In [47], the authors consider tracking multiple targets. They perform an iterative local search to minimize the PCRB and find a subset of antennas to be employed at each time.

In [48], the authors investigate a CRN system for the joint estimation of the target state comprising the positions and velocities of multiple targets, and the channel state comprising the propagation conditions of an urban transmission channel. They develop a measurement model for the received signal by considering a finite-dimensional representation of the time-varying system function which characterizes the urban transmission channel. The authors employ sequential Bayesian filtering at the receiver to estimate the target and the channel state. They propose a hybrid Bayesian filter that operates by partitioning the state space into smaller subspaces and thereby reducing the complexity involved with high-dimensional state space. The feedback loop that embodies the radar environment and the receiver enables the transmitter to employ approximate greedy programming to find a suitable subset of antennas to be employed in each tracking interval, as well as the power transmitted by these antennas. The PCRB on the target and channel state estimation is used as an optimization criterion for designing the antenna selection and power allocation algorithms.

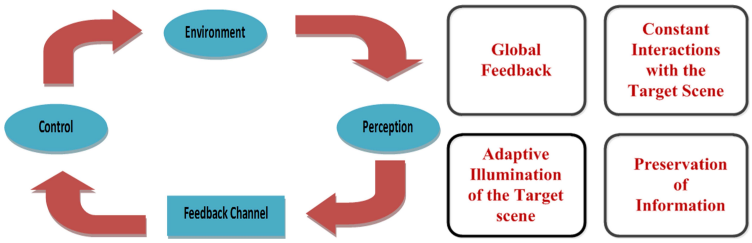

Figure 1.4: Cognitive Radar Building blocks

1.4 Major Contributions and Thesis Outline

In this thesis, we develop and analyze cognitive radar architectures to improve target parameter extraction from a radar scene. The radar scene considered is dynamic with mobile target and non-target scatterers. Specifically this work focuses on the intelligent illumination techniques for the radar scene based on cognition. As discussed previously, this thesis aims at developing cognitive mechanisms which would gain from adaptive waveform design methods, continual learning based on constant interactions with the radar environment and developing feedback mechanisms which would make the radar transmitter more "intelligent" and aware about the dynamic target scene.

In particular, we try to incorporate the above mentioned recent advances in radar systems design within the cognitive radar framework. We develop cognitive architectures for MIMO radar, UWB radar and joint communication-radar waveform design applications. Specifically, we incorporate the cognitive framework for MIMO radar through a novel waveform optimization algorithm, we develop a cognitive strategy for target detection and tracking for UWB radars and finally we investigate the radar systems with added functionality by developing joint communication-radar systems. Chapter-wise major contributions of this thesis are as follows:

- In Chapter 2, a detailed literature survey on the research ideas mentioned in Section 1.2 is presented. Specifically recent advances in MIMO, UWB and joint communication-radar systems are discussed in detail in this Chapter.

- In Chapter 3, a cognitive MIMO radar waveform design method is developed and analyzed. In this approach the target parameter estimates formed by the radar receiver through successive interactions with the radar environment are used in order to design MIMO radar waveforms. This novel two-step ap-

proach employs information theoretic concepts in order to design the MIMO waveforms. As demonstrated by this work the cognitive MIMO waveform design approach improves the target parameter extraction capability. Simulation results also demonstrate that the cognition improves target detection probability, target impulse response or target signature extraction capability and delay-Doppler resolution.

- In Chapter 4, a CRN is developed for facilitating intelligent illumination of the radar scene. This approach employs spatial discretization of the radar scene and develops a HMM enabled approach to learn about the target trajectory. This work considers a distributed radar network which has been deployed to track the trajectory of a target. The radar system learns from the target trajectory and updates its understanding about the radar scene with every subsequent scan. This updated understanding of the radar scene facilitates the intelligent illumination in the succeeding time instant. As demonstrated by the simulation results, the performance gain in terms of probability of target detection, root mean squared (RMS) error on location and tracking performance is compared with the benchmark methods for tracking.

- In Chapter 5, a joint communication-radar waveform design is developed based on cognition. In this chapter a novel approach for encapsulating communication and radar functionalities in a single waveform design for CRR networks is proposed. This approach aims at extracting the target parameters from the radar scene, as well as facilitating high data rate communications between CRR nodes by adopting a single waveform optimization solution. Each CRR node encapsulates its communication data into the radar signal such that the radio and radar information is always separable and can be shared over the entire network. Such CRR networks are aimed at addressing the communication and radar detection problems in mission-critical and military applications, where there is a need of integrating the knowledge about the target scene gained from distinct radar entities functioning in tandem with each other.

- In Chapter 6, a novel approach to spectrum and power allocation is proposed for cognitive radio networks by integrating cognitive radio and cognitive radar network paradigms to achieve intelligent utilization of spectral resources in a

wireless network. This approach exploits the intelligent location information offered by cognitive radars combined with user detection capability of cognitive radios to aid spectrum and power allocation to minimize interference between wireless devices. Such a system requires sharing of channel perception between the radio and radar devices involved, to aid better spectral resource utilization. The second aspect of this research is investigating the inclusion of cognitive mechanism in predicting the spectral holes over the network by adopting a HMM learning approach. To realize opportunistic spectrum access, cognitive spectrum sensing is applied to detect the presence of spectrum holes. Simulation results indicate improvement in throughput and reduction in interference between neighboring wireless devices.

- Finally, Chapter 7 provides concluding remarks and associated future works for this research.

Throughout this work, $\det(\cdot)$ denotes the determinant of a matrix, $(\cdot)^H$ denotes the Hermitian transpose, $\mathrm{tr}(\cdot)$ denotes the trace, and $\mathrm{E}\{\cdot\}$ denotes the expectation operator.

1.5 Publications Arising From This Research

1. Y. Nijsure, Y. Chen, C. Litchfield and P. B. Rapajic, "Hidden Markov model for target tracking with UWB radar systems", in *Proc. IEEE* 20^{th} *International Symposium on Personal, Indoor and Mobile Radio Communications*, pp. 2065-2069, 13-16 Sept. 2009.

2. Y. Nijsure, Y. Chen, P. Rapajic, C. Yuen, Y. H. Chew, and T. F. Qin, "Information-theoretic algorithm for waveform optimization within ultra wideband cognitive radar network", in *Proc. IEEE International Conference on Ultra-Wideband (ICUWB)*, vol. 2, Sept. 2010, pp. 1-4.

3. Y. Nijsure, Y. Chen, C. Yuen, Y. H. Chew, "Location-aware spectrum and power allocation in joint cognitive communication-radar networks", in *Proc. Cognitive Radio Oriented Wireless Networks and Communications (CROWNCOM)*, pp.171-175, 1-3 June 2011.

4. H. Ahmadi, Y. H. Chew, P. K. Tang and Y. Nijsure,"Predictive opportunistic spectrum access using learning based hidden Markov models", in *Proc. IEEE* 22^{nd} *International Symposium on Personal Indoor and Mobile Radio Communications (PIMRC)*, pp.401-405, 11-14 Sept. 2011.

5. Y. Nijsure, Y. Chen, Y. Chau, Y. H. Chew, Z. Ding and S. Boussakta,"Adaptive Distributed MIMO Radar Waveform Optimization Based on Mutual Information", *IEEE Transactions on Aerospace and Electronic Systems* (Journal accepted for publication in September 2012).

6. Y. Nijsure, Y. Chen, P. Rapajic, C. Yuen and Y.H. Chew,"Mobile target tracking using hidden-Markov-model-enabled Cognitive Radar Network", *IEEE Transactions on Aerospace and Electronic systems* (Journal under 2^{nd} stage review).

7. Y. Nijsure, Y. Chen, Y. Chau, Y. H. Chew, Z. Ding and S. Boussakta,"Novel system architecture and waveform design for cognitive radar radio Networks", *IEEE Transactions on Vehicular Technology*(Journal accepted for publication in May 2012).

Chapter 2

Literature Survey

2.1 Introduction

As mentioned in Chapter 1, this thesis provides a cognitive approach to design the modern radar systems. In Section 1.2, the link between the existing research ideas and the contribution of this thesis was presented. In this Chapter, a detailed literature survey on these research ideas is provided. Specifically, recent advances in MIMO, UWB and joint communication-radar systems are discussed in detail. We incorporate the cognitive framework for MIMO radar through a novel waveform optimization algorithm, we develop a cognitive strategy for target detection and tracking for UWB radars and finally we investigate the radar systems with added functionality by developing joint communication-radar systems. We further investigate the fusion of the cognitive radar and cognitive radio paradigms for enhanced spectrum and power resource allocation in wireless networks.

2.2 MIMO Radar System

MIMO radar is an emerging technology that is attracting the attention of radar researchers. Unlike a standard phased array radar, which transmits scaled versions of a single waveform, a MIMO radar system can transmit via its antennas multiple probing signals that may be chosen quite freely. The notion of MIMO radar is simply that there are multiple radiating and receiving sites [49]. The collected information is then processed together. In some sense, MIMO radars are a generalization of multi-static radar [50, 51]. The underlying concepts have most likely

been discovered independently numerous times. By the most general definition, many traditional systems can be considered as special cases of MIMO radars. As an example, synthetic aperture radar (SAR) can be considered as a form of MIMO radar. Although SAR traditionally employs a single transmit antenna and a single receive antenna, the positions of these two antennas are translated and images are formed by processing all the information jointly. The significant difference between this radar and a "typical" MIMO radar, which takes full advantage of the degrees of freedom, is that SAR does not have access to channel measurements for all transmit-receive position pairs. Equivalently, one may say that only the diagonal elements of the channel matrix are measured. Similarly, a fully polarimetric radar, that is, a radar that measures both receive polarizations for each transmit polarization, is an example of MIMO radar [50]. Clearly, it is a MIMO radar with a relatively small dimensionality. In addition, some spatial interpretations of MIMO radar have to be considered in a different context for polarimetric radars.

The transmit antennas radiate signals, which may or may not be correlated, and the receive antennas attempt to disentangle these signals. In much of the current literature, it is assumed that the waveforms coming from each transmit antenna are orthogonal, but this is not a requirement for MIMO radar. However, orthogonality can facilitate the processing. Two simple approaches to obtain orthogonality are to use time division or frequency division multiplexing. However, both approaches can suffer from potential performance degradation (assuming coherent operation) because of the loss of coherence of the target response. The scattering response of the target or background is commonly time-varying or frequency-selective, limiting the ability to coherently combine the information from the antenna pairs. In some applications, it is desirable to introduce correlation between the transmitted signals. For some tracking problems, optimal asymptotic angle estimation performance is given by employing strongly correlated signals [49].

There is a continuum of MIMO radar system concepts; however, there are two basic regimes of operation considered in the current literature. In the first regime, the transmit array elements (and receive array elements) are broadly spaced, providing independent scattering responses for each antenna pair, sometimes referred to as statistical MIMO radar. In the second regime, the transmit array elements (and receive array elements) are closely spaced so that the target is in the far field of the transmit or receive array, sometimes referred to as coherent MIMO radar.

Here it is assumed that the targets scattering response is the same for each antenna pair, up to some small delay. While the answer to the question,"how large must the angular separation be to get independent scattering responses?" is dependent on the details of the target, a sense of scale is provided by thinking of the target as an array of scatterers with phase responses optimized to focus energy toward one of the antennas. If an array of appropriately phased scatterers of the physical size of the target can resolve individual locations of the antennas, then independent scattering responses would theoretically be possible [49]. The waveform diversity enables superior capabilities compared with a standard phased array radar.

In [11, 49, 52, 53], the diversity offered by widely separated transmit/receive antenna elements was exploited. Many other papers, including, for instance, [54], have considered the merits of a MIMO radar system with collocated antennas. The advantages of a MIMO radar system with both collocated and widely separated antenna elements are investigated in [55]. For collocated transmit and receive antennas, the MIMO radar paradigm has been shown to offer higher resolution [50,56], higher sensitivity to detecting slowly moving targets [57], better parameter identifiability [58], and direct applicability of adaptive array techniques [58, 59]. On the other hand, MIMO radars employing widely separated antennas have an advantage of viewing the target from several distinct aspect angles. The radar cross section (RCS) of the target varies with the aspect angle and thus widely separated MIMO radar systems can exploit spatial diversity more effectively [49]. Waveform optimization has also been shown to be a unique capability of a distributed MIMO radar system. For example, it has been used to achieve flexible transmit beam pattern designs [60] as well as for MIMO radar imaging and parameter estimation [54].

In the MIMO radar receiver, a matched filter bank is used to extract the orthogonal waveform components. There are two different approaches for using the non-coherent waveforms:

1. Increased spatial diversity can be obtained [52,53]. In this scenario, the transmitting antenna elements are far enough from each other relative to the distance from the target. The target RCSs are independent random variables for different transmitting paths. When the orthogonal components are sent from different antennas, each orthogonal waveform will carry independent information about the target. This spatial diversity can be utilized to perform better

detection [52, 53].

2. A better spatial resolution for clutter can be obtained. In this scenario, the distances between transmitting antennas are small enough compared to the distance between the target and the radar station such that the target RCS is identical for all transmitting paths. The phase differences caused by different transmitting antennas along with the phase differences caused by different receiving antennas can form a new virtual array steering vector. With judiciously designed antenna positions, one can create a very long array steering vector with a small number of antennas. Thus the spatial resolution for clutter can be dramatically increased at a small cost.

The adaptive techniques for processing the data from airborne antenna arrays are called space time adaptive processing (STAP) techniques. The basic theory of STAP for the traditional single-input multiple-output (SIMO) radar has been well developed [61]. Many algorithms have been proposed for improving the complexity and convergence of the STAP in the SIMO radar. With a slight modification, these methods can also be applied to the MIMO radar case. The MIMO radar STAP for multipath clutter mitigation can be found in [62]. However, in the MIMO radar, STAP becomes even more challenging because of the extra dimension created by the orthogonal waveforms. On one hand, the extra dimension increases the rank of the jammer and clutter subspace, especially the jammer subspace. This makes the STAP more complex. On the other hand, the extra degrees of freedom created by the MIMO radar allow us to filter out more clutter subspace with little effect on signal-to-interference-and-noise ratio (SINR).

2.3 UWB Radars

UWB radio is a fast emerging technology with uniquely attractive features inviting major advances in wireless communications, networking, radar, imaging, and positioning systems. By its rule-making proposal in 2002, the Federal Communications Commission (FCC) in the United States essentially unleashed huge new bandwidth ($3.6 - 10.1$ GHz) at the noise floor, where UWB radios overlaying coexistent radio frequency (RF) systems can operate using low-power ultra-short information bearing pulses. With similar regulatory processes currently under way in many

countries worldwide, industry, government agencies, and academic institutions respond to this FCC ruling with rapidly growing research efforts targeting a host of exciting UWB applications. These include short-range very-high-speed broadband access to the Internet, covert communication links, localization at centimeter-level accuracy, high-resolution ground-penetrating radar, through-wall imaging, precision navigation and asset tracking, just to name a few. UWB characterizes transmission systems with instantaneous spectral occupancy in excess of 500 MHz or a fractional bandwidth of more than 20%. Such systems rely on ultra-short (nanosecond scale) waveforms that can be free of sine-wave carriers and do not require intermediate frequency processing because they can operate at baseband. As information-bearing pulses with ultra-short duration have UWB spectral occupancy, UWB signals come with unique advantages that have long been appreciated by the radar and communications communities:

- Enhanced capability to penetrate through obstacles.
- Ultra high precision ranging at the centimeter level.
- Potential for very high data rates along with a commensurate increase in user capacity.
- Potentially small size and low processing power.

Despite these attractive features, interest in UWB devices prior to 2001 was primarily limited to radar systems, mainly for military applications.

UWB technology emerges as a promising physical layer candidate for Wireless Personal Area Networks (WPAN), because it offers high-rates over short range, with low cost, high power efficiency, and low duty cycle.

- **UWB radio networks:**

  Sensor networks consist of a large number of nodes spread across a geographical area. The nodes can be static, if deployed for, e.g., avalanche monitoring and pollution tracking, or mobile, if equipped on soldiers, firemen, or robots in military and emergency response situations. Key requirements for sensor networks operating in challenging environments include low cost, low power and multi functionality. High data-rate UWB communication systems are well motivated for gathering and disseminating or exchanging a vast quantity of

sensory data in a timely manner. Typically, energy is more limited in sensor networks than in WPANs because of the nature of the sensing devices and the difficulty in recharging their batteries. Studies have shown that current commercial Bluetooth devices are less suitable for sensor network applications because of their energy requirements and higher expected cost. In addition, exploiting the precise localization capability of UWB promises wireless sensor networks with improved positioning accuracy. This is especially useful when GPS are not available, e.g., due to obstruction.

- **UWB radar and imaging systems:**
  As described previously, the wireless sensors can aid in detection of various phenomenon of interest like avalanche monitoring, fire detection, pollution tracking etc. UWB radar and imaging systems comprise wireless radar sensor network (WRSN). WRSN is an enabling technology for applications such as border surveillance, intrusion monitoring for unauthorized movement of targets around critical facilities. Surveillance applications, i.e., real-time detection, tracking and classification of intrusion, require mission critical networking capabilities in WRSN. Generally, low power UWB radar sensors are used in detection, tracking and localization of an intruder in sensor field [63–67]. However, detection and tracking do not surface for a complete target classification in mission critical surveillance applications. To address this need, target imaging is imperative to effectively determine the features of the mobile target.

  Object detection and imaging via sensor network is presented in [63], with multi-static imaging of fixed objects by using mobile radar sensors. Here, to obtain high quality radar image, large number of samples of the object need to be taken and transported to the sink, which incur huge amount of traffic, and hence, potentially lead to congestion in the network. Furthermore, radar image quality and communication challenges are not investigated in [63]. In fact, UWB radar technology can be used for networked collaborative target imaging over a field due to its unique features. UWB radar sensors can provide detection, localization and imaging of targets in short range regardless of environmental conditions [63], as they can operate in all weather conditions, including fog, rain, sleet, hail, snow, and sand. In the classification process,

UWB radar image of the mobile target is required to accurately assess the threat level of the mobile intruder. Spatially distributed radar sensor nodes can gather significant information, e.g., feature and shape, on mobile targets in sensor field. However, UWB-based WRSN is yet to be developed for high quality imaging of mobile targets.

Different from conventional radar systems where targets are typically considered as point scatterers, UWB radar pulses are shorter than the target dimensions. UWB reflections off the target exhibit not only changes in amplitude and time shift but also changes in the pulse shape. As a result, UWB waveforms exhibit pronounced sensitivity to scattering relative to conventional radar signals. This property has been readily adopted by radar systems and references therein and can be extended to additional applications, such as underground, through-wall and ocean imaging, as well as medical diagnostics and border surveillance devices.

- **Vehicular radar systems:**
  UWB-based sensing has the potential to improve the resolution of conventional proximity and motion sensors. Relying on the high ranging accuracy and target differentiation capability enabled by UWB, intelligent collision-avoidance and cruise-control systems can be envisioned. These systems can also improve airbag deployment and adapt suspension/braking systems depending on road conditions. UWB technology can also be integrated into vehicular entertainment and navigation systems by downloading high-rate data from airport off ramp, road-side, or gas station UWB transmitters.

2.3.1 Overview on UWB Indoor Target Tracking Algorithms:

With respect to the UWB tracking technique itself, parametric and non-parametric approaches can be distinguished. Parametric approaches compute the location based on the *a priori* knowledge of a model, while non-parametric approaches process straightforward the data with the usage, in some cases, of some statistic parameters [68]. Specifically, the following algorithms are considered in the current literature: Trilateration, weighted least square with

multidimensional scaling (WLS-MDS), least square with distance contraction (LS-DC), extended Kalman filter (EKF) and particle filter (PF) [68].

Trilateration is a non-parametric algorithm that computes the position based on the distance estimated between the target and three anchor nodes using a geometrical method for determining the intersection of three sphere surfaces [69]. Consequently, regardless of the number of anchors selected, only the three with the smallest estimated distances to the target are used for position computation.

The algorithm WLS-MDS is a completely non-parametric approach combining multidimensional scaling (MDS) with weighted least square minimization (WLS) [70]. MDS is a multivariate data analysis technique used to map "proximities" into a space. These "proximities" can be dissimilarities (distance-like quantities). Given the points and corresponding dissimilarity, MDS finds a set of points in a space such that a one-to-one mapping between the original configuration and the reconstructed one exists. MDS is used to obtain a previous estimation of the solution. Then the Procrustes transformation is used to map back the solution to the absolute reference system. Finally, an iterative low-complexity minimization algorithm known as *scaling by majorizing a complicated function* or SMACOF is applied to optimize the solution. Weights based on the dispersion of the estimated distances are used in the optimization phase in order to diminish the importance of less reliable estimations.

LS-DC aims to correct the distance measurements by subtracting a certain value in order to minimize the impact of biased measurements on the least square (LS) objective function [71]. First the existence of a feasibility region, defined as the area formed by the intersection of the circles with centre at the anchors is checked and an initial solution is computed inside the feasibility area. The contracted distances are computed as the shortest distance from each anchor to the feasibility region. Once the contracted distances are computed, then the LS-objective function is generally convex, and any optimization method (i.e. global distance continuation, steepest descent) can be used to find the global minimum, thus reducing complexity.

The EKF is a Bayesian technique known for its low-complexity and stability as a tracking algorithm [72]. The Kalman-based tracking algorithm has two

major stages, namely, the update and the correction stages, which are iterated a few times for every observation occurring at a given time. A state vector is defined, which contains the variables of the process, namely target position and speed. A measure vector is defined containing the process observations, namely the estimated distances between the target and the anchors. A function that describes the evolution of the state vector through time, and a function that describes the relation between the state vector and the measure vector, are identified. Process noise (acceleration) and measurement noise (ranging error) are Gaussian with a certain variance that is optimized through simulations.

Finally, PFs are recursive implementations of Monte Carlo based statistical signal processing. The use of PFs for positioning in wireless networks was proposed in [73]. It is based on a large number of samples of the state vector (particles), which are weighted according to their importance (likelihood) in order to provide an estimation of the state vector. On each step, the particles are moved according to the process model and the weights are updated according to the likelihood of the observations (estimated distances) according to the distribution of the measurement error. The advantage of the PFs over other parametric solutions is that non-linear models and non-Gaussian noise can be defined. Specifically, two different measurement error models have been defined as a weighted sum of two and three Gaussian components for the different channel configurations. Consequently, the filter is defined by the variance of process noise (acceleration) and the parameters of the measurement error model that were optimized through simulations. As a drawback, its computational complexity is higher, so it is suitable in applications where computational power is rather cheap and the sampling rate is slow.

2.4 Joint Communication-Radar System

Multi-functional software defined radio for both radar and communication has become a hot research topic recently [23, 26, 27, 29]. In current technological development, RF front-end architectures in radar and wireless communication technologies have become more and more similar. In particular, an increasing number of functions, traditionally realized by hardware components, are being replaced by digital signal processing. At the same time, the carrier frequencies used for communica-

tion systems, have shifted to the microwave regime and have become of the same order of magnitude as those traditionally used for radar applications. Hence, a joint RF hardware platform for communications and radar applications could easily be realized with today's technology. Such a kind of platform would offer unique possibilities for novel system concepts and applications. A typical communication waveform with good autocorrelation properties is the spread spectrum signal, which is a well-known candidate for joint radar and communications applications [23]. In addition, advanced concepts, based on multicarrier communication waveforms, have appeared recently. With multicarrier waveforms, processing techniques in the frequency domain can be applied that allow relaxing the autocorrelation requirement.

Not only the employed waveform, but also general system parameters, e.g., the bandwidth, have to be chosen according to the requirements derived from both applications. At first glance, the conditions for optimum signal parameters, from the communications and radar perspective, seem different. That is, in order to achieve high resolution, a radar sensor needs a large signal bandwidth, which is usually much wider than the bandwidth of typical communication signals. Furthermore, the waveform design should satisfy a number of additional requirements. Most importantly, it should be possible to perform radar sensing with arbitrary transmit data. Only in that case is an efficient reuse of the spectrum possible. While the Doppler shift of the received signal, which occurs in environments with moving objects, represents a deteriorating factor for the quality of information transmission, it contains valuable information on the velocities of the reflecting objects at the same time. Hence a strategy must be found that allows for tolerating the Doppler shift in the case of information transmission and for exploiting the velocity information in the radar processing. The radar processing algorithm should support the independent estimation of range and velocity of multiple objects. The acquisition of Doppler information, in addition to a simple range measurement is important for active vehicular safety applications like pre-crash detection. In practical automotive applications, in addition to the range and the velocity also the azimuth position of objects must be determined, in order to get the full two-dimensional (2D) scenario information. However, rotating narrow-beam antennas, as typically utilized for surveillance radar systems, are hardly applicable in automotive radar and would also imply low update rates and restricted communication coverage. A practical solution is to use digital beam-forming techniques, which is currently an important

research area. In this approach, the received signals from multiple antenna elements, with a wider, dedicated coverage, are first individually converted to baseband and digitized. Then, they are processed to form an arbitrary, but limited, number of beams covering the illuminated scene. It can be foreseen that this technique will provide advanced flexibility and performance in many radar applications, from small automotive radar sensors (adaptive cruise control, short range parking aid and so on) to space-borne SAR.

Even more importantly, by using a joint waveform for both applications, the occupied spectrum would be used very efficiently and both applications could be operated simultaneously, which would guarantee a permanent availability of both functions, and help to partially overcome the limited availability of spectral resources. Such systems, providing radar and communication functions on a single hardware platform with a single waveform is feasible [74]. Classical radar waveform design aims at creating signals with optimum autocorrelation properties, which guarantee the high dynamic range of the measurements when applying correlation processing in the receiver. The most popular example fulfilling this requirement is linear frequency modulated pulses, also known as chirp signals. The most intuitive approach for designing a joint waveform, hence, would be to use the linear frequency modulation also for encoding data.

OFDM waveform has also been used in the current radar literature [75–77]. The key feature of OFDM waveform is that the multiple frequencies can be exploited simultaneously and in an orthogonal way. Meanwhile, the radio resources of all frequencies in OFDM waveform can be adjusted dynamically. Digital generation, inexpensive implementation, pulse-to-pulse shape variation, interference mitigation, noise-like waveform for low probability of intercept/detection, and so on are the benefits of adopting OFDM waveforms. The research about the joint OFDM-based radar and communication system has been carried about in Karlsruhe Institute of Technology, Germany [74, 78–82], especially for the future intelligent transportation systems. Range estimation, angle estimation, and Doppler estimation are extensively studied. Besides, a communication waveform is proposed for radar in [74]. OFDM waveform can be used to solve the unambiguous radial speed in a single transmission and improve the signal-to-background contrast [74].

Meanwhile, in the radar network, the communication message for instance the reports on the detected targets can be embedded into the OFDM radar waveform [32].

A unique covert opportunistic spectrum access solution to enable the coexistence of OFDM based data communication with UWB noise radar is presented in [33]. A multi-functional waveform has been designed, by embedding an OFDM signal within a spectrally notched UWB random noise waveform [33]. Besides, the performance of a cognitive WiMAX system in the presence of S-band swept pulse radar is studied in [33]. WiMAX can still work with opportunistic transmission as long as it avoids interfering with the radar system.

Communication-radar integration based on Direct-sequence spread spectrum (DSSS) has been discussed in [83]. As shown in [83], a multi-functional RF system that integrates radar and communication can avoid mutual interference by using different pseudo random (PR) codes. Direct sequence UWB signals like the Oppermann sequences have been applied in [84, 85] to generate the weighted pulse trains for the integrated radar and communication system. Thus, Oppermann sequences can facilitate both radar application and multiple-access communication. Communication information can also be embedded in the radar system through waveform diversity as shown in [30, 31].

In Chapter 5, we investigate the above mentioned joint communication-radar waveform design concepts by designing a novel system architecture for cognitive radar radio (CRR) systems. In this work we consider mobile radar units capable of exchanging target scene information utilizing the same radar waveform. To further extend this idea of the integrating cognitive radar and cognitive radio paradigms a different system architecture for CRR systems is presented in Chapter 6 of this thesis. In essence Chapter 5 and Chapter 6 explore the design of the CRR systems with two distinct architectures. The former considers the CRR units to be mobile radar units with communications capability while the latter envisions the CRR units to be radio users which are also radar targets in the CRR network. We combine the functionalities of cognitive radio and cognitive radar to facilitate localization as well as intelligent spectrum and power allocation. Thus before discussing the potential advantages offered by the fusion of these two cognitive schemes, in the following discussion a brief introduction to the basic concepts and challenges in cognitive radio design are provided.

The report from the FCC's spectrum policy task force indicates that at any given location and time, a high percentage of the scarce radio spectrum remains unused. What we have learnt from the study is that looking for novel spectrum management

approaches to replace the existing static allocation scheme is necessary to solve the spectrum scarcity problem. Dynamic spectrum access (DSA) allows frequency bands to be assigned based on the needs of the radio. Opportunistic spectrum access is a class of DSA where secondary users (SUs) exploit the temporary unused frequency bands, known as *white spaces* or *spectrum holes*, for transmission. However, SUs must guarantee that their transmissions would not cause harmful interference to primary users (PUs) which are the licensed users. An occupied channel needs to be released when a licensed user would like to use it for transmission. To detect the presence of white spaces, SUs have to frequently sense the channels in the spectrum band under consideration. Some commonly known sensing techniques include energy detection, matched filter and the cyclostationary feature detection.

A cognitive radio system may coexist with a primary network or PUs on an either interference-free or interference-tolerant basis [86]. For the former case, the cognitive radio system only exploits the unused spectra of the primary network. While, for the latter case, the cognitive radio system is allowed to share the spectra assigned to primary network under the condition of not imposing detrimental interference on the primary network. In this thesis, Chapter 6 considers a interference-free cognitive radio system, in which location aware spectrum and power allocation scheme and opportunistic spectrum access technique is investigated.

Unfortunately, most cognitive devices might not be able to sense all the targeted channels concurrently. If SUs need to sequentially sense through all the channels before a decision is made, significant amount of the scarce spectrum resources can be wasted in performing spectrum sensing. For example, comparing an algorithm which on average needs to sense four channels before it can find a channel to transmit, to that which on average needs to sense only two channels, the latter has the advantage that the transmission can begin earlier. The waste therefore is significantly reduced. This motivates the idea to search for an intelligent predictive method so that SUs can learn from the past channel utilization and predict which channel is likely to be available for transmission. By prioritizing the order in which channels are sensed according to the channels availability likelihoods, the probability that an SU gets a channel upon it first attempt significantly increases. In other words, being able to learn from the previous experiences helps to find the appropriate time and frequency bands to sense, and subsequently the predicted knowledge of the channel status helps the SU to exploit the spectrum more efficiently. Cognitive radio has been

proposed to promote efficient utilization of the spectrum by exploiting the existence of spectrum holes as mentioned in [87].

Location information of cognitive radio users (CRU) can prove to be beneficial in identifying spectrum holes over the network, which can be used to assist in spectrum allocation in order to avoid interference among users in close vicinity. This information can be obtained from a dedicated cognitive radar network as discussed in [37,88]. This motivates the design of a novel CRR system presented in the current work.

Essentially in Chapter 6, we combine the functionalities of cognitive radio and cognitive radar to facilitate localization as well as intelligent spectrum and power allocation. Specifically, in a CRR network, *radar targets are also radio users*, which results in coexistence of radio environment and radar scene. Furthermore, the knowledge about the location and identification of a specific radar target, which uses certain radio channels for communications, can be fed into the cognitive radio network to assist in decision making about spectrum assignment strategies. Similarly, the cognitive radio network can also localize and identify the radio users by analyzing the received signal. This information can be fed into the cognitive radar network to assist in radar waveform design and selection, target state estimation, and power allocation [37, 88–90]. This leads to sharing of perception of radio and radar scenes under surveillance.

2.5 Note on Thesis Organization

Based on the current research developments as discussed in this Chapter, this thesis further extends these research ideas in Chapters 3, 4, 5 and 6. As mentioned earlier, the thesis focuses upon a cognitive approach to design MIMO, UWB and joint communication-radar systems. The subsequent Chapters are organized in this mentioned order.

Chapter 3

Waveform Optimization in Cognitive MIMO Radars Based on Information Theoretic Concepts

This chapter provides treatment on the novel approach for optimizing cognitive MIMO radar waveforms. This Chapter aims at improving target detection and feature extraction performance by maximizing the MI between the target impulse response and the received echoes in the first step, and then minimizing the MI between successive backscatter signals in the second step. The waveform optimization algorithm is based upon adaptive learning from the radar scene, which is achieved through a feedback loop from the receiver to the transmitter. This feedback includes vital information about the target features derived from the reflected pulses. In this way, the transmitter adapts its probing signals to suit the dynamically changing environment by applying a cognitive approach. Simulation results demonstrate better target response extraction using the proposed two-step algorithm as compared to each single-step optimization method. This approach also results in improved target detection probability and delay-Doppler resolution as the number of iteration increases.

3.1 Introduction

Adaptive waveform design for radar applications has been a well investigated subject in the past. Some of the pioneering works like [3], have applied information-theoretic

measures for the design of radar waveforms in order to facilitate improved target detection and classification. In recent years, the research on the development of knowledge-aided waveform design has received great impetus. Some of the noteworthy works in this area include [4–8]. In these works the radar transmission parameters are modified in order to improve the target parameters estimation in a dynamic radar environment. Another such recent development is the design of cognitive radar systems which represent an innovative paradigm to describe brain-empowered radar systems that constantly employ information-gathering mechanisms to facilitate intelligent illumination of the dynamic radar scene. Subsequently, the updated information about the environment can be utilized to allocate crucial resources such as transmit power and spectrum in a more efficient manner [35, 37]. For a cognitive radar, the information of the radar scene collected at the receiver is relayed to the transmitter through a continuous feedback mechanism. Such a constant learning approach allows the development of waveform design techniques offering better target resolution capability as shown in [91, 92].

Recent results have also shown that a MIMO radar, which employs multiple transmit and receive antenna elements, can fully exploit waveform and spatial diversity gains by illuminating the target in different directions [93, 94]. MIMO radars employ orthogonal signals at distinct transmit antenna elements which excite different scattering centers on the extended targets, thus enhancing the information content in the received backscatter signal. Since the target returns are strongly dependent on the cross sectional area of the scatterers in the line-of-sight (LOS) of the radars, the spatial diversity provided by the distributed MIMO radar elements improves the target parameters extraction as shown in [95–97]. In terms of MIMO radar pulse design, an important school of thought is to apply information theory to radar signal processing. Bell [3] studied the design of waveforms in the context of illumination of extended objects for target detection and information extraction. Yang and Blum [49] extended the work in [3] by using the MI between random target response and the reflected signal as a waveform optimization criterion in the MIMO radar configuration. Thus it is interesting to study the performance of a cognitive MIMO radar that combines the strength of "cognition" and "MIMO". Specifically, the problem of optimizing radar waveforms in order to improve target detection and impulse response extraction will be addressed in this Chapter.

The previous works [49, 95–99] mainly utilize the MI between the target impulse

response and the backscatter signal as a waveform optimization criterion.

This Chapter extends these previously presented ideas on adaptive radar waveform design and cognitive radar principles by presenting a novel two-stage waveform optimization strategy, which can be summarized as follows.

- *Step 1: Waveform design*

  This module involves the design of transmission waveform for each of the distinct MIMO transmit antenna elements. The main objective is to maximize the MI between the backscatter signal and the estimated target response, subject to the transmission power constraint [98]. This design approach ensures that the target echoes at each time instant become more statistically dependent on the target features. Once the set of optimal waveform ensembles is designed, the next step is to select the appropriate signals for transmission.

- *Step 2: Waveform selection*

  This module is based on the principle of minimizing the MI between successive received signals. This selection criterion ensures that we always acquire target echoes that are more statistically independent on each other in time, with an intention of gaining more knowledge about the target features in each time instant of reception.

Furthermore, the optimization process is preceded by channel estimation, wherein an estimate of the target response and noise characteristics is formed by the receiver through measurements carried out in the previous time instant. A feedback loop from the receiver to the transmitter allows the delivery of this radar scene information to the transmitter. Consequently, the probing signal optimization process becomes cognitive by enabling the transmitter to dynamically adapt its operational mode to suit the changing radar environment. The contributions of this chapter can be summarized as follows:

- Developing a practical framework for cognitive waveform design based on ideas presented in works like [35].

- Developing a comprehensive algorithm for cognitive MIMO configuration comprising waveform design and selection.

- Comparison of prevalent target detection and classification techniques with the proposed approach for waveform optimization.

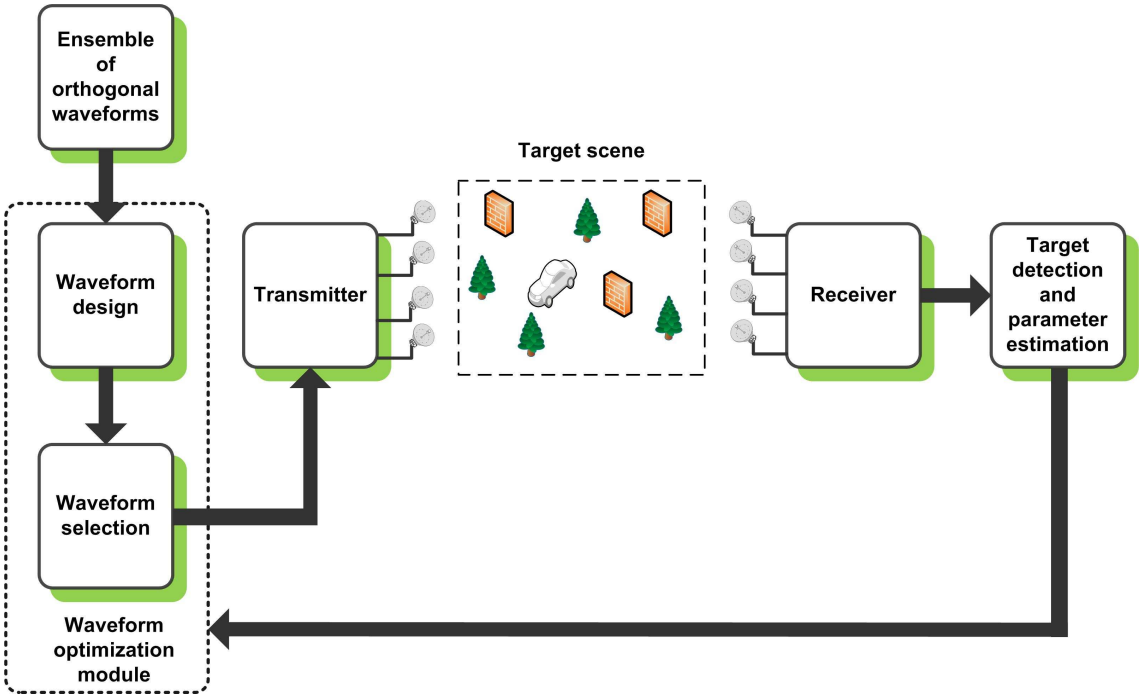

Figure 3.1: Cognitive MIMO radar architecture.

- Performance evaluation of the novel waveform optimization approach in terms of target detection, target features extraction, receiver operating characteristics (ROC) and ambiguity function (AF) analysis.

3.2 Cognitive Waveform Optimization Strategy

3.2.1 System Architecture

Fig. 3.1 represents the general architecture of the cognitive MIMO radar under consideration. As discussed extensively in the existing literature, modern radar applications make use of the pulse compression techniques such as linear frequency modulation or phase coded waveforms employing Barker codes or Costas codes in order to improve the target delay-Doppler resolution [2]. Here we adopt the idea of utilizing phase coded waveforms for generation of orthogonal sequences required for transmission over various transmit antennas. Phase-coded waveforms are selected since they can fully exploit the transmit power with sufficient variability unlike traditional linear frequency modulated (LFM) waveforms [10]. Phase coded waveforms divide the pulse into time segments, referred to as chips, and apply a different phase to each. Binary phase codes limit the chip phase to 0 or π, while polyphase codes

support more levels. In case of the extended target detection, where the target signature is approximated by a finite impulse response comprising of a collection of scattering centers, the phase coded waveforms offer the advantage of exciting the phase-sensitive scattering centers on the target, thus allowing a better target discrimination [99].

We will consider the UWB probing signals [37], though the general methodology is also applicable to any other type of excitation. The waveform comprises a sequence of UWB Gaussian pulses in which the phase of each pulse is modulated in accordance with the orthogonal sequences corresponding to the column vectors of a Hadamard matrix [2]. Each Gaussian monocycle u(t) takes the following form

$$u(t) = \frac{1}{\sqrt{2\pi}T} \exp\left(-\frac{t^2}{T^2}\right) \tag{3.1}$$

where T determines the pulse width and is assumed to be 0.2 ns.

As indicated in Fig. 3.1, we initially form an *ensemble of orthogonal sequences* of Gaussian waveforms ready to be sent over each of the transmit antenna elements of the MIMO radar. These pulses are then modified at the *waveform optimization module* and the optimized waveforms are transmitted over the radar channels. The backscatter signals are gathered by each of the receive antenna elements and passed on to a matched filter bank, which matches the received signals to each individual transmit waveform stored in the receiver. Target response is thus extracted by the *target detection and parameter estimation* module, which attempts to discriminate the target from the surrounding clutter. The estimated channel response and received signal characteristics such as noise covariance are forwarded to the waveform optimization module through a feedback link. The radar channel is comprised of target and non-target scatterer contributions. In this thesis, channel response or scattering matrix refers to this combined radar channel response. Also in this work, the terms, back-scattered radar signal, target echoes and radar returns all refer to the received radar signal. In the light of updated radar scene, the optimization module designs and selects suitable sequences for each of the transmit antennas in order to acquire the best knowledge on the target in the next time instant. This operation facilitates adaptive illumination of the radar environment and essentially leads to a cognitive system featuring the following two important properties described in [35]: (i) intelligent signal processing, which builds on real-time learning through

continuous interaction of the radar with the surroundings; and (ii) feedback from the receiver to the transmitter, which is a facilitator of intelligence.

3.2.2 Signal Model

Without loss of generality, we consider the bistatic radar configuration, where the transmitter and receiver are connected but not collocated. It is assumed that the direct path between the transmitter and the target as well as the one between the receiver and the target have been extracted through some preprocessing steps [100]. For example, the MIMO radar may employ beam-steering [37] and delay windowing [101] to suppress non-target impulse responses.

Suppose that the MIMO system has M transmit and N receive antennas. For simplicity of discussion, it is assumed that $M = N$. We can express the received signal vector at the nth ($n = 1, 2, \cdots, N$) antenna element as

$$\mathbf{y}_n = \sum_{m=1}^{M} h_{m,n}\mathbf{x}_m + \eta_n. \tag{3.2}$$

In the preceding equation, $\mathbf{y}_n \in \mathbb{C}^{k\times 1}$ where $\mathbb{C}$ indicates the complex number domain. The parameter K= $K_s + K_d$, where K_s is the length of the pseudo-random sequence generated and K_d is the maximum excess delay with respect to the first arrival among all the links. The term $\mathbf{x}_{m,n} = [\mathbf{0}_{1\times L_{m,n}}\ \hat{\mathbf{x}}_m^T\ \mathbf{0}_{1\times(K_d - L_{m,n})}]^T$, where $\mathbf{0}_{1\times l}$ is a null vector of length l, $L_{m,n}$ is the propagation delay between the m^{th} transmit and the n^{th} receive antennas via the target, and $\mathbf{x}_m \in \mathbb{C}^{K_s\times 1}$ is the probing signal sent by the m^{th} transmitter. $h_{m,n}$ represents the channel response between the m^{th} transmit and the n^{th} receive antennas. Finally, $\eta_n \in \mathbb{C}^{K\times 1}$ denotes the noise at the n^{th} receiver, which characterizes the combination of both additive white Gaussian noise (AWGN) and joint nuisance of the channel estimation and measurement errors. In this work, we consider the scenario that the length of the pseudo-random sequence is much larger than the excess delay. As a result, $K \approx K_s$ and $\hat{\mathbf{x}}_m$ can be used to approximate $\mathbf{x}_{m,n}$. We further assume that the minimum transmit/receive antenna spacing is sufficiently larger than half wavelength (distributed MIMO configuration). Hence, the correlation introduced by finite antenna element spacing is low enough that the fades associated with two different antenna elements can be considered independent. Subsequently, the reflection coefficient $h_{m,n}$ is assumed to

be different for various pairs of transmitter and receiver, and its phase is assumed to be uniformly distributed between 0 and 2π. Following these above mentioned assumptions on radar channel, the effective convolution in (3.1) between the channel response and transmitted signal can be replaced by multiplication of matrices. A similar assumption has also been made in other recent works like [10, 98].

Let $\mathbf{Y} = [\mathbf{y}_1\ \mathbf{y}_2\ \cdots\ \mathbf{y}_N] \in \mathcal{C}^{K\times N}$ be the ensemble of received signals, $\mathbf{X} = [\mathbf{x}_1\ \mathbf{x}_2\ \cdots\ \mathbf{x}_M] \in \mathcal{C}^{K\times M}$ be the set of orthogonal sequences to be used for transmission, $\mathbf{H} = [h_{m,n}]_{M\times N} \in \mathcal{C}^{M\times N}$ be the radar channel response matrix or scattering matrix, and $\mathbf{\Theta} = [\eta_1\ \eta_2\ \cdots\ \eta_N] \in \mathcal{C}^{K\times N}$ be the noise matrix. We can conveniently express (3.2) as

$$\mathbf{Y} = \mathbf{XH} + \mathbf{\Theta}. \tag{3.3}$$

Each $h_{m,n}$ in the scattering matrix $\mathbf{H}$ is proportional to the target RCS, whose scintillation can vary slowly or rapidly depending on the target size, shape, dynamics, and its relative motion with respect to the radar. The two random matrices $\mathbf{H}$ and $\mathbf{\Theta}$ are assumed to be independent of each other.

3.2.3 Target RCS Modeling

RCS is a measure of how detectable an object is with a radar. A larger RCS indicates that an object is more easily detected. An object reflects a limited amount of radar energy. A number of different factors determine how much electromagnetic energy returns to the source as mentioned in [102],

- Material of which the target is made;
- Absolute size of the target;
- Relative size of the target (in relation to the wavelength of the illuminating radar);
- The incident angle (angle at which the radar beam hits a particular portion of target which depends upon shape of target and its orientation to the radar source);
- Reflected angle (angle at which the reflected beam leaves the part of the target hit, it depends upon incident angle);

- The polarization of transmitted and the received radiation in respect to the orientation of the target.

Swerling target models are special cases of the Chi-Squared target models with specific degrees of freedom. There are five different Swerling models, numbered I through V [102],

1. Swerling I:

   A model where the RCS varies according to a Chi-squared probability density function with two degrees of freedom. This applies to a target that is made up of many independent scatterers of roughly equal areas. As little as half a dozen scattering surfaces can produce this distribution. Swerling I describes a target whose radar cross-section is **constant throughout a single scan**, but **varies independently from scan to scan**. This case is known as **slow fluctuation**. In this case, the pdf reduces to

   $$p(\xi) = \frac{1}{\xi_{av}} \exp\left\{-\frac{\xi}{\xi_{av}}\right\}$$

   where $\xi > 0$ represents the variance of RCS fluctuations and ξ_{av} is the average RCS. Swerling I has been shown to be a good approximation when determining the RCS of objects in aviation.

2. Swerling II

   Similar to Swerling I, except the RCS values returned are **independent from pulse to pulse, instead of scan to scan**. This case is known as **fast fluctuation**.

3. Swerling III

   A model where the RCS varies according to a Chi-squared probability density function with four degrees of freedom. This pdf approximates an object with one large scattering surface with several other small scattering surfaces. The RCS is constant through a single scan just as in Swerling I. This is again a case of **slow fluctuation**. The pdf becomes

   $$p(\xi) = \frac{4\xi}{\xi_{av}^2} \exp\left\{\frac{-2\xi}{\xi_{av}}\right\}.$$

4. Swerling IV

   Similar to Swerling III, but the RCS varies from pulse to pulse rather than from scan to scan. This is a case of **fast fluctuation**.

5. Swerling V (Also known as Swerling 0)

   Constant RCS as degrees of freedom approaches infinity.

While important in detecting targets, strength of emitter and distance are not factors that affect the calculation of a RCS because the RCS is a property of the target reflectivity. RCS of a target depends heavily upon the target aspect angle. Since the target radar cross section depends heavily upon the frequency of operation of the radar (since the target response is frequency selective).

In this thesis we consider the case of slow fluctuations of the RCS as represented by the Swerling III model.

Let the target be a point scatterer amidst several clutter sources. In Swerling III, the RCS samples measured by the radar are correlated throughout an entire scan, but are uncorrelated from scan to scan (slow fluctuation) and the radar scene comprises a single powerful scattering center and many weak reflectors in its vicinity. This model will be applied here, where we assume that the radar scene is dominated by the target and the amplitude returns from non-target scatterers are lower than those from the target. The random RCS takes the following form

$$f(\xi) = \frac{1}{\xi_{av}} \exp\left(-\frac{\xi}{\xi_{av}}\right). \tag{3.4}$$

We would expect the target echoes between successive scans to be uncorrelated for the Swerling III model. Towards this end, we seek to use excitation sequences that will produce uncorrelated received signals between two consecutive scans. Swerling models are used to describe the variations in RCS of complex targets. Also note that, this variation cannot be analytically expressed in terms of Doppler spread and bandwidth of the radar system, but is instead expressed in terms of statistical variations in RCS given by the probability distributions as mentioned earlier.

3.2.4 Two-Stage Waveform Optimization

The waveform design and selection process can be formulated as the following two-step algorithm. Note that the subscript $_t$ will be used to indicate the parameters

for a particular round of radar system adaptation at time t.

Step 1: Maximization of MI between the estimated target response and the received target echoes at time t

Following the classical definition of MI [103],

$$\mathcal{I}(\cdot)(\mathbf{Y}_t; \mathcal{H}(\cdot)_t|\mathbf{X}_t) = \mathcal{H}(\mathbf{Y}_t|\mathbf{X}_t) - \mathcal{H}(\mathbf{Y}_t|\mathbf{H}_t, \mathbf{X}_t) = \mathcal{H}(\mathbf{Y}_t|\mathbf{X}_t) - \mathcal{H}(\mathbf{\Theta}_t) \tag{3.5}$$

where $\mathcal{I}(\mathbf{Y}_t; \mathbf{H}_t|\mathbf{X}_t)$ is the MI between two random variates $\mathbf{Y}_t$ and $\mathbf{H}_t$ given the transmission matrix $\mathbf{X}_t$, and $\mathcal{H}(\mathbf{Y}_t|\mathbf{X}_t)$ represents the conditional entropy or the average information that $\mathbf{X}_t$ conveys about $\mathbf{Y}_t$.

Our aim is to maximize $\mathcal{I}(\mathbf{Y}_t; \mathbf{H}_t|\mathbf{X}_t)$ between $\mathbf{Y}_t$ and $\mathbf{H}_t$ given $\mathbf{X}_t$, i.e., we intend to maximize the MI between the received target echoes and the channel response given the ensemble of transmit waveforms. This implies that the backscatter signals would be more statistically dependent upon the actual radar scene. We can simplify (3.5) by applying the classical definition of entropy as follows [103]

$$\mathcal{H}(\mathbf{Y}_t|\mathbf{X}_t) = \int -p(\mathbf{Y}_t|\mathbf{X}_t) \ln \left[p(\mathbf{Y}_t|\mathbf{X}_t)\right] d\mathbf{Y}_t \tag{3.6}$$

where $p(\mathbf{Y}_t|\mathbf{X}_t)$ denotes the conditional pdf of $\mathbf{Y}_t$ given $\mathbf{X}_t$. The above expression for the entropy can be further simplified by evaluating $p(\mathbf{Y}_t|\mathbf{X}_t)$ to be

$$\begin{aligned} p(\mathbf{Y}_t|\mathbf{X}_t) &= \prod_{n=1}^{N} p(\mathbf{y}_{n,t}|\mathbf{X}_t) \\ &= \prod_{n=1}^{N} \frac{1}{\pi^K \det\left(\mathbf{X}_t^H \mathbf{R}_{\mathbf{H}_t} \mathbf{X}_t + \mathbf{R}_{\mathbf{\Theta}_t}\right)} \exp\left[-\mathbf{y}_{n,t}^H \left(\mathbf{X}_t^H \mathbf{R}_{\mathbf{H}_t} \mathbf{X}_t + \mathbf{R}_{\mathbf{\Theta}_t}\right)^{-1} \mathbf{y}_{n,t}\right] \\ &= \frac{1}{\pi^{NK} \left[\det\left(\mathbf{X}_t^H \mathbf{R}_{\mathbf{H}_t} \mathbf{X}_t + \mathbf{R}_{\mathbf{\Theta}_t}\right)\right]^N} \exp\left\{-\mathrm{tr}\left[\left(\mathbf{X}_t^H \mathbf{R}_{\mathbf{H}_t} \mathbf{X}_t + \mathbf{R}_{\mathbf{\Theta}_t}\right)^{-1} \mathbf{Y}_t^H \mathbf{Y}_t\right]\right\} \end{aligned} \tag{3.7}$$

where $\mathbf{R}_{\mathbf{H}_t} = \mathrm{E}\left\{\mathbf{H}_t^H \mathbf{H}_t\right\}$ and $\mathbf{R}_{\mathbf{\Theta}_t} = \mathrm{E}\{\mathbf{\Theta}_t^H \mathbf{\Theta}_t\}$ are the covariance matrices of the target response $\mathbf{H}_t$ and the noise $\mathbf{\Theta}_t$, respectively. Solving (3.6) and (3.7) gives rise to the following result for the entropy [98]

$$\mathcal{H}(\mathbf{Y}_t|\mathbf{X}_t) = NK \ln(\pi) + NK + N \ln\left[\det\left(\mathbf{X}_t^H \mathbf{R}_{\mathbf{H}_t} \mathbf{X}_t + \mathbf{R}_{\mathbf{\Theta}_t}\right)\right] \tag{3.8}$$

Similarly, we can derive the entropy of the noise as

$$\mathcal{H}(\boldsymbol{\Theta}_t) = NK\ln(\pi) + NK + N\ln\left[\det(\mathbf{R}_{\boldsymbol{\Theta}_t})\right] \tag{3.9}$$

Using (3.5), (3.8), and (3.9), we can compute the MI as

$$\mathcal{I}(\mathbf{Y}_t;\mathbf{H}_t|\mathbf{X}_t) = N\ln\left[\det(\mathbf{X}_t^H\mathbf{R}_{\mathbf{H}_t}\mathbf{X}_t + \mathbf{R}_{\boldsymbol{\Theta}_t})\right] - N\ln\left[\det(\mathbf{R}_{\boldsymbol{\Theta}_t})\right] \tag{3.10}$$

Hence, the maximization in Step 1 can be simplified as

$$\begin{aligned} &\max_{\mathbf{X}_t}\left\{N\ln\left[\det(\mathbf{X}_t^H\mathbf{R}_{\mathbf{H}_t}\mathbf{X}_t + \mathbf{R}_{\boldsymbol{\Theta}_t})\right] - N\ln[\det(\mathbf{R}_{\boldsymbol{\Theta}_t})]\right\} \\ &\text{subject to } \mathrm{tr}[\mathbf{X}_t^H\mathbf{X}_t] \le P \end{aligned} \tag{3.11}$$

with P being the total transmission power.

A rigorous solution of (3.11) has been provided in [98]. We can then find the set of optimal waveform ensembles $\mathbb{S}_{\widetilde{\mathbf{X}}_t}$ out of the entire set of orthogonal sequences from the Hadamard matrix, and the corresponding power allocation vector over different antenna elements, $\boldsymbol{\Psi}_{\widetilde{\mathbf{X}}}$, for each $\widetilde{\mathbf{X}}_t \in \mathbb{S}_{\widetilde{\mathbf{X}}_t}$.

Step 2: Minimization of MI between the received target echoes at time t and the estimated target echoes at time t+1

We now proceed to the second module of the waveform optimization process, in which we intend to ensure that successive target echoes are as different from each other as possible. This would ensure that at every instant of reception, we learn something more about the radar scene.

We can express the MI between the received signals in two consecutive times, t and $t+1$, as

$$\mathcal{I}\left(\mathbf{Y}_t, \mathbf{Y}_{t+1}\right) = \mathcal{H}\left(\mathbf{Y}_t|\mathbf{X}_t\right) + \mathcal{H}\left(\mathbf{Y}_{t+1}|\mathbf{X}_{t+1}\right) - \mathcal{H}\left(\mathbf{Y}_t, \mathbf{Y}_{t+1}|\mathbf{X}_t, \mathbf{X}_{t+1}\right). \tag{3.12}$$

In the preceding equation, $\mathcal{H}\left(\mathbf{Y}_t|\mathbf{X}_t\right)$ (or $\mathcal{H}\left(\mathbf{Y}_{t+1}|\mathbf{X}_{t+1}\right)$) denotes the measure of the uncertainty in the received signal at time t (or $t+1$) given the knowledge of the transmitted signal $\mathbf{X}_t$ (or $\mathbf{X}_{t+1}$). Furthermore, $\mathcal{H}\left(\mathbf{Y}_t, \mathbf{Y}_{t+1}|\mathbf{X}_t, \mathbf{X}_{t+1}\right)$ is the entropy of the received signal pair $(\mathbf{Y}_t, \mathbf{Y}_{t+1})$ given the transmitted signal pair $(\mathbf{X}_t, \mathbf{X}_{t+1})$. We can simplify (3.12) in the same way as we did for (3.6) to obtain the following

results

$$\begin{aligned}\mathcal{H}(\mathbf{Y}_t|\mathbf{X}_t) &= \int -p\left(\mathbf{Y}_t|\mathbf{X}_t\right)\ln\left[p\left(\mathbf{Y}_t|\mathbf{X}_t\right)\right]d\mathbf{Y}_t \\ &= NK\ln(\pi) + NK + N\ln\left[\det(\mathbf{X}_t^H\mathbf{R}_{\mathbf{H}_t}\mathbf{X}_t + \mathbf{R}_{\mathbf{\Theta}_t})\right],\end{aligned} \tag{3.13}$$

$$\begin{aligned}\mathcal{H}(\mathbf{Y}_{t+1}|\mathbf{X}_{t+1}) &= \int -p\left(\mathbf{Y}_{t+1}|\mathbf{X}_{t+1}\right)\ln\left[p(\mathbf{Y}_{t+1}|\mathbf{X}_{t+1})\right]d\mathbf{Y}_{t+1} \\ &= NK\ln(\pi) + NK + N\ln\left[\det(\mathbf{X}_{t+1}^H\mathbf{R}_{\mathbf{H}_t}\mathbf{X}_{t+1} + \mathbf{R}_{\mathbf{\Theta}_t})\right],\end{aligned} \tag{3.14}$$

and

$$\begin{aligned}\mathcal{H}(\mathbf{Y}_t, \mathbf{Y}_{t+1}|\mathbf{X}_t, \mathbf{X}_{t+1}) &= 2NK\ln(\pi) + 2NK \\ &\quad + N\ln\left[\det\left(\mathbf{X}_t^H\mathbf{R}_{\mathbf{H}_t}\mathbf{X}_t + \mathbf{R}_{\mathbf{\Theta}_t}\right)\right] + N\ln\left[\det\left(\mathbf{X}_{t+1}^H\mathbf{R}_{\mathbf{H}_t}\mathbf{X}_{t+1} + \mathbf{R}_{\mathbf{\Theta}_t}\right)\right] \\ &\quad + N\ln\left\{\det\left\{\mathbf{I}_{M\times M} - \left[\mathbf{D}^{(t,t+1)}\right]^2\right\}\right\}.\end{aligned} \tag{3.15}$$

In the preceding equation, $\mathbf{I}_{M\times M}$ is the identity matrix of dimension $M \times M$ and $\mathbf{D}^{(t,t+1)}$ is the diagonal matrix obtained by singular value decomposition (SVD) of the covariance matrix $\mathbf{R}_{\overline{\mathbf{Y}}_t,\overline{\mathbf{Y}}_{t+1}}$, given as the cross-covariance of the whitened expressions for $\mathbf{Y}_t$ and $\mathbf{Y}_{t+1}$:

$$\begin{aligned}\mathbf{R}_{\overline{\mathbf{Y}}_t,\overline{\mathbf{Y}}_{t+1}} = \mathrm{E}\left\{\overline{\mathbf{Y}}_t^H\overline{\mathbf{Y}}_{t+1}\right\} &= \mathrm{E}\left\{\left(\mathbf{Y}_t\sqrt{\mathbf{R}_{\mathbf{Y}_t}^{-1}}\right)^H\mathbf{Y}_{t+1}\sqrt{\mathbf{R}_{\mathbf{Y}_{t+1}}^{-1}}\right\} \\ &= \left(\sqrt{\mathbf{R}_{\mathbf{Y}_t}^{-1}}\right)^H\mathbf{R}_{\mathbf{Y}_t,\mathbf{Y}_{t+1}}\sqrt{\mathbf{R}_{\mathbf{Y}_{t+1}}^{-1}}\end{aligned} \tag{3.16}$$

where

$$\begin{aligned}\mathbf{R}_{\mathbf{Y}_t} &= \mathrm{E}\left\{\mathbf{Y}_t^H\mathbf{Y}_t\right\}, = \mathbf{X}_t^H\mathbf{R}_{\mathbf{H}_t}\mathbf{X}_t + \mathbf{R}_{\mathbf{\Theta}_t}, \\ \mathbf{R}_{\mathbf{Y}_{t+1}} &= \mathrm{E}\left\{\mathbf{Y}_{t+1}^H\mathbf{Y}_{t+1}\right\} = \mathbf{X}_{t+1}^H\mathbf{R}_{\mathbf{H}_t}\mathbf{X}_{t+1} + \mathbf{R}_{\mathbf{\Theta}_t}, \\ \mathbf{R}_{\mathbf{Y}_t,\mathbf{Y}_{t+1}} &= \mathrm{E}\left\{\mathbf{Y}_t^H\mathbf{Y}_{t+1}\right\} = \mathbf{X}_t^H\mathbf{R}_{\mathbf{H}_t}\mathbf{X}_{t+1}.\end{aligned} \tag{3.17}$$

Note that $\mathbf{R}_{\mathbf{Y}_t,\mathbf{Y}_{t+1}}$ in (3.17) does not include a noise term as noise at two different time instants is assumed to be uncorrelated. Furthermore, the covariance matrices of $\mathbf{H}$ and $\mathbf{\Theta}$ estimated at time t are used to approximate the two matrices at time

$t+1$ in (3.14)-(3.17). Solving (3.13)-(3.15), we obtain

$$\mathcal{I}(\mathbf{Y}_t, \mathbf{Y}_{t+1}) = -N \ln \left\{ \det \left\{ \mathbf{I}_{M\times M} - \left[\mathbf{D}^{(t,t+1)}\right]^2 \right\} \right\} = -N \sum_{m=1}^{M} \ln \left\{ 1 - \left[d_m^{(t,t+1)}\right]^2 \right\} \tag{3.18}$$

where $d_m^{(t,t+1)}$ are the diagonal elements of the matrix $\mathbf{D}^{(t,t+1)}$ arranged in the descending order as $d_1^{(t,t+1)} \geq d_2^{(t,t+1)} \geq d_3^{(t,t+1)} \geq \cdots \geq d_M^{(t,t+1)}$.

Finally, we can form the minimization problem in Step 2 as

$$\begin{aligned} &\min_{\mathbf{X}_{t+1}\in\mathbb{S}_{\widetilde{\mathbf{X}}_t}} \left\{ -N \sum_{m=1}^{M} \ln \left\{ 1 - \left[d_m^{(t,t+1)}\right]^2 \right\} \right\} \\ &\text{subject to } \mathrm{tr}[\mathbf{X}_{t+1}^H \mathbf{X}_{t+1}] \leq P \end{aligned} \tag{3.19}$$

$d_m^{(t,t+1)}$ are the diagonal elements of the matrix or the singular values of the covariance matrix $\mathbf{R}_{\overline{\mathbf{Y}}_t, \overline{\mathbf{Y}}_{t+1}}$. The minimization criterion presented in (3.19) is solved by choosing $\mathbf{X}_{t+1} \in \mathbb{S}_{\widetilde{\mathbf{X}}_t}$ such that its corresponding singular value minimizes the expression in (3.19). The set of waveform ensembles $\mathbb{S}_{\widetilde{\mathbf{X}}_t}$ obtained in Step 1 are designed with the purpose of maximizing MI over the *spatial* domain, whereas Step 2 selects the transmission sequence for each transmit antenna element from $\mathbb{S}_{\widetilde{\mathbf{X}}_t}$ with an objective of minimizing MI over the *temporal* domain. The proposed waveform optimization algorithm can be summarized as follows.

1. At the initial time $t = 0$, $\mathbf{R}_{\mathbf{H}_0}$ and $\mathbf{R}_{\boldsymbol{\Theta}_0}$ can be estimated through successive measurements with uniform power allocation over the transmit antenna elements by solving equations in (3.17) simultaneously. This can be done by estimating the target echoes in the next time instant by using (3.3) and the prospective transmission waveforms from the ensemble $\mathbb{S}_{\widetilde{\mathbf{X}}_0}$.

2. Solve for the optimum power allocation $\boldsymbol{\Psi}_{\widetilde{\mathbf{X}}_0}$ and the set of optimal waveform ensembles $\mathbb{S}_{\widetilde{\mathbf{X}}_0}$ as per the maximization criterion stated in (3.11).

3. Form an estimate of the received signal $\mathbf{Y}_1$ at time $t = 1$ based on the current estimate for target impulse response and by using (3.3). The target impulse response in the current time instant is estimated by de-convolving the received signal with the transmitted signal. Since it is assumed that the target is the most dominant scatterer in the radar environment, the result of this deconvolution is assumed to be the target impulse response.

4. Solve for $\widetilde{\mathbf{X}}_1 \in \mathbb{S}_{\widetilde{\mathbf{X}}_0}$ using the minimization approach stated in (3.19).

5. Transmit $\widetilde{\mathbf{X}}_1$ and process the received signal to obtain the updated $\mathbf{R}_{\mathbf{H}_1}$ and $\mathbf{R}_{\mathbf{\Theta}_1}$ at time $t = 1$.

6. Repeat Steps $1 - 5$ iteratively.

It is worth emphasizing that cognition is integrated in the above waveform optimization process through the feedback operation implemented in Step 5.

3.3 Delay-Doppler Resolution of MIMO Radar

The radar AF represents the time response of a filter matched to a given finite energy signal when the signal is received with a delay τ and a Doppler shift υ relative to the nominal values expected by the filter as described in [2]. Different from the communication systems, the matched filter for a radar receiver is designed to match the transmit waveform but not the channel itself. The radar AF thus explains the ability of the radar receiver to boost the backscatter signal from the target (assumed to be at the origin of the AF plot) in comparison with the backscatter signal from non-target scatterers [2]. The closer the AF response to unity at the origin the better the delay-Doppler resolution. Ideally the AF plot must be a thumb-tack response at the origin as suggested in [2].

The radar AF can be mathematically represented as [102]

$$\chi(\tau, \upsilon)_0(\tau, \upsilon) = \left| \int_{-\infty}^{\infty} u(t) u^*(t + \tau) \exp(j2\pi\upsilon t) dt \right| \tag{3.20}$$

where u is the complex envelope of the signal. A positive υ implies a target moving toward the radar, whereas a positive τ implies a target being farther from the radar than the reference position with $\tau = 0$. The radar AF for a single UWB Gaussian pulse as shown in (3.1) can be represented as [1]

$$\chi_1(\tau, \upsilon) = \left| \int_{-\infty}^{\infty} \exp\left(-\frac{t^2}{T^2}\right) \exp\left[-\frac{(t+\tau)^2}{T^2}\right] \exp(j2\pi\upsilon t) dt \right| \tag{3.21}$$

where T determines the Gaussian pulse width. For a train of UWB pulses, the radar

AF is given by

$$\chi_2(\tau,\upsilon)=\frac{1}{Q}\sum_{q=-(Q-1)}^{Q-1}\left|\chi_1\left(\tau-qT,\upsilon\right)\frac{\sin(\pi\upsilon-|q|T)}{\sin(\pi\upsilon T)}dt\right| \tag{3.22}$$

where Q represents the total number of pulses. However, the preceding equations are only applicable to the single-input single-output (SISO) radar architecture. For an MIMO radar the equation needs to be modified and is derived in [100]. The received signal after matched filtering can be expressed as

$$\chi_3\left(\tau,\upsilon,f\right)=\left|\int\left[\mathbf{y}\left(t,\tau',\upsilon',f'\right)\right]^H\mathbf{y}\left(t,\tau,\upsilon,f\right)dt\right| \tag{3.23}$$

where τ,υ,f represent the delay, Doppler shift, and spatial frequency, respectively; and τ',υ',f' are the corresponding parameters used by the matched filter at the receiver. We can match the spatial frequency at each of the receive antenna element by adopting receiver beamforming. In terms of the transmitted waveform for non-collocated antennas, the above equation can be written as

$$\chi_3\left(\tau,\upsilon,f\right)=\underbrace{\left|\sum_{n=1}^{N}\exp\left[j2\pi(f-f')n\right]\right|}_{\text{Receiver beamforming}}\sum_{m_1=1}^{M}\sum_{m_2=1}^{M}\underbrace{\left|\chi_{m_1,m_2}(\tau,\upsilon)\right|}_{\text{Cross AF}}\exp\left[j2\pi(f_{m_1}-f_{m_2})\tau\right] \tag{3.24}$$

where M and N are the number of transmit and receive antenna elements. The cross AF is obtained as

$$\chi_{m_1,m_2}(\tau,\upsilon)=\int u_{m_1}(t-\tau)u_{m_2}^H(t-\tau')\exp\left[j2\pi(\upsilon-\upsilon')t\right]dt. \tag{3.25}$$

As the radar AF is a function of the transmit waveform, we can evaluate the performance of the proposed waveform optimization strategy in terms of the delay-Doppler resolution by using (3.24).

3.4 Simulation Results

We employ orthogonal sequences of the Gaussian UWB pulse over the transmit antenna elements. The received waveform ensemble is matched filtered at the receiver and the transmitted signals are later modified by the waveform optimization

module as shown in Fig. 3.1. Fig. 3.2(a) indicates the optimized transmission sequence at one particular transmit antenna element after the two-step optimization process. The sampling frequency of these UWB pulses is 10 GHz and the bandwidth is 700 MHz.

Fig. 3.2(b) shows the received radar pulse sequence for the transmission sequence in Fig. 3.2(a). Fig. 3.2(c) shows the target response extracted from the received target echoes after matched filtering at the end of 20 iterations of the algorithm, where an excellent performance of the target response extraction can be observed. At each iteration of the algorithm, the RCS for the target and non-target scatterers in $\mathbf{H}$ varies as described by the Swerling III variations. This causes the amplitude returns of the backscatter signal from target and clutter sources to vary at each instance. However the amplitude returns from the target are always assumed to be stronger than those from the clutter sources.

Fig. 3.3(a) indicates the mean squared error (MSE) achieved by the algorithm with regard to the estimation of target impulse response. This plot demonstrates an improved MSE performance for the two-step optimization approach as compared to the individual maximization (Step 1) and minimization (Step 2) modules, particularly at the first few iterations. Fig. 3.3(b) indicates the probability of target detection achieved by the proposed method, which is obtained by averaging over 1000 simulations each at a particular value of the received signal-to-clutter-plus-noise ratio (SCNR). We apply the hypothesis testing method based on the optimal Neyman-Pearson algorithm [2] for target detection. The numerical value of the amplitude threshold is determined by fixing the probability of false alarm $P_{fa} = 0.00001$. By Neyman-Pearson detection algorithm as mentioned in [2] we have the threshold value $\varepsilon = \sqrt{n\sigma^2}\mathbb{Q}^{-1}(P_{fa})$ where σ^2 is the variance of the normalized received signal amplitudes, n represents the number of samples and $\mathbb{Q}$ is the complementary error function. Fig. 3.3(b) shows that for a fixed probability of detection, the required SCNR value decreases as the number of iterations increases. An SCNR gain of more than 5.5 dB at a detection probability of 0.8 is observed between iterations 1 and 20. Nevertheless, the system performance does not show any significant improvement beyond 20 iterations.

Fig. 3.4(a) illustrates the normalized 2×2 MIMO radar AF contours after the 1st iteration of the optimization algorithm. As can be seen from Fig. 3.4(a), the resolution of the delay and Doppler of the target deteriorates due to the presence

of surrounding clutter. This is particularly evident if the non-target scatterers are positioned in the vicinity along the line joining the target and the antenna element, assuming that the target is located at the origin of the plot. However, as we increase the number of iterations using the two-step waveform optimization approach, we observe that the target discrimination ability is greatly improved as shown in Fig. 3.4(b). Specifically, at the end of 20 iterations, the clutter interference is suppressed by approximately 2 dB. This plot was generated for the first transmitter receiver pair of the MIMO radar configuration.

The delay-Doppler resolution is directly related to the AF of the radar waveforms. It represents the matched filter output of the radar receiver and should ideally be a thumb-tack response (with unity at origin which corresponds to the delay-Doppler for the target). The ideal AF response would be observed if we use statistically independent waveforms for transmission with optimum phase shifts and amplitude for the pulses. In the two-step waveform optimization approach, we design and select the waveforms that are matched to the approximate target impulse response which is estimated and updated at each iteration. The improvement in AF for the two-step setup can be attributed to the improved waveform design due to this continual upgrade in the target impulse response estimates. The optimum power allocation $\mathbf{\Psi}_{\widetilde{\mathbf{X}}_0}$ ensures that we suppress the clutter interference over the MIMO radar channels and thus improve the SCNR of the received signal. The probability of target detection result presented in Fig. 3.3(b) displays this improvement in SCNR with the number of iterations of the algorithm in the presence of strong clutter. This result demonstrates the improved capability of the radar system to discriminate the target from its surroundings and resolve it in terms of its range and velocity.

In Fig. 3.5, we provide simulation data for the target scene shown in Fig. 3.1. In this simulation, we compare the performance of different radar configurations with respect to their target signature extraction or target discrimination capability. The radar scene is simulated by placing the target (the vehicle in Fig. 3.1) and non-target scatterers (trees and brick walls in Fig. 3.1) at fixed locations on the 2D map. The map is spatially discretized in the form of range bins or cells in both the X and Y directions. The boundary cells of all the scatterers in the target scene fluctuate over subsequent scans as defined by the Swerling III. The target scene is illuminated by sequences of the UWB Gaussian pulse over each of the antenna

elements, as described in the earlier sections. The samples of the signals received at each antenna element are captured and utilized to perform range estimation for the scatterer boundaries, which is achieved by estimating the delays that maximize the cross-correlation between the received signal samples and the delayed version of the transmission waveform. The range cells corresponding to the boundary of each scatterer are identified by using these estimated delays. This approach to target range estimation is similar to the one adopted in [24, 104]. Based on this range resolution technique, an approximated map of the target scene is created.

Fig. 3.5(a) shows the target scene image recreated using the conventional SAR, where the phased antenna arrays are employed at both the transmitter and the receiver. For the SAR, we utilize the same Gaussian UWB sequence over each of the antenna elements but with different delays and with the uniform power allocation. As can be seen from Fig. 3.5(a), the target discrimination offered by this technique is poor. Although the presence of the object can be successfully detected, the SAR fails to discriminate the object from the surrounding clutter. Furthermore, the target signature extraction is suboptimal as shown in the image. Fig. 3.5(b) represents the approximated target scene by using the 4×4 MIMO radar and employing the MI maximization approach for designing waveforms as discussed in [98]. The target scene is clearer since the scatterers are better resolved spatially. The enhanced spatial resolution can be attributed to the MIMO radar configuration, which exploits the spatial diversity by illuminating the target scene from different directions. The waveform design solution employed in this case results in excitation signals better matched to the target impulse response. Hence, the target signature extraction is superior compared to the SAR. Fig. 3.5(c) shows the recreated target scene by employing the MI minimization algorithm alone. The target scene discrimination is comparable to the MI maximization case but no significant improvement is observed. Fig. 3.5(d) indicates the proposed two-step waveform design solution. As can be seen from the image, the target resolution has been significantly improved. The target discrimination is also superior as compared to the previous examples. Fig. 3.5(e) depicts the ROC for 4 different radar configurations, which are

- Constant false alarm rate (CFAR) detection using the phased antenna arrays at both the transmitter and the receiver as indicated in [105];
- 2×2 MIMO radar employing the waveform design solution based on maxi-

mization of the MI as indicated in [98];

- 2×2 MIMO radar employing the proposed two-step MI optimization approach for waveform design; and
- Conventional SAR architecture employing the phased antenna arrays.

For a probability of false alarm at 0.02, the probability of target detection offered by the proposed scheme is approximately 0.8 as compared to 0.64 offered by the MI maximization approach, 0.42 by the CFAR, and 0.38 by the SAR. The plot for MI maximization and two-step waveform optimization was generated at the end of 50 iterations.

Fig. 3.5(f) represents the ROC curves for 4×4 MIMO radar configuration. As can be seen from this result the area under the ROC curve is much greater than in the case of the 2×2 MIMO configuration, thus indicating the gain due to spatial diversity of the MIMO radar channel.

The proposed waveform optimization comprises of maximization of MI over the spatial domain by designing optimum ensemble of transmission waveforms. In this module, we intend to make the received signal more statistically dependant upon the estimated target impulse response. This design step has been well investigated in the existing literature like [98]. This designed waveform matches the target response. More specifically, the waveform design approach ensures that, the left singular vectors of the optimal waveform are the eigenvectors of the colored noise and the right singular vectors become the eigenvectors of the target covariance matrix. In other words all the transmitted waveform energy is focussed in the direction where the target exists and the energy of the clutter is minimum. This means that the Step 1 of the algorithm ensures that the optimum transmission waveform preserves and boosts the target energy whereas suppresses the clutter and noise contributions at the same time. The Step 2 of the algorithm ensures that we receive the back-scatter signal which has low cross correlation over the temporal domain. This allows better discrimination of the target features from the back-scatter signal. Thus the proposed waveform optimization offers better target discrimination and suppression of non-target contributions.

In order to evaluate the advantage of the proposed waveform optimization other than its MSE performance, we analyze the detection variation brought about by the waveform optimization as compared to the other MI algorithms. Fig. 3.6 represents

the detection variation brought about by the proposed waveform optimization algorithm, the detection constraint optimization has been recently explored in works like [10]. In [10] the authors address the problem of radar phase-coded waveform design for extended target recognition in the presence of colored Gaussian disturbance. The objective function in [10] aims to maximize the weighted average Mahalanobis distance or Euclidean distance between the ideal echoes from different target hypotheses. This objective is similar to Step 1 of the proposed waveform optimization which is waveform design, this means that the optimization problem in (11) is similar to [10, Eq. (8)]. As seen from Fig. 3.6, a radar scene with 7 target scatterers is simulated in a 8 m $\times$ 8m map. The backscatter signal from the radar scene is normalized and the radar attempts to discriminate the targets on the map based on a fixed detection threshold. There is a significant improvement in the target SCNR at the end of 20 iterations of the proposed waveform optimization as compared with the same number of iterations of MI minimization and MI maximization individually. This result also agrees with the probability of detection result in Fig. 3.3(b). As seen in Fig. 3.6 the radar is able to discriminate 7 targets successfully on the 2-D map, by suppressing the clutter and noise. This improved detection performance is because the waveform design step in the proposed method ensures that the Euclidean distance between the ideal echoes from different targets is maximized through the optimization problem in (3.11) and the most optimum waveform has been selected based upon the MI minimization problem mentioned in (3.19).

Fig. 3.7 indicates the MSE performance for the 4 $\times$ 4 MIMO configuration with the application of MI minimization, MI maximization and the proposed two-step optimization. As seen from the plot the two-step waveform optimization offers better MSE performance than both the individual MI based approaches. This result agrees with the target discrimination result indicated in Fig. 3.5.

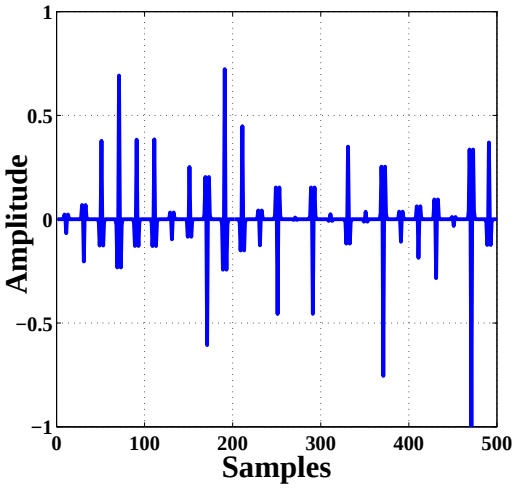

(a)

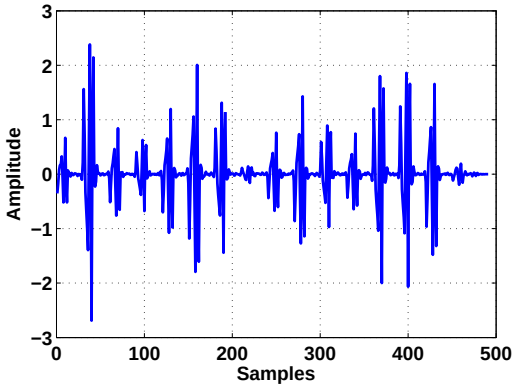

(b)

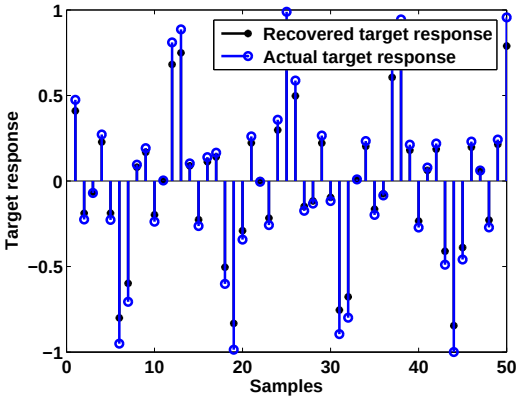

(c)

Figure 3.2: (a) Transmission waveform at a particular antenna after the two-step optimization, (b) received signal after matched filtering for the transmitted signal shown in (a), and (c) target response extraction.

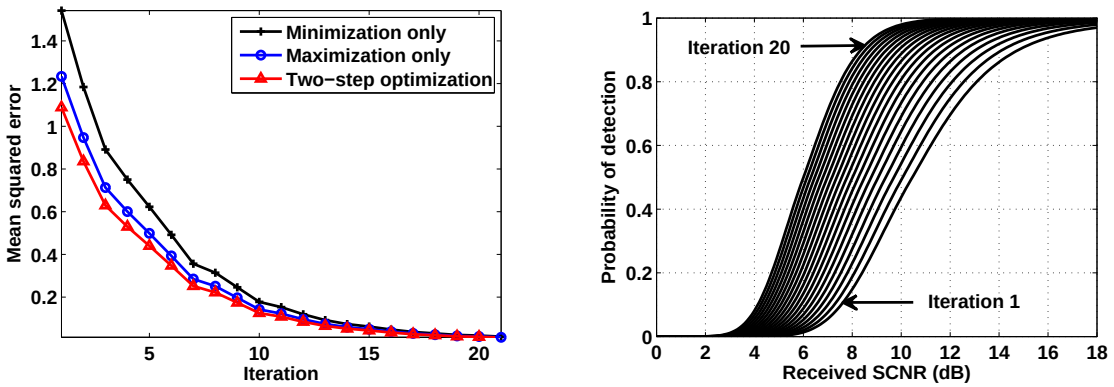

(a) (b)

Figure 3.3: (a) MSE in target response extraction and (b) probability of target detection.

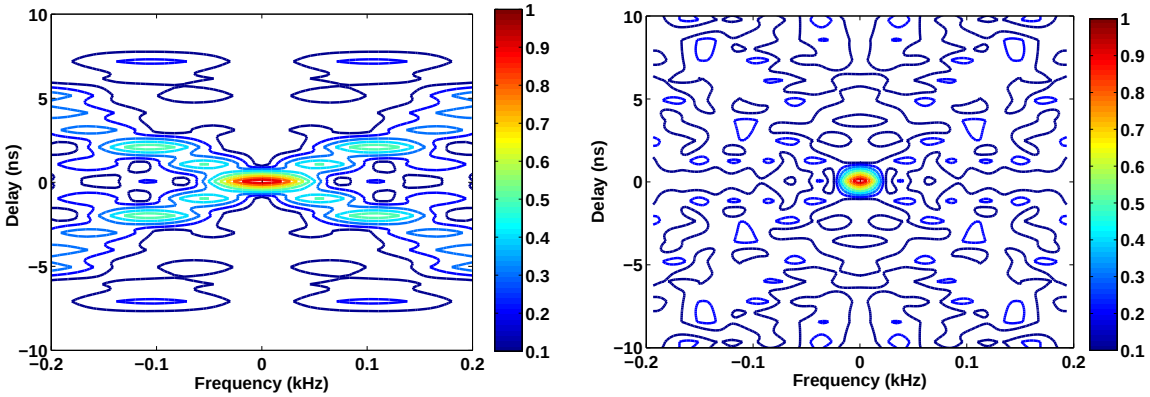

(a) (b)

Figure 3.4: AF contours indicating target resolution at (a) iteration 1 and (b) iteration 20 for a 2×2 MIMO radar, which demonstrates a smaller focal area and an improved signal-to-clutter ratio in (b) as compared to (a).

3.5 Chapter Summary

This chapter presents a two-stage waveform optimization algorithm for a cognitive MIMO radar, which unifies the waveform design and selection procedures. The proposed algorithm is based upon constant learning of the radar environment at the transceiver and adaptation of the transmit waveforms to suit the non-stationary radar scene. This ensures maximum information extraction from the target of interest. Simulation results have demonstrated that the proposed approach results in an improved performance in terms of target response estimation, target detection, delay-Doppler resolution, and target discrimination.

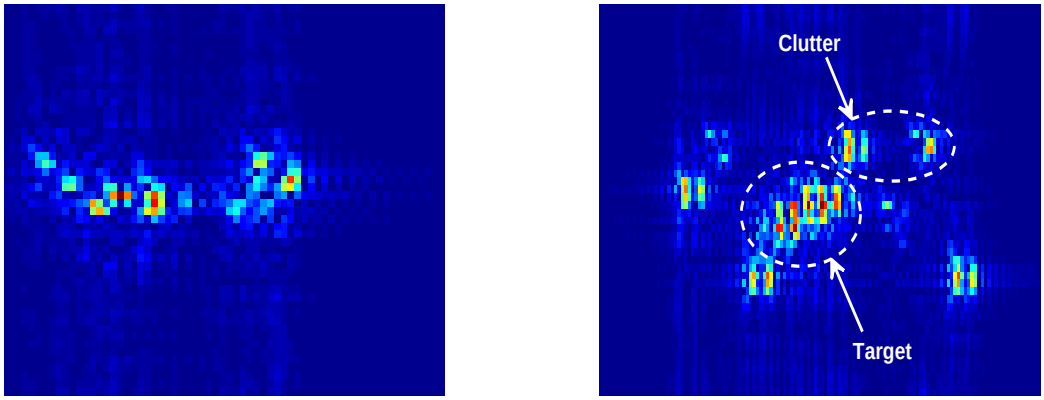

(a)

(b)

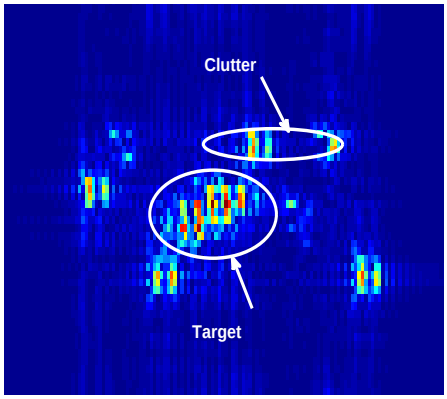

(c)

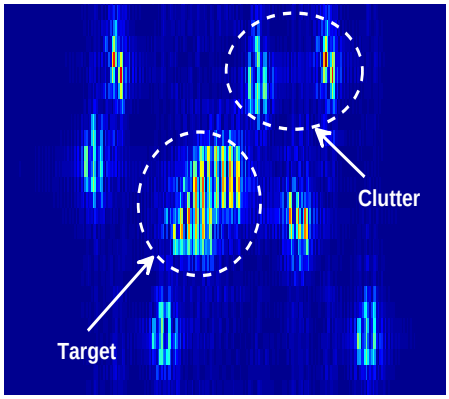

(d)

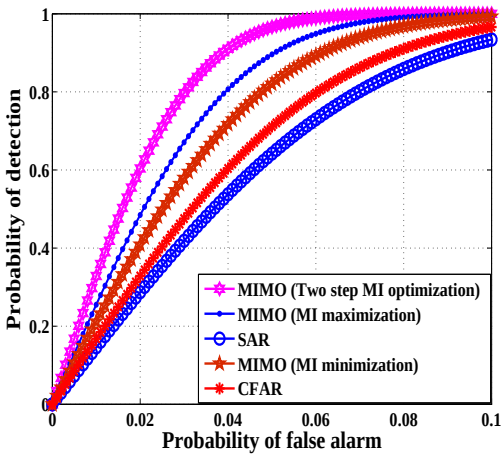

(e)

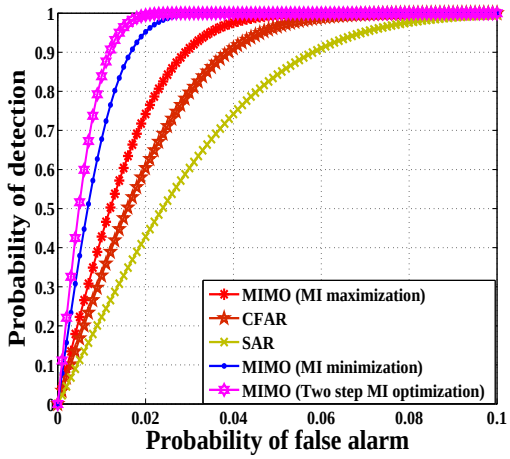

(f)

Figure 3.5: (a) SAR image, (b) 4×4 MIMO radar (MI maximization), (c) 4×4 MIMO radar (MI minimization), and (d) 4×4 MIMO radar two step MI optimization. (e) ROC for 2×2 MIMO radar (f) ROC for 4×4 MIMO radar.

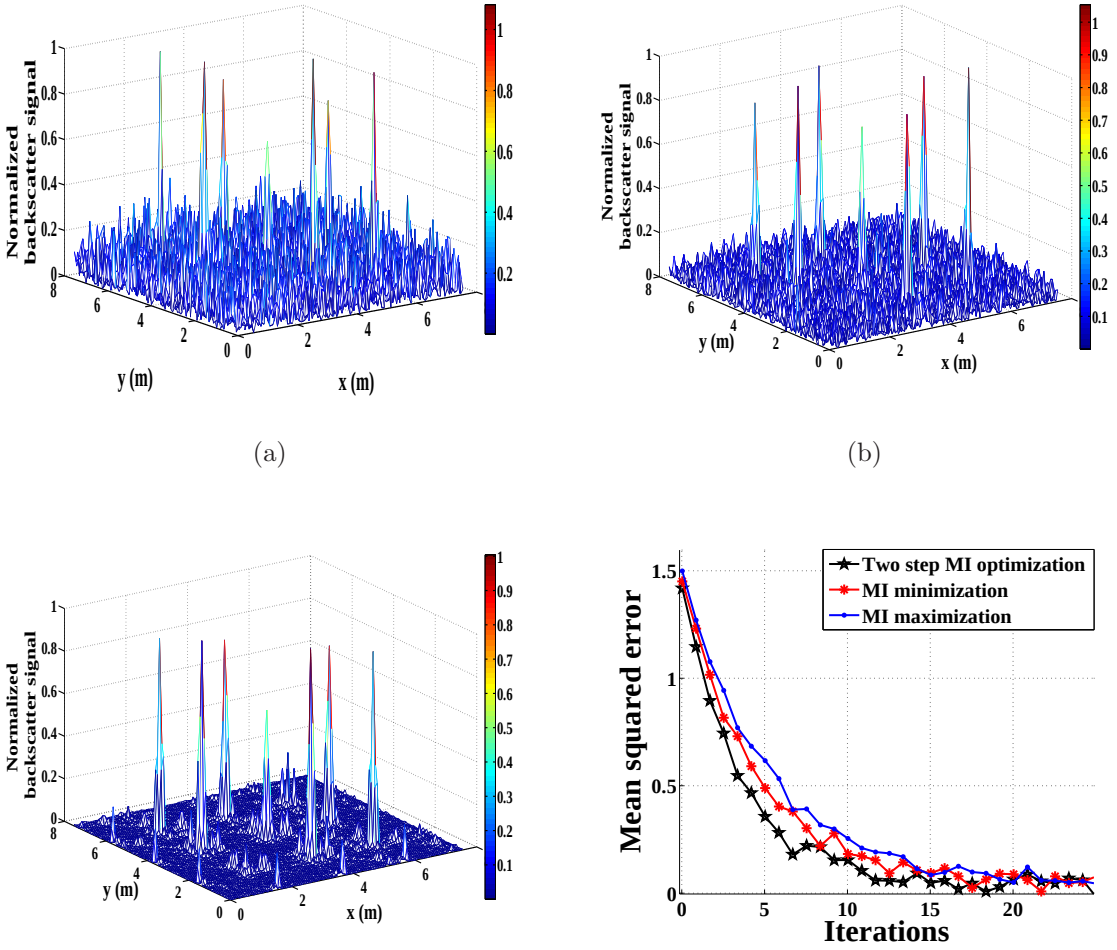

Figure 3.6: (a) Backscatter signal profile for MI minimization at iteration 20, (b) Backscatter signal profile for MI maximization at iteration 20, (c) Backscatter signal profile for two-step waveform optimization at iteration 20, and (d) MSE performance for 4×4 MIMO configuration.

Chapter 4

Target Detection and Tracking Using Hidden-Markov-model-enabled Cognitive Radar Network

In this chapter a novel HMM for describing the movement of an object, monitored by a CRN, is developed. The problem of tracking the target is tackled using the proposed HMM approach, which is integrated into the CRN that constantly learns about its surroundings and adopts its operational mode accordingly. Both the received signal strength (RSS) and time-of-arrival (TOA) of the backscatter signals acquired at different radar units are applied to establish the HMM for characterizing the non-stationary radar scene and enabling subsequent target detection and tracking. The system performance predicted using the proposed technique is then compared to other widely-used algorithms including the EKF and maximum likelihood estimation (MLE). Simulation results demonstrate the advantage of the proposed cognitive tracking scheme as compared to the other approaches in terms of its higher probability of detection and lower computational complexity, while maintaining the same level of location accuracy.

4.1 Introduction

In wireless positioning systems, localization is usually achieved through the measurement of relevant propagation parameters such as RSS, TOA, time-difference-of-arrival (TDOA), and angle-of-arrival (AOA) [106–109]. Accurate ranging could be obtained, in theory, by estimating RSS or TOA of the received waveforms. However, dense multipath and large delay spread, often found in indoor environments, complicate the channel measurement process and deteriorate the performance of the line-of-sight (LOS) signal acquisition. As a result, we use the hybrid RSS/TOA measurements for localization instead of the conventional approach based upon RSS or TOA only. On the other hand, the RSS information recorded at various radar components is employed to construct the HMM for describing the dynamic radar scene and subsequently enabling target detection and tracking. Specifically, the HMM forms the basis of the adaptive learning module in the CRN, which continuously collects the RSS/TOA information from the environment under surveillance and estimates the HMM parameters responsible for generating the set of observations. The target trajectory can then be estimated as an output of the HMM parameter estimation process, which is fed back to the data fusion center for activation of the nearby radars in accordance with the updated target location estimate. We will consider UWB radars in the following discussions due to the high-resolution ranging capability of UWB pulses [69, 110–113]. Nevertheless, the general methodology is also applicable to any other types of radar waveforms.

HMM has been used for multiple target tracking applications in works like [114], where superimposition of HMMs was applied. In [114], the parameters like target location, velocity, etc. were classified as the underlying latent states for detection through noisy observations. HMM was first applied to the problem of target localization in [106]. However, the proposed HMM algorithm differs in the definition of the Markov states and observations compared to those defined in [106]. The current approach also differs from [106] in the way to perform spatial discretization of the area under surveillance. In addition, we utilize a two-way propagation model for radar signals, which is different from the one-way model for radio localization in [106]. One possible solution for the target position and tracking estimation is the one presented in [115] which has utilized particle filtering approach for tracking of multiple targets within indoor localization scenarios. Other related contributions in

Table 4.1: Related Works

Relevant contributions	References
CRN	[34–36]
Application of CRN in object tracking	[37]
HMM	[118]
Application of HMM in indoor localization using RSS/TOA	[106]
RSS/TOA based tracking with nonlinear system models	[119]

indoor localization and tracking include [107, 110, 116, 117].

We build upon the ideas presented in Table 4.1, namely CRN [34–36] and its application in object tracking [37], HMM [118] and its application in indoor localization [106], and RSS/TOA based tracking [119], to propose a novel intelligent target tracking platform.

The main contributions of this Chapter encompass the following aspects:

1. Development of a HMM-enabled CRN to detect and track an object by accurately predicting the nearest radar units in an indoor environment; and

2. Evaluation of the probability of target detection and the root-mean-squared-error (RMSE) of location estimate, and comparison of the results with the benchmark algorithms including the EKF and the MLE.

4.2 Preliminaries of HMM-Enabled CRN

As indicated in Fig. 4.1, the target moves within a 2 D indoor environment and is monitored using a CRN. As discussed in works like [37,106,119], a 2 D environment is used to simplify the tracking problem under consideration. The height or the azimuth information of the target is irrelevant to the radar scene under consideration, since we are interested to locate the target within the 2D indoor map. This type of approach is used for ground targets in which the radar units employ beam-steering techniques to illuminate the radar scene in a direction parallel to the ground plane. This greatly simplifies the problem since the spatial discretization need not be carried out in a 3 D space. Each radar unit in the CRN is fixed at a known location and transmits UWB pulses at fixed time intervals to probe the surroundings. The service area under surveillance is divided into a number of Voronoi regions, where the radars distributed in the region form the Voronoi centers as shown in Fig. 4.1. The locations of the object are classified into discrete "states" following the Voronoi regions where

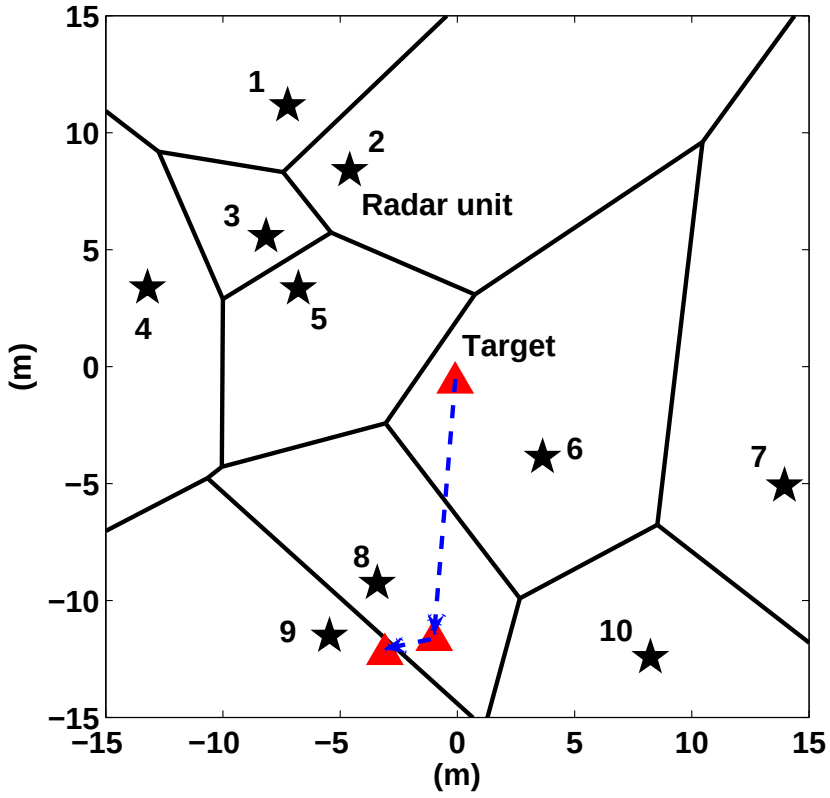

Figure 4.1: 10 Voronoi regions formed based on the distribution of 10 radars in the CRN. The target locations are classified into discrete "states" corresponding to the Voronoi regions where the target is located. In the above plot, the sequence of target states is $6 \rightarrow 8 \rightarrow 9$.

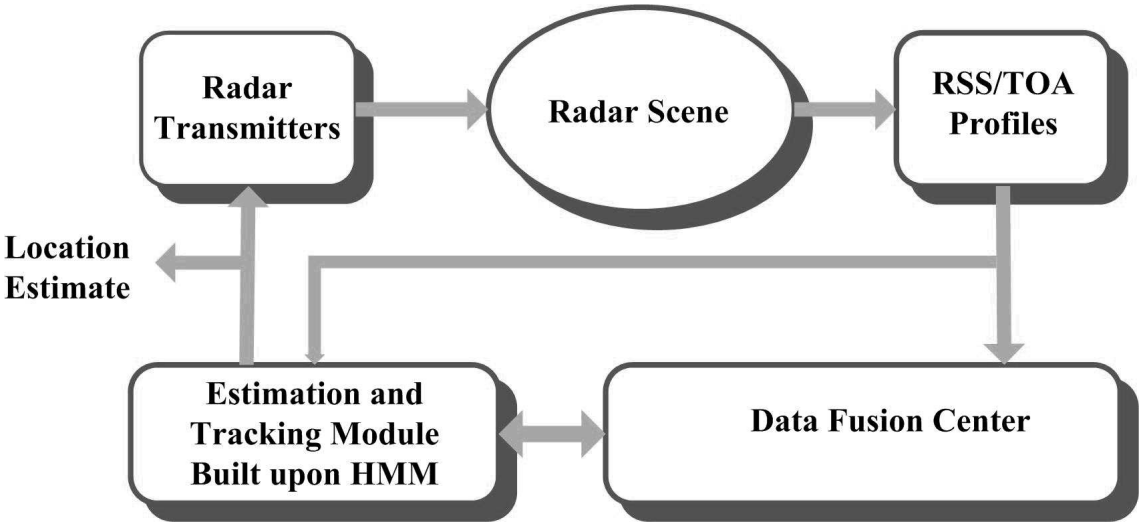

Figure 4.2: System architecture of the HMM-enabled CRN.

the object is located. We further assume that the target states in consecutive time instants are correlated.

A block diagram of the system architecture is illustrated in Fig. 4.2. Each *radar transmitter* probes the environment to obtain a *radar scene* by sending UWB waveforms. The signals reflected from the target are sampled and the *RSS/TOA profiles* are extracted, which are relayed to a central *data fusion center*. Subsequently, the data fusion center stores the measurements recorded by all radars and constructs a global RSS/TOA map. The global RSS/TOA map comprises the first arrived pulse of the backscatter signal at each radar unit as well as the corresponding TOA lag. It then identifies the nearest set of radars based upon this profile at the current time instant to facilitate triangulation of the object. The index of the nearest radar (or equivalently, the Voronoi region in which the target is located) is identified as the state of the target to establish the HMM. Next, the data fusion center forwards this information to the *estimation and tracking module*, which then estimates the required HMM parameters. This process is repeated until the convergence of the parameters is achieved. The estimation and tracking module then computes the target position, which is fed back to the data fusion center and is subsequently used for activating the appropriate group of radars in the vicinity of the object in the next time interval. This operation facilitates adaptive illumination of the radar scene and essentially leads to a CRN featuring the following two properties described in [34,35]: (i) intelligent signal processing, which builds on real-time learning through continuous interactions of the CRN with the surroundings; and (ii) feedback from the

receiver to the transmitter, which is a facilitator of intelligence.

We consider a monostatic radar configuration, where the transmitter and the receiver are collocated. The radar channel comprises a forward connection and a backward connection. The former describes signal propagation from the transmitter to the target, while the latter characterizes the target-to-receiver link. Each radar measures the RSS and TOA of the backscatter signal from the object. The method of least square is then applied for location estimation from the noisy set of measurements. To solve the multimodal optimization problem due to the nonlinearity of the relationship between RSS/TOA and target position, the Taylor-series expansion method is used to linearize the measurement model following the procedures in [108, 109]. It is worth noting that a radio frequency identification (RFID) tag could be attached to the object to enhance its radar cross section [37, 120, 121]. In this case, a radar unit also serves as a RFID reader, and the RFID tag could facilitate boosting of the backscatter signal (e.g., enhanced RSS, more recognizable target signature) from the target, potentially leading to improved localization accuracy.

It is assumed that each LOS path has been extracted through some preprocessing steps. For example, each radar may employ beam-steering [37, 122] and delay windowing [101] to suppress undesirable clutter interference. As a result, we focus on the direct path in the subsequent analysis. The TOA is equal to the round-trip propagation time $\tau = 2d/c$, where d is the one-way propagation distance and c is the speed of the electromagnetic wave. To account for the dependence of RSS on d, the received power can be expressed as [120]

$$P_{\mathrm{R}} = -10\alpha \log \tau + \varrho, \tag{4.1}$$

where α is the two way path loss exponent, and $\varrho = 10 \log P_{\mathrm{T}} + K$ is a constant that depends on the power P_{T} of the transmit antenna and a propagation constant K that depends on the indoor path loss model that we adopt. The value of $\alpha = 4.8$ and $K = -25$ dB is as shown in [123]. Thus (4.1) represents the log-normal shadowing and fast fading effect for the received signal power. The received signal could also be represented as where P_{T} represents the transmission power, and α denotes the one-way path loss exponent. The extension to noisy LOS data due to channel shadowing and fading, imperfect LOS acquisition, and measurement errors can be realized by modeling P_{R} and τ as log-normal random variables as discussed in the subsequent

analysis.

4.3 HMM for Target Tracking

4.3.1 Problem Formulation

All radars are assumed to be randomly distributed in the service area, which is divided into distinct Voronoi regions with each radar acting as the center. In the beginning, the target is supposed to be equiprobable anywhere in the region. As indicated in Fig. 4.1, the target makes random walks in the indoor environment. Hence, the transition from one location to another is governed by the following relationship

$$\mathbf{x}_{t+1} = \mathbf{x}_t + \nu_t. \tag{4.2}$$

In (4.2), $\mathbf{x}_{t+1}$ and $\mathbf{x}_t$ denote the position vectors at time instants $t+1$ and t, respectively. The term ν_t is a random perturbation at time t, which can be modeled using various perturbation distributions as described in [106]. In the current work, ν_t is assumed to follow a 2D Gaussian process. The following terms will be used henceforth to characterize the HMM.

- *Radar index* defines the unique identity number assigned to each radar in the CRN.
- *State* q_t defines the Voronoi region where the target belongs, and is the same as the index of the nearest radar at time t.
- *Position vector* $\mathbf{x}_t$ defines the target location in the Cartesian coordinates at time t.
- *Trajectory* $\mathbf{X}_T \triangleq (\mathbf{x}_1, \mathbf{x}_2, \cdots, \mathbf{x}_T)$ defines the sequence of position vectors from time $t = 1$ to $t = T$.
- *Observation sequence* $\mathbf{z}_t$ defines the sequence of quantized RSS levels observed at time t (see also Fig. 4.3). Note that in order to simplify the analysis and implementation, we only apply the RSS to establish the HMM. Nevertheless, both the RSS and TOA data could be utilized through a 2D quantization of the RSS-TOA space in Fig. 4.3.

- *Transition matrix* **A** defines the matrix of probabilities of transition between states.

- *Observation matrix* **B** defines the matrix of probabilities of observing each quantized RSS level given the state of the target.

- *Initial state probability vector* π defines the vector of probabilities of the initial state where the target belongs.

- *HMM parameter set* λ defines the set of **A** and **B**.

The main objective is to establish the HMM model π and λ, which describes the target trajectory in the environment. Once the model is developed, we can utilize it to address the following two problems.

- **Problem 1:** Given λ, estimating the most probable set of target locations in the next time instant.

- **Problem 2:** Optimizing λ by updating the parameters **A** and **B** at each time instant.

Subsequently, a scheme utilizing both the training and prediction phases for the HMM (see also the flowchart in Fig. 4.4) is developed. In the training phase, we construct the HMM model. In the prediction phase, we address the two problems mentioned above. A brief description of the Baum-Welch algorithm mentioned in [118] in order to re-estimate the HMM parameters like the state transition matrix A and the observation matrix B as a solution to Problem 2 is also presented. This is achieved by using the newly observed data and old values of A and B.

4.3.2 Training Phase

During the training stage when the HMM model is being built, all the radar components in the region are powered up to detect and locate the target by triangulation [108, 109]. The state or the physical location of the target is treated as an unknown (hidden) variable. The only observable part of the process is the backscatter signal from the target.

Initially, the target under monitoring is supposed to be equiprobable in any state. As the object changes from one state to another, its transitions are recorded during

the training phase. Based upon this learning process, the transition matrix $\mathbf{A}$ can be constructed. For developing the observation matrix $\mathbf{B}$, we discretize the RSS at the nearest radar into distinct levels as illustrated in Fig. 4.3. Each RSS level corresponds to a particular target-to-radar distance following (4.1). Subsequently, the relative frequency of each level can be calculated by applying the entire set of RSS samples associated with this specific Markov state (i.e., the index of the nearest radar), which yields the probability of observation of each quantized RSS level.

Let M be the total number of states or equivalently, the number of radars in the CRN; K be the number of quantized RSS levels; a_{mn} $(m, n \in \{1, 2, \cdots, M\})$ be the probability of transition from state m to state n, and b_{mk} $(m \in \{1, 2, \cdots, M\}$ and $k \in \{1, 2, \cdots, K\})$ be the probability of observing the kth RSS level when the target is in state m. The following relationships can be obtained:

$$a_{mn} = \frac{\text{Number of transitions from state } m \text{ to state } n}{\text{Total number of transitions from state } m},$$

$$b_{mk} = \frac{\text{Number of occurences of RSS level } k \text{ when target is in state } m}{\text{Total number of times when target is in state } m}.$$

The HMM model π and λ can thus be formulated as

$$\pi = \begin{pmatrix} \frac{1}{M} \\ \vdots \\ \frac{1}{M} \end{pmatrix}, \qquad \mathbf{A} = \begin{pmatrix} a_{11} & \cdots & a_{1M} \\ \vdots & \ddots & \vdots \\ a_{M1} & \cdots & a_{MM} \end{pmatrix}, \qquad \mathbf{B} = \begin{pmatrix} b_{11} & \cdots & b_{1K} \\ \vdots & \ddots & \vdots \\ b_{M1} & \cdots & b_{MK} \end{pmatrix}. \tag{4.3}$$

4.3.3 Prediction Phase

Once the HMM parameter set λ is derived, we can start utilizing the two matrices $\mathbf{A}$ and $\mathbf{B}$ to predict the most probable set of target locations and RSS measurements. Essentially, we attempt to solve both Problem 1 and Problem 2 during the prediction phase.

4.3.3.1 Solution to Problem 1

Let $\mathbf{Z}_T = (\mathbf{z}_1, \mathbf{z}_2, \cdots, \mathbf{z}_T)$ be the sequence of observations up to time T. The most straightforward way of finding $\Pr(\mathbf{Z}_T|\lambda)$, where $\Pr(\cdot)$ denotes probability, is through

identifying every possible state sequence of length T. Consider one such state sequence

$$\mathbf{Q}_T = (q_1, \cdots, q_T) \tag{4.4}$$

The probability of observing $\mathbf{Z}_T$, given $\mathbf{Q}_T$ and the HMM parameter set λ, can be stated as

$$\Pr(\mathbf{Z}_T|\mathbf{Q}_T, \lambda) = \prod_{t=1}^{T} \Pr(\mathbf{z}_t|q_t, \lambda) \tag{4.5}$$

where we have assumed statistical independence of observations. Next, the probability of the state sequence $\mathbf{Q}_T$ given λ can be written as

$$\Pr(\mathbf{Q}_T|\lambda) = \pi(q_1) \times \Pr(q_2|q_1) \times \Pr(q_3|q_2) \times \cdots \times \Pr(q_T|q_{T-1}) \tag{4.6}$$

where $\pi(q_1) = 1/M$ is the probability of the initial state. The joint probability of $\mathbf{Z}_T$ and $\mathbf{Q}_T$ is simply the product of (4.5) and (4.6)

$$\Pr(\mathbf{Z}_T, \mathbf{Q}_T|\lambda) = \Pr(\mathbf{Z}_T|\mathbf{Q}_T, \lambda) \times \Pr(\mathbf{Q}_T|\lambda). \tag{4.7}$$

The probability of $\mathbf{Z}_T$ given λ is obtained by summing this joint probability over all possible state sequences, yielding

$$\Pr(\mathbf{Z}_T|\lambda) = \sum_{\forall \mathbf{Q}_T} \Pr(\mathbf{Z}_T, \mathbf{Q}_T|\lambda) = \sum_{\forall \mathbf{Q}_T} \Pr(\mathbf{Z}_T|\mathbf{Q}_T, \lambda) \times \Pr(\mathbf{Q}_T|\lambda). \tag{4.8}$$

Substituting (4.5) and (4.6) into (4.8) for all possible $\mathbf{Q}_T$ gives the result of $\Pr(\mathbf{Z}_T|\lambda)$. The numerical values of all the terms in the righthand side of (4.8) can be obtained from their corresponding entries in the transition matrix $\mathbf{A}$ and the observation matrix $\mathbf{B}$. Given the sequence of states and the observations from the training phase, the observations that maximize the probability in (4.8) can be identified.

Due to large computational complexity and latency in state estimation, both the forward-backward and Viterbi algorithms are not suitable for real-time tracking. Therefore, there is a need to consider tracking as a forward-only process that estimates q_T based on all the measurements $\mathbf{Z}_T$ collected up to the Tth time instant. The mathematical representation of this approach can be found in [118] and will be applied here. Let the forward variable α_T be the joint probability of observation

sequence $\mathbf{Z}_T$ and state q_T at time T,

$$\alpha_T = \Pr(\mathbf{Z}_T, q_T|\lambda). \tag{4.9}$$

The observation probability $\Pr(\mathbf{Z}_T|\lambda)$ is the summation of α_T over all possible states, viz.,

$$\Pr(\mathbf{Z}_T|\lambda) = \sum_{m=1}^{M} \alpha_T(m) = \sum_{m=1}^{M} \Pr(\mathbf{Z}_T, q_T = m|\lambda) \tag{4.10}$$

where $\alpha_T(m)$ is the joint probability of $\mathbf{Z}_T$ and $q_T = m$. One possible optimality criteria is to choose the state that is individually most likely. To implement this solution, we define

$$\gamma_T(m) = \Pr(q_T = m|\mathbf{Z}_T, \lambda) \tag{4.11}$$

which is the probability of the target being in state m at time T, given the observation sequence $\mathbf{Z}_T$ and the HMM parameter set λ. Thus we can write (4.11) in the form of the forward variables $\alpha_T(m)$ as

$$\gamma_T(m) = \frac{\alpha_T(m)}{\Pr(\mathbf{Z}_T|\lambda)} = \frac{\alpha_T(m)}{\sum_{m=1}^{M} \alpha_T(m)}. \tag{4.12}$$

Using $\gamma_T(m)$, we can solve for the individually most likely state $\hat{m}$ at time T as

$$\hat{m} = \arg\max_{m} [\gamma_T(m)] \tag{4.13}$$

where m takes the values of $1, 2, \cdots, M$.

Subsequently, the most probable $\mathbf{z}_T$ and q_T at time T can be identified from (4.8) and (4.13) respectively, and with the help of $\mathbf{A}$ and $\mathbf{B}$. This depends on our knowledge of the trajectory until now through the sequence of states, $\mathbf{Q}_T$, which we assume to have since the prediction module follows the training phase and therefore we are aware of these parameters. Using (4.13) we can predict the most likely state $\hat{m}$ during the next time instant. The predicted future state and the observation matrix $\mathbf{B}$ can be utilized to find out the most probable RSS level. Finally, the target distance from the nearest radar in the next time instant can be predicted. Thus the current illumination strategy can be designed in accordance with this prediction to address Problem 1.

4.3.3.2 Solution to Problem 2

In this problem, we wish to optimize the parameters, **A** and **B** of the HMM model. Before each instance of reception, the HMM algorithm predicts the most probable target location and accordingly illuminates the target scene. Since we aim at optimizing the HMM parameters at every iteration, the error in prediction does not propagate. The approach towards optimization of λ was introduced in [118] and termed as the Baum-Welch algorithm. As shown in (4.11) and (4.12),

$$\gamma_T(m) = \Pr(q_T = m|\mathbf{Z}_T, \lambda) = \frac{\alpha_T(m)}{\sum_{m=1}^{M} \alpha_T(m)}. \tag{4.14}$$

We also define the quantity

$$\xi_{mn}(T) = \Pr(q_T = m, q_{T+1} = n|\mathbf{Z}_T, \lambda) \tag{4.15}$$

which is the probability of being in state m at time T and being in state n at time $T+1$. ξ_{mn} can also be expanded as

$$\xi_{mn}(T) = \frac{\Pr(q_T = m, q_{T+1} = n, \mathbf{Z}_T|\lambda)}{\Pr(\mathbf{Z}_T, \lambda)}. \tag{4.16}$$

Thus

$$\xi_{mn}(T) = \frac{\Pr(\mathbf{Z}_T, q_T = m|\lambda) a_{mn} \Pr(\mathbf{Z}_T, q_{T+1} = n|\lambda)}{\sum_{m=1}^{N} \sum_{n=1}^{N} \Pr(\mathbf{Z}_T, q_T = m|\lambda) a_{mn} \Pr(\mathbf{Z}_T, q_{T+1} = n|\lambda)}. \tag{4.17}$$

In order to estimate the new parameters for the HMM using the old parameters and the data, we can simplify the relative frequencies as follows

$$\tilde{\pi}_m = \gamma_1(m) \tag{4.18}$$

which is the expected relative frequency spent in state m at time $T = 1$. The updated transition probability

$$\tilde{a}_{mn} = \frac{\sum_{t=1}^{T} \xi_{mn}(t)}{\sum_{t=1}^{T} \gamma_t(m)} \tag{4.19}$$

which is the expected number of transitions from state m to state n relative to the expected total number of transitions from state m. This can be used to update the

transition matrix $\mathbf{A}$. The updated observation probability

$$\tilde{b}_{mk} = \frac{\sum_{t=1}^{T} \delta_{v_k} \gamma_t(m)}{\sum_{t=1}^{T} \gamma_t(m)} \tag{4.20}$$

where δ_{v_k} is the number of times the output observations have been equal to RSS level v_k. $\tilde{b}_{mk}$ can be used to update the observation matrix $\mathbf{B}$. The detailed procedure to implement the aforementioned re-estimation process is presented in [118].

The matrix $\mathbf{A}$ is largely sparse due to the comparatively slow target motion in indoor environments (i.e., each random-walk step is much smaller than the inter-radar distances). In realistic scenarios, only partial prior knowledge of λ is available. A training procedure has to be implemented for optimally adapting λ to some observed data $\mathbf{Z}_T$ of length T in practical systems. We can analytically derive the maximum likelihood estimate $\hat{\lambda} = \arg\max_{\lambda} \Pr(\mathbf{Z}_T|\lambda)$ through the Baum-Welch algorithm [118]. It involves an expectation-maximization (EM) process that, starting from an estimate λ_{j-1} at iteration $j-1$, evaluates the posterior probabilities of the state transition, given the observation sequence $\mathbf{Z}_T$. These posterior probabilities acquired by assuming $\hat{\lambda} = \lambda_{j-1}$ are then used to re-estimate the HMM parameters by approximating the probabilities constrained in λ in terms of the expected frequencies of state transitions. The new parameter set λ_j is defined such that

$$\Pr(\mathbf{Z}_T|\lambda_j) \geq \Pr(\mathbf{Z}_T|\lambda_{j-1}).$$

The process terminates when the convergence is reached or some limiting criteria are met. Global convergence is not guaranteed since this is a local algorithm and the solution quality depends on the selected initial parameters [118].

4.3.4 Summary

The strategy for tracking is illustrated as a flowchart in Fig. 4.4, which is summarized below.

- *Training Phase*
  - All the radar components in the CRN are powered up to detect the presence and location of the target.
  - The RSS/TOA profile is extracted from the reflected signal at each radar

and is sent to the central data fusion center.

  - The data fusion center identifies the set of four radars closest to the object (which include the nearest one indicating the "state" of the target location) from the gathered RSS/TOA profiles.
  - The set of four nearest radars are used to triangulate the position of the target by applying the methods of least square and Taylor series expansion [108, 109]. This information is used to build the HMM.
  - The preceding steps are repeated until the convergence of the HMM parameters is achieved.

- *Prediction Phase*

  - Once the training phase is completed, the system makes predictions about the future target location and the corresponding set of radars in the vicinity. This prior knowledge of the nearest radars facilitates stimulation of only those nearby radars in the next time instant.
  - Based on the values of $\mathbf{A}$ and $\mathbf{B}$ estimated during the training phase, four nearest radars are deduced by the data fusion center. The four radar units collect the first arrived backscatter signal as shown in the RSS/TOA profile in Fig. 4.3.
  - The data fusion center then detects the presence of the target by comparing the RSS values with a pre-specified threshold, and triangulates its position based on the RSS/TOA profiles, which are collected from the radars activated in the previous step. Any error in estimation of the target state is identified by the fusion center based upon the latest RSS/TOA profiles and is used to update the transition matrix and the observation matrix in the HMM. The process of estimating the nearest four radars is also repeated. In this way adaptability is incorporated in the CRN.

During the entire tracking process, the overall power transmitted by the CRN to probe the surroundings is fixed and equally parceled out to the activated radars. In the next section, we will evaluate the Cramer-Rao Lower Bound (CRLB) on the estimation of the target position using the RSS/TOA profiles and analyze the

convergence of the proposed HMM algorithm. Other works like [124] and [125] have derived the CRLB on RSS/TOA measurements. We use a similar approach to establish the CRLB for our case to gauge the RMSE performance of the HMM and other tracking algorithms.

4.4 Theoretical Analysis

4.4.1 CRLB on Location Error

At an arbitrary time instant, let us define the observed RSS/TOA profile $\mathbf{\Theta}$ to be

$$\mathbf{\Theta} = (\tau_1, \tau_2, \tau_3, \cdots, \tau_M, P_1, P_2, P_3, \cdots, P_M) \tag{4.21}$$

where τ_m and P_m $(m = 1, 2, \cdots, M)$ are the TOA and RSS of the backscatter signals at the mth radar.

Define the actual location of the target in the Cartesian coordinates as $\psi_0 = (x_0, y_0)$. The positioning problem then consists of finding an estimate of ψ_0, $\hat{\psi}_0$, given the vector of the radar locations $\mathbf{\Psi} = [\Psi_1, \cdots, \Psi_M]$, where $\Psi_m = (x_m, y_m)$ $(m = 1, 2, \cdots, M)$ gives the Cartesian coordinates of the mth radar. To obtain a lower bound on the estimation error, we assume that the TOA and RSS measurements are independent. This is because correlation in measured data usually reduces the degrees of freedom and thus increases the positioning error. Furthermore, the pdf of TOAs is assumed to follow $\tau_m \sim \mathcal{N}(2d_m/c, \sigma_\tau^2)$, where $\mathcal{N}$ indicates the normal distribution, d_m is the distance between the mth radar and the target, c is the speed of the electromagnetic wave, and σ_τ is the parameter describing the joint nuisance of the channel estimation and measurement errors. The RSSs are supposed to be lognormal random variables with $P_m \sim \mathcal{N}(P_{\mathrm{R},m}(\mathrm{dB}), \sigma_P^2)$, where $P_{\mathrm{R},m}(\mathrm{dB}) = P_0(\mathrm{dB}) - 20\alpha \log_{10}(d_m) + 20\alpha \log_{10} d_0$ following (4.1) and σ_P is the standard deviation of lognormal shadowing.

The CRLB of an unbiased estimator $\hat{\psi}_0$ is given by the inverse of the Fisher information matrix (FIM), which has the form

$$\begin{aligned} \mathfrak{I}(\psi_0) &= -\mathbb{E}\left\{\nabla_{\psi_0}\left(\nabla_{\psi_0}\mathcal{L}\left(\mathbf{\Theta}|\psi_0, \mathbf{\Psi}\right)\right)\right\} \\ &= \begin{pmatrix} \mathfrak{I}_{xx} & \mathfrak{I}_{xy} \\ \mathfrak{I}_{xy} & \mathfrak{I}_{yy} \end{pmatrix} \end{aligned} \tag{4.22}$$

where ∇_{ψ_0} denotes the derivative with respect to ψ_0, $\mathbb{E}\{\cdot\}$ is the expectation operator, and $\mathcal{L}(\boldsymbol{\Theta}|\psi_0, \boldsymbol{\Psi})$ is the logarithm of the conditional pdf

$$\mathcal{L}(\boldsymbol{\Theta}|\psi_0, \boldsymbol{\Psi}) = \sum_{m=1}^{M} \ln\left[f_{\tau_m|\psi_0,\Psi_m}(\tau_m|\psi_0, \Psi_m)\right] + \sum_{m=1}^{M} \ln\left[f_{P_m|\psi_0,\Psi_m}(P_m|\psi_0, \Psi_m)\right]. \tag{4.23}$$

Subsequently, $\mathcal{I}_{xx}$ is derived as

$$\mathcal{I}_{xx} = -\sum_{m=1}^{M} \mathbb{E}\left\{\frac{\partial^2}{\partial x_0^2} \ln\left[f_{\tau_m|\psi_0,\Psi_m}(\tau_m|\psi_0, \Psi_m)\right]\right\} - \sum_{m=1}^{M} \mathbb{E}\left\{\frac{\partial^2}{\partial x_0^2} \ln\left[f_{P_m|\psi_0,\Psi_m}(P_m|\psi_0, \Psi_m)\right]\right\}. \tag{4.24}$$

The other two terms $\mathcal{I}_{xy}$ and $\mathcal{I}_{yy}$ can be similarly computed. Subsequently, the CRLB on the variance of the RSS/TOA location estimation is given by

$$\sigma_{\psi_0}^2 = \frac{\mathcal{I}_{xx} + \mathcal{I}_{yy}}{\mathcal{I}_{xx}\mathcal{I}_{yy} - \mathcal{I}_{xy}^2}. \tag{4.25}$$

A detailed derivation of the CRLB can be found in [125].

Following [125], the FIM for our case can be expressed as

$$\mathcal{I}(\psi_0) = \begin{pmatrix} \frac{1}{c^2\sigma_\tau^2}\sum_{m=1}^{M}\frac{(x_0-x_m)^2}{d_m^2} + \Upsilon\sum_{m=1}^{M}\frac{(x_0-x_m)^2}{d_m^4} & \frac{1}{c^2\sigma_\tau^2}\sum_{m=1}^{M}\frac{(x_0-x_m)(y_0-y_m)}{d_m^2} + \Upsilon\sum_{m=1}^{M}\frac{(x_0-x_m)(y_0-y_m)}{d_m^4} \\ \frac{1}{c^2\sigma_\tau^2}\sum_{m=1}^{M}\frac{(x_0-x_m)(y_0-y_m)}{d_m^2} + \Upsilon\sum_{m=1}^{M}\frac{(x_0-x_m)(y_0-y_m)}{d_m^4} & \frac{1}{c^2\sigma_\tau^2}\sum_{m=1}^{M}\frac{(y_0-y_m)^2}{d_m^2} + \Upsilon\sum_{m=1}^{M}\frac{(y_0-y_m)^2}{d_m^4} \end{pmatrix} \tag{4.26}$$

where $\Upsilon = \left(\frac{20\alpha}{\sigma_P \ln 10}\right)^2$. Using (4.24) and (4.25), $\sigma_{\psi_0}^2$ can be determined. It is worth noting that the CRLB is proportional to the factor Υ linked to RSS measurements and also proportional to $1/(c^2\sigma_\tau^2)$ linked to TOA measurements. The CRLB also depends upon the number of the radars, M.

4.4.2 Convergence of the HMM Algorithm

The HMM parameters **A** and **B** can be optimized using the Baum-Welsh algorithm or the EM algorithm as stated in [118]. Each iteration of the EM algorithm consists of two stages: the expectation step (E-step) and the maximization step (M-step). In the E-step, the missing data are estimated given the observed data and the current

estimate of the model parameters. This is achieved using the expectation. In the M-step, the likelihood function is maximized under the assumption that the missing data are known. The results acquired from the E-step are used in lieu of the actual missing data.

Let $\mathbf{Z}$ be the sequence of RSS observations at an arbitrary time. In order to estimate the parameter set λ representing $\mathbf{A}$ and $\mathbf{B}$, it is typical to introduce the log-likelihood function defined as

$$\mathcal{L}(\lambda) = \ln\left[\Pr(\mathbf{Z}|\lambda)\right]. \tag{4.27}$$

Since $\ln(\cdot)$ is a strictly increasing function, the value of λ that maximizes $\Pr(\mathbf{Z}|\lambda)$ also maximizes $\mathcal{L}(\lambda)$. The EM algorithm is an iterative procedure for maximizing $\mathcal{L}(\lambda)$. Assume that after the $(j-1)$th iteration the current estimate for λ is given by λ_{j-1}. Since the objective is to maximize $\mathcal{L}(\lambda)$, we wish to compute an updated estimate λ_j such that,

$$\mathcal{L}(\lambda_j) \geq \mathcal{L}(\lambda_{j-1}). \tag{4.28}$$

By determining the conditional expectation of the unobserved likely states q (which are the missing data) and maximizing it with respect to λ, the local convergence is guaranteed as it increases the likelihood at each iteration. A detailed discussion on the convergence properties of the EM algorithm is presented in [126]. For the sake of completeness, we provide a brief analysis of the convergence of the algorithm in the current context of target tracking.

We aim at maximizing the difference as indicated in (4.27),

$$\mathcal{L}(\lambda_j) - \mathcal{L}(\lambda_{j-1}) = \ln\left[\Pr(\mathbf{Z}|\lambda_j)\right] - \ln\left[\Pr(\mathbf{Z}|\lambda_{j-1})\right]. \tag{4.29}$$

Denote the likely state of the moving target as q, which corresponds to the Voronoi region where the target is located, as shown in Fig. 4.1. q is considered to be the hidden or unobserved variable in both the HMM and EM algorithm setting.

Subsequently, we have

$$\begin{aligned}
\mathcal{L}(\lambda_j) - \mathcal{L}(\lambda_{j-1}) &\overset{\langle 1 \rangle}{=} \ln\left[\sum_q \Pr(\mathbf{Z}|q,\lambda_j)\Pr(q|\lambda_j)\right] - \ln\left[\Pr(\mathbf{Z}|\lambda_{j-1})\right] \\
&= \ln\left[\sum_q \Pr(q|\mathbf{Z},\lambda_{j-1})\frac{\Pr(\mathbf{Z}|q,\lambda_j)\Pr(q|\lambda_j)}{\Pr(q|\mathbf{Z},\lambda_{j-1})}\right] - \ln\left[\Pr(\mathbf{Z}|\lambda_{j-1})\right] \\
&\overset{\langle 2 \rangle}{\geq} \sum_q \Pr(q|\mathbf{Z},\lambda_{j-1}) \ln\left[\frac{\Pr(\mathbf{Z}|q,\lambda_j)\Pr(q|\lambda_j)}{\Pr(q|\mathbf{Z},\lambda_{j-1})}\right] - \ln\left[\Pr(\mathbf{Z}|\lambda_{j-1})\right] \\
&= \sum_q \Pr(q|\mathbf{Z},\lambda_{j-1}) \ln\left[\frac{\Pr(\mathbf{Z}|q,\lambda_j)\Pr(q|\lambda_j)}{\Pr(q|\mathbf{Z},\lambda_{j-1})\Pr(\mathbf{Z}|\lambda_{j-1})}\right] \\
&\triangleq \Delta_{j,j-1}
\end{aligned} \tag{4.30}$$

where $\langle 1 \rangle$ follows the relationship that $\Pr(\mathbf{Z}|\lambda_j) = \sum_q \Pr(\mathbf{Z}|q,\lambda_j)\Pr(q|\lambda_j)$ and $\langle 2 \rangle$ applies the Jensen's inequality for the concave $\ln(\cdot)$ function.

It can be easily shown that if the estimated parameter at the jth iteration, $\hat{\lambda}_j$, maximizes $\Delta_{j,j-1}$ in (4.30), it also maximizes the following function

$$\mathbb{E}_{q|\mathbf{Z},\lambda_{j-1}}\left\{\ln\left[\Pr(\mathbf{Z},q|\lambda_j)\right]\right\} = \sum_q \Pr\left(q|\mathbf{Z},\lambda_{j-1}\right)\ln\left[\Pr(\mathbf{Z},q|\lambda_j)\right]. \tag{4.31}$$

This essentially corresponds to the expectation and maximization steps in the EM algorithm. Apparently, $\Delta_{j,j-1} = 0$ for $\lambda_j = \lambda_{j-1}$. Furthermore, $\hat{\lambda}_j$ is chosen such that $\Delta_{j,j-1}$ is maximized and thus is no less than 0. Consequently, for each iteration the likelihood $\mathcal{L}(\lambda_j)$ is non-decreasing following (4.30). More detailed discussions on the convergence behavior of the EM algorithm can be found in [126].

4.5 Numerical Examples

In this section we compare the performance of the proposed HMM algorithm to the benchmark EKF and MLE schemes for detection and tracking of a target.

4.5.1 EKF and MLE Algorithms

The use of the Kalman filter to assist in tracking targets has been proposed in [117] and [127], where the TOA ranging technique is applied in conjunction with a modified Kalman algorithm to track Universal Mobile Telecommunications System

(UMTS) mobiles in non-line-of-sight conditions. It is assumed that the measurement process is Gaussian, which is characterized by a mean (i.e., the actual position) and by a covariance (i.e., the measurement or projection uncertainties). A further assumption is that, in the Cartesian coordinate system, the positioning error along the x-axis is independent of the error along the y-axis.

On the other hand, the MLE attempts to maximize the likelihood function $\Pr(\boldsymbol{\Theta}|\psi_0)$ at an arbitrary time instant [106], where ψ_0 is the target location and $\boldsymbol{\Theta}$ is the observed RSS/TOA profiles as mentioned previously. Assuming independent observations at different radars, the MLE can be expressed as

$$\hat{\psi}_0 = \arg\max_{\psi_0} \Pr(\boldsymbol{\Theta}|\psi_0) = \arg\max_{\psi_0} \prod_{m=1}^{M} \Pr(\boldsymbol{\Theta}_m|\psi_0). \tag{4.32}$$

The parameter M indicates the total number of radars and $\boldsymbol{\Theta}_m = (\tau_m, P_m)$ is the RSS/TOA profile recorded at the mth radar. For simualtion purposes we adopt a similar approach for MLE as mentioned in [128].

4.5.2 Application of EKF Algorithm to Target Tracking

We adopt a similar approach to the design of EKF tracking algorithm as stated in [129,130]. For simulation purposes we model the state of the EKF by incorporating the position and the velocity of the moving target. In 2D space, the RSS/TOA profile generated by the moving object can be used to obtain the distance from the radar units, which can be expressed as

$$d_m = \sqrt{(x_0 - x_m)^2 + (y_0 - y_m)^2} \tag{4.33}$$

where x_m and y_m $(m = 1, ..., M)$ are the coordinates of the mth fixed radar units and (x_0, y_0) are the coordinates of the target. One way of modeling motion is by setting up a linear system composed of the kinematic equations for each dimension of the tracked movement. Thus the following expression represents an object's 2D motion using the position and velocity at time step T, and corresponds to the current state

$\mathbf{X}_T$ in the EKF formulation

$$\mathbf{X}_T = \begin{pmatrix} x_{0,T} \\ y_{0,T} \\ \dot{x}_{0,T} \\ \dot{y}_{0,T} \end{pmatrix} = \mathbf{C} \cdot \begin{pmatrix} x_{0,T-1} \\ y_{0,T-1} \\ \dot{x}_{0,T-1} \\ \dot{y}_{0,T-1} \end{pmatrix} + \mathbf{E} \tag{4.34}$$

where $\dot{x}_{0,T}$ and $\dot{y}_{0,T}$ are the velocities in the X and Y directions, $\mathbf{C}$ is the state transition matrix for the EKF, and $\mathbf{E}$ is the process noise vector accounting for any unmodeled factors of the system. At time step T, let $\tilde{d}_{m,T}$ $(m = 1, .., M)$ be the distance measurement errors. The measured distances are given by

$$\begin{aligned} d_{1,T} &= \sqrt{(x_{0,T} - x_1)^2 + (y_{0,T} - y_1)^2} + \tilde{d}_{1,T} \\ d_{2,T} &= \sqrt{(x_{0,T} - x_2)^2 + (y_{0,T} - y_2)^2} + \tilde{d}_{2,T} \\ &\vdots \\ d_{M,T} &= \sqrt{(x_{0,T} - x_M)^2 + (y_{0,T} - y_M)^2} + \tilde{d}_{M,T}. \end{aligned} \tag{4.35}$$

The above set of equations can also be written as

$$\begin{pmatrix} d_{1,T} \\ d_{2,T} \\ \vdots \\ d_{M,T} \end{pmatrix} = \mathbf{S} \cdot \begin{pmatrix} x_{0,T} \\ y_{0,T} \\ \dot{x}_{0,T} \\ \dot{y}_{0,T} \end{pmatrix} + \begin{pmatrix} \tilde{d}_{1,T} \\ \tilde{d}_{2,T} \\ \vdots \\ \tilde{d}_{M,T} \end{pmatrix}. \tag{4.36}$$

Where $\mathbf{S}$ is the measurement matrix that relates the current state to the output. Since the output equations (4.35) are nonlinear, the Jacobian should be used [129, 130]. Hence,

$$\mathbf{S} = \begin{pmatrix} \frac{\partial d_1}{\partial x} & \frac{\partial d_1}{\partial y} & 0 & 0 \\ \frac{\partial d_2}{\partial x} & \frac{\partial d_2}{\partial y} & 0 & 0 \\ \vdots & \vdots & \vdots & \vdots \\ \frac{\partial d_M}{\partial x} & \frac{\partial d_M}{\partial y} & 0 & 0 \end{pmatrix} \tag{4.37}$$

where $\frac{\partial d_m}{\partial x} = \frac{x_0 - x_m}{\sqrt{(x_0 - x_m)^2 + (y_0 - y_m)^2}}$ and $\frac{\partial d_m}{\partial y} = \frac{y_0 - y_m}{\sqrt{(x_0 - x_m)^2 + (y_0 - y_m)^2}}$ $(m = 1, 2, \cdots, M)$.

Subsequently, the following procedures can be applied iteratively to track the moving object. In each iteration, five steps are performed as listed below [129, 130].

1. Project the state ahead: $\mathbf{X}_T^- = \mathbf{C} \cdot \mathbf{X}_{T-1}$;

2. Project the error covariance ahead: $\mathbf{W}_T^- = \mathbf{C} \cdot \mathbf{W}_{T-1} \cdot \mathbf{C}^T + \mathbf{\Omega}$;

3. Evaluate the Kalman gain: $\mathbf{K}_T = \mathbf{W}_T^- \cdot \mathbf{S}^T \cdot \left(\mathbf{S} \cdot \mathbf{W}_T^- \cdot \mathbf{S}^T + \mathbf{R}\right)^{-1}$;

4. Update estimation with measurements: $\mathbf{X}_T = \mathbf{X}_T^- + \mathbf{K}_T \cdot \left(\mathbf{D}_T - \mathbf{S} \cdot \mathbf{X}_T^-\right)$;

5. Update the error covariance: $\mathbf{W}_T = (\mathbf{I} - \mathbf{K}_T \cdot \mathbf{S}) \cdot \mathbf{W}_T^-$.

In Step 1, the current state $\mathbf{X}_{T-1}$ is used to estimate the location at the next time instant. The error covariance matrix $\mathbf{W}_T^-$ in the next time step is projected using the state space model $\mathbf{C}$ and the process noise covariance matrix $\mathbf{\Omega}$ in Step 2, where $(\cdot)^T$ denotes the matrix transpose. In Step 3, the Kalman gain $\mathbf{K}_T$ is computed, where $\mathbf{R}$ is a diagonal matrix representing the independent distance measurement noises at different radars. The Kalman gain is used in Step 4, when the distance measurements $\mathbf{D}_T = [d_{1,T}, d_{2,T}, \cdots, d_{M,T}]^T$ from the radars to the target are employed to update the state, $\mathbf{X}_T$. In Step 5, the error covariance matrix $\mathbf{W}_T$ is updated. The current position $(x_{0,T}, y_{0,T})$ is readily available from the state $\mathbf{X}_T$.

In the simulation study of the EKF algorithm presented previously, the same area under surveillance of dimensions 30 m $\times$ 30 m was chosen with the same distribution of radar units as illustrated in Fig. 4.1. The sampling time or the time step was chosen to be 1 ms. The step size standard deviation of the target trajectory was set to be $\sigma_\nu = 50$ cm. The process noise covariance matrix $\mathbf{\Omega}$, the state space model $\mathbf{C}$, and the measurement noise matrix $\mathbf{R}$ were assumed to be

$$\mathbf{\Omega} = \begin{pmatrix} 400\ \text{cm}^2 & 0 & 0 & 0 \\ 0 & 400\ \text{cm}^2 & 0 & 0 \\ 0 & 0 & 100\ \text{cm}^2/\text{s}^2 & 0 \\ 0 & 0 & 0 & 100\ \text{cm}^2/\text{s}^2 \end{pmatrix},$$

$$\mathbf{C} = \begin{pmatrix} 1 & 0 & 1\ \text{ms} & 0 \\ 0 & 1 & 0 & 1\ \text{ms} \\ 0 & 0 & 1 & 0 \\ 0 & 0 & 0 & 1 \end{pmatrix},$$

$$\mathbf{R} = \begin{pmatrix} 10\ \text{cm} & \cdots & 0 \\ \vdots & \ddots & \vdots \\ 0 & \cdots & 10\ \text{cm} \end{pmatrix}.$$

Table 4.2: Simulation Setup: Radar Positions

Radar index	x **position (m)**	y **position (m)**
Radar 1	−7.239	11.15
Radar 2	−4.593	8.387
Radar 3	−8.158	5.565
Radar 4	−13.21	3.367
Radar 5	−6.78	3.328
Radar 6	3.636	−3.874
Radar 7	13.96	−5.094
Radar 8	−3.42	−9.268
Radar 9	−5.455	−11.52
Radar 10	8.237	−12.43

4.5.3 Simulation Results

Simulations have been carried out to evaluate the performance of the HMM algorithm with regards to the probability of detection, the RMSE for target tracking, and the CRLB on RSS/TOA localization. The probing radar waveforms are Gaussian monocycles with a central frequency of 4 GHz at a bandwidth of 700 MHz and the sampling frequency used is 10 GHz. The acquisition time for RSS/TOA acquisition is set to be 0.01 ms. The layout of the CRN under consideration is illustrated in Fig. 4.1, where 10 radar units are normally distributed in a 30 m $\times$ 30 m region. The observation space of RSS levels has been fixed for simulation purposes and has a value of $K = 6$. The target makes random walks in the service area, where each step follows a normal distribution with a standard deviation of 50 cm. The sampling time for RSS/TOA acquisition has been selected to be small enough to cater to the target movement. Finally, the one-way path loss exponent is chosen to be $\alpha = 2.4$ following the value suggested in [131]. We assume that the radar units operate asynchronously. In the case of a synchronous operation of different radars, various orthogonal maximum length UWB sequences (see e.g., [132]) can be employed to handle the interference rather than using a single pulse at distinct radars. The radar positions for the simulation setup are as shown in Table 4.2 and Fig. 4.1. The simulations are carried out by fixing the number and positions of the radar units and varying the target trajectory.

Once the training phase is completed and the HMM model is constructed, subsequent locations of the target are estimated using the proposed HMM algorithm as well as the benchmark EKF and MLE algorithms. The probability of detection is evaluated for various Signal to Noise Ratio (SNR) values ranging from 5 dB to

20 dB. In the HMM algorithm, only the radar units in the vicinity of the target are activated, which is based upon prediction of the nearest radar. For the EKF and MLE algorithms all the radar units are powered up. Based upon the target position estimates made by the three tracking algorithms, the received signal is estimated and a hypothesis testing approach is used to compare the signal amplitude with a pre-specified threshold value for detecting the presence of the target. This threshold is determined by fixing the probability of false alarm at $P_{fa} = 0.0001$. Following the Neyman-Pearson algorithm [2], we can calculate the threshold value to be $\varepsilon = \sqrt{n\sigma^2}Q^{-1}(P_{fa})$, where σ^2 is the variance of the normalized received signal amplitude, n is the number of samples, and Q is the complementary error function. If we assume that the noise floor $\sigma^2 = 0.01$, then the threshold translates into the value of 0.3 V for a single normalized signal sample. To combine the binary decisions made at different radars about the presence or absence of a target, the majority rule is adopted. Fig. 4.5 is a result of averaging over 100 simulations each at a particular SNR value. It demonstrates that as the SNR increases, the probability of target detection is improved. In the case of the HMM algorithm, the probability of detection is superior since only the nearby radar units are activated, thus avoiding the noise contributions of distant radar components.

The RMSE of the target location is evaluated in Fig. 4.6(a). At each random-walk step, the error in the location estimation is calculated. It can be seen that the EKF and MLE algorithms achieve better target localization accuracy. This is due to the fact that the EKF and MLE algorithms have superior degrees of freedom in terms of the activated radar units. The parameters of the proposed HMM algorithm have to be estimated at each step simultaneously with the location of the target, which affects its RMSE performance. Nevertheless, as the random-walk step increases, the achievable accuracy for all the three algorithms is similar and less than 1 m, which is acceptable for indoor positioning applications as indicated in [133].

We evaluate the CRLB for the RSS/TOA based localization using (4.24) and (4.25), which serves as a benchmark for comparison of the RMSE accuracy of the tracking algorithms under consideration. In the current work, the data fusion center selects the set of four nearest radar units for target localization. Hence, we consider four radars placed at the following four locations: $(-10\text{ m}, -10\text{ m})$, $(10\text{ m}, -10\text{ m})$, $(-10\text{ m}, 10\text{ m})$, and $(10\text{ m}, 10\text{ m})$, which synthesizes the scenario that a set of close-by radars are activated for target positioning. As shown in Fig. 4.6(b), at

Table 4.3: Execution Times for Various Tracking Algorithms

Tracking algorithm	**Probability of detection > 0.9**			**RMSE < 0.3** m		
	$\sigma_\nu = 10$ cm	$\sigma_\nu = 20$ cm	$\sigma_\nu = 50$ cm	$\sigma_\nu = 10$ cm	$\sigma_\nu = 20$ cm	$\sigma_\nu = 50$ cm
MLE	220 ms	240 ms	310 ms	200 ms	275 ms	325 ms
EKF	337 ms	350 ms	376 ms	309 ms	329 ms	345 ms
HMM	105 ms	127 ms	157 ms	308 ms	335 ms	357 ms

the central locations the maximum achievable accuracy is around 0.019 m, and the CRLB reduces as the target moves towards one of the radar units.

Table 4.3 indicates the execution times for the three tracking algorithms under consideration. The radar units are activated every 1 ms and the probability of successful target detection is evaluated over an epoch of 50 such activations. The simulation is repeated for various values of σ_ν, which is the standard deviation defining the step size of the 2D motion of the target. The time demanded to achieve a probability of detection greater than 0.9 for each of the tracking techniques is evaluated over subsequent epochs. The HMM method displays the fastest detection of the target due to its ability to spatially discretize the area under surveillance. A similar analysis is carried out with respect to the execution time required to achieve a RMSE < 0.3 m. In this case, the performance for the three algorithms is similar particularly at larger σ_ν, though the HMM algorithm requires slightly longer execution times as compared to the EKF and MLE approaches.

Finally, we study the performance of the three techniques if only the nearest set of radar units are activated for all the algorithms. Specifically, we look into the influence of standard deviation of the step size σ_ν on the RMSE, where σ_ν is resolved into two components, σ_{ν_x} and σ_{ν_y} along the X and Y directions, respectively. As shown in Fig. 4.7, the HMM yields the least RMSE for higher values of σ_ν as compared to the EKF and MLE when all the algorithms have the same degrees of freedom in terms of the activated radars. Furthermore, the performance of the EKF and MLE for target position estimation is sensitive to the increase in the step size. In other words, they are suboptimal for tracking rapid target movements. The HMM algorithm on the other hand gains advantage from the spatial discretization of the area under surveillance and hence, its performance will not be affected even if there is an increase in the target velocity. These observations justify the use of the HMM algorithm over the other two techniques for tracking fast target movements, and also prove that intelligent illumination of the target scene alone is necessary but

not sufficient for achieving an enhanced RMSE performance.

Fig. 4.8 gives an illustrative example for the initialization of **A** and **B** as well as their values after the training phase is completed. This example corresponds to an arbitrary five-state HMM with six RSS levels of observation. As shown in Fig. 4.8, the state transition matrix **A** is initialized with all states being equiprobable and the observation matrix **B** is initialized with all observation levels being equiprobable for each state. After achieving the convergence of **A** and **B**, each current state is most likely to remain in the same state in the next time instant.

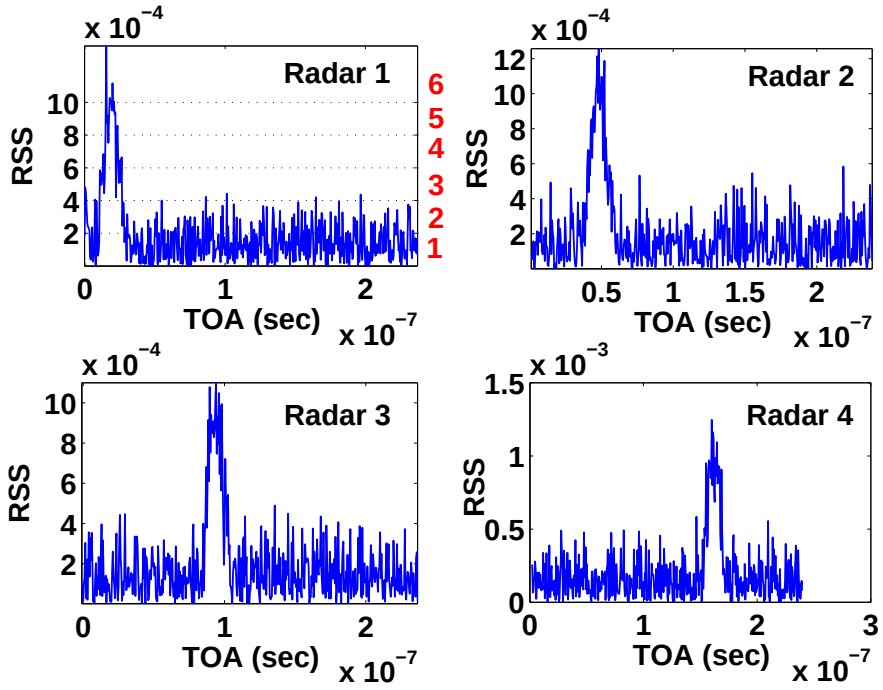

Figure 4.3: Typical RSS/TOA profiles received at 4 radars. RSS at Radar 1 (the nearest radar) is quantized into 5 levels. Each level corresponds to a particular distance from Radar 1 following (4.1). The quantized level corresponding to the highest RSS is selected.

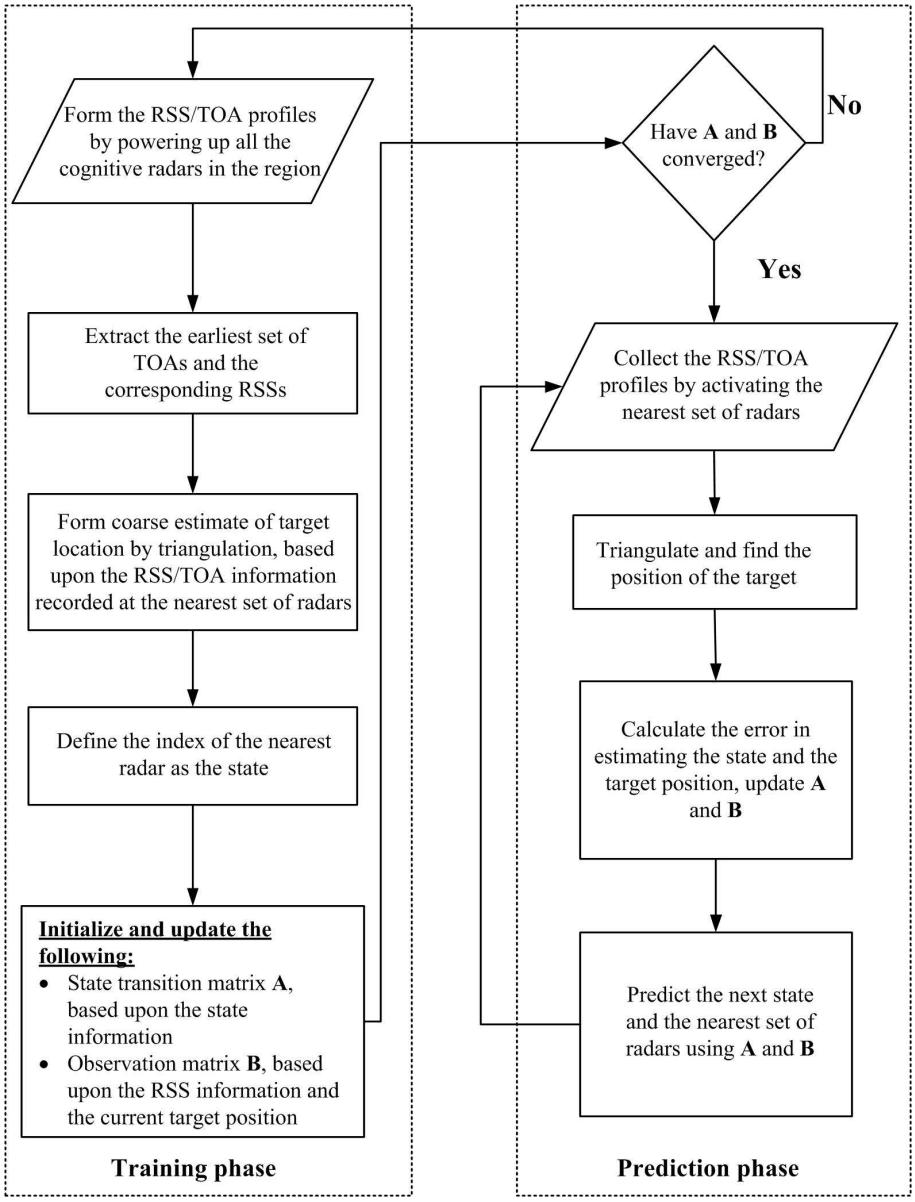

Figure 4.4: Flowchart for the HMM-based target tracking algorithm.

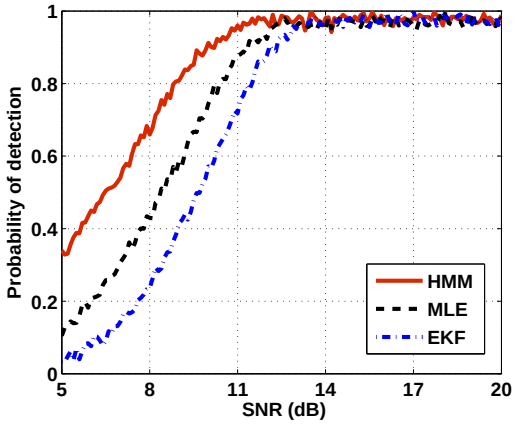

Figure 4.5: Probability of detection for various target tracking algorithms.

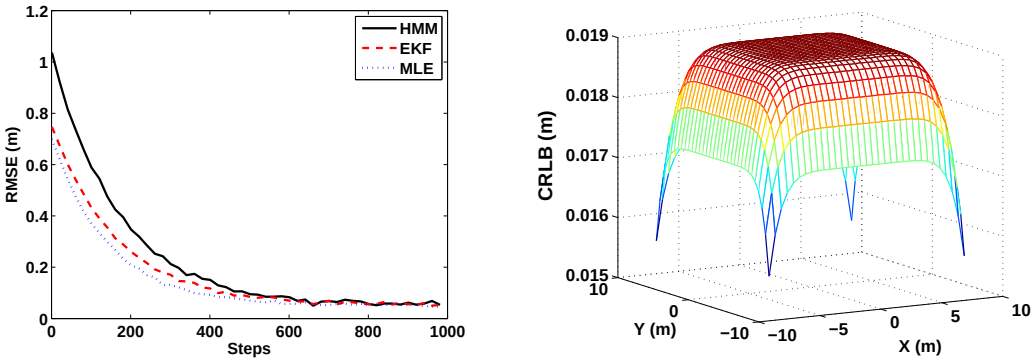

(a) (b)

Figure 4.6: (a) Location estimation errors for various target tracking algorithms, (b) CRLB on RSS/TOA localization

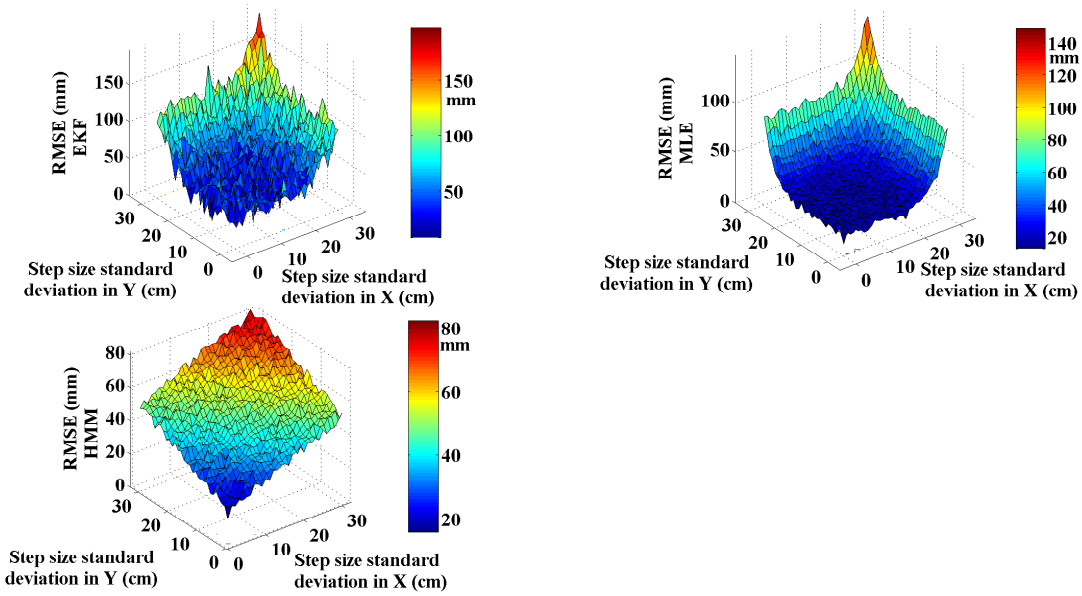

Figure 4.7: RMSE performance of the 3 tracking algorithms with respect to varying values of σ_{ν_x} and σ_{ν_y}.

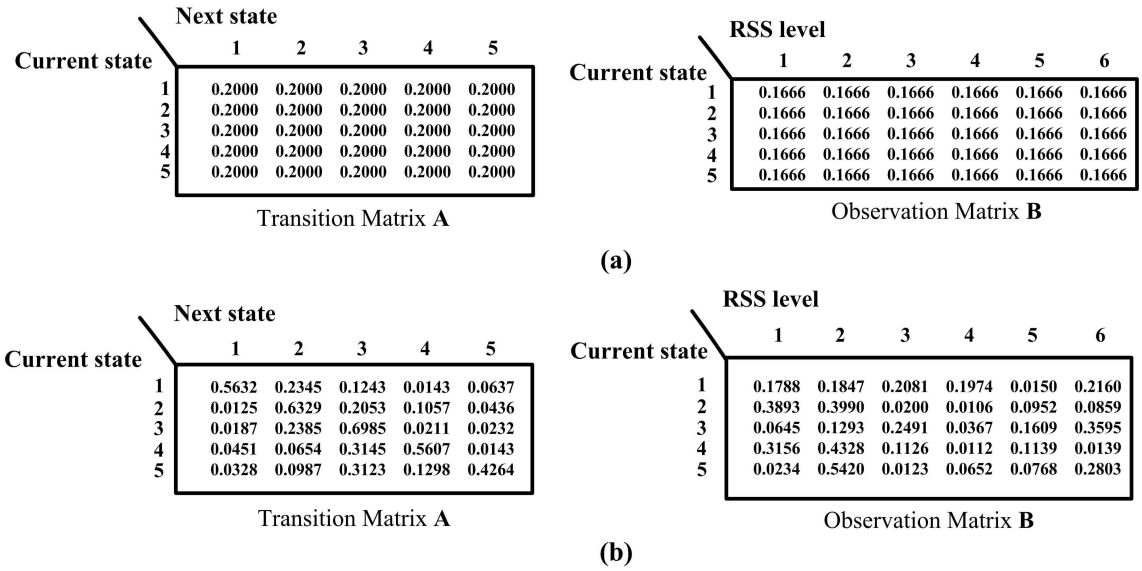

Figure 4.8: An illustrative example for initial and final values (before and after the training phase) of matrices **A** and **B**.

4.6 Chapter Summary

In this chapter, the application of HMM to the design of a CRN for indoor target tracking is proposed. Simulation results have demonstrated a superior performance of the HMM technique as it offers higher probability of target detection while maintaining the same level of location accuracy as compared to the conventionally used EKF and MLE. We have also derived the CRLB on localization error based on the hybrid RSS/TOA method and analyzed the convergence of the HMM algorithm. The proposed approach can be applied to real-time systems wherein there is a need of cognitive algorithms, which define the operation of radar transceivers in response to the changing radar scene due to target movement.

Chapter 5

Novel System Architecture and Waveform Design for Cognitive Radar Radio Networks

In this chapter, a novel approach to combining communication and radar functionalities in a single waveform design for CRR networks is proposed. This approach aims at extracting the target parameters from the radar scene, as well as facilitating high-data-rate communications between CRR nodes by adopting a single waveform optimization solution. The system design technique aims at addressing the coexisting communication and radar detection problems in mission-critical services, where there is a need of integrating the knowledge about the target scene gained from distinct radar entities functioning in tandem with each other. The high spatial resolution and immunity to multipath fading make UWB signals an appropriate choice for such applications. The proposed solution is achieved by applying the MI based strategy to design the sequence of UWB transmission pulses and embed into them the communication data with the pulse position modulation (PPM) scheme. With subsequent iterations of the algorithm, simulation results demonstrate an improvement in extraction of the parameters from the radar scene such as target position and impulse response, while still maintaining high-throughput radio links with low bit error rates (BERs) between CRR nodes.

5.1 Introduction

5.1.1 Background on Cognitive Radar Waveform Design and Joint Communication-Radar Systems

In a cognitive radar, the information of the target scene parameters is relayed to the transmitter by the receiver through a continuous feedback loop, which allows the development of waveform design techniques that offer better target resolution capabilities [132]. Excitation pulses can be optimized by application of information theory to radar signal processing. Bell [3] studied the design of waveforms in the context of illumination of extended targets for target detection and information extraction. Yang and Blum [134] extended the work of Bell [3] by using MI as a waveform optimization criterion subject to the limited transmission power in the MIMO radar configuration.

The work in [134] in particular focuses upon the problem of radar waveform design for target classification and identification, where the conditional MI between the random target impulse response and the reflected signals is maximized given the knowledge of the transmitted signals. Another problem that [135] addresses is the design of waveforms based on minimization of mean square error (MMSE) in estimating the target response. Analysis in [135] indicates that the above mentioned two problems lead to the same waveform solution. The work in [132] focuses upon designing UWB transmission waveforms with an aim of minimizing the MI between the received radar pulses at successive instants of time. This is achieved by designing the probing signals that will result in independent responses from the target scene in a bid to gain more knowledge about the changing target parameters at each instant of time.

In this chapter, we try to develop a novel cognitive architecture for the joint communication-radar waveform design. Before we describe the actual architecture, we provide a general background on the existing proposal of joint communication-radar networks.

In recent years, the research in integrating the communication and radar system designs under a common platform has gained significant momentum [24,25,28]. Such a joint radar and communication system would constitute a unique cost-efficient solution for future intelligent surveillance applications, for which both environmental

sensing and establishment of *ad hoc* communication links is essential.

Recent contributions such as [24] and [25] in particular focus upon the development of devices that have multiple radio functions and combine communication and radar in a small portable form with ultra-low power consumption. These works have adopted the OFDM techniques fused with UWB technologies to realize the communication-radar integration. However, these designs create other implementation issues, such as excessive demand of signal processing power, high speed analog-to-digital circuitry, agile radio frequency frontend for multi-mode operation, etc. Furthermore, systems employing UWB-OFDM for localization [24,25,28] utilize the same waveform family for designing the joint communication-radar signals. Consequently, these methods share a common drawback due to the fact that the auto-correlation (related to the range resolution of radar) of UWB-OFDM signals depends on both the location of the notch and the OFDM signal bandwidth. Hence, although the radar target range estimation is unaffected by the presence of an OFDM signal, its range resolution depends on the notch bandwidth into which the OFDM signal is embedded.

5.1.2 Joint Communication-Radar Waveform Design from a CRR Perspective

We combine the cognitive waveform selection algorithm presented in [132] and the UWB-PPM technique to obtain a unified waveform design solution, which offers superior radar performance and high-data-rate communication capability between CRR nodes. In our method, the radio and radar signals can coexist by sharing the same frequency band. Hence, the range resolution of the radar module is not affected by the communication signal design parameters. This makes the proposed UWB-PPM method superior to the existing UWB-OFDM solutions. The CRR waveforms obtained would not only benefit from an information-theoretic approach for efficient target parameter extraction but also utilize the same signal for establishing *ad hoc* communication links by adopting the UWB-PPM transmission strategy.

We consider the IEEE 802.15.4 MAC layer for the CRR network and adopt the relevant multipath indoor channel model proposed in [136] with the existence of a LOS path. In the case of the radar link, the LOS component corresponds to the direct target echo, whose RCS scintillation is characterized by the Swerling III

model [137]. Each CRR node is assumed to be a monostatic radar unit where the transmitter and receiver subsystems are collocated and hence, can share the information about the target parameters between themselves. We also assume perfect synchronization between CRR nodes in order to eliminate the multiple access interference between different users, and leave the more complicated asynchronous operation scenario for future investigation. In addition, we have chosen the UWB-PPM instead of continuous waveforms for the following reasons:

- The operational environment could be harsh to radio communications caused by densely populated scatterers. UWB signals are relatively immune to multipath channel fading in this case.
- The UWB-PPM waveform design is robust to hostile environments by providing low probability of interception and avoiding jamming interference.
- The UWB-PPM waveform solution enables rapid low-transmission-power *ad hoc* links, which can be configured "on-the-fly" without reservation or contention of available spectra.

The above benefits offered by UWB-PPM make it suitable for the current system design problem. The key contributions of this chapter can be summarized as follows:

- We develop a novel cognitive radar probing strategy based on the concept of MI minimization between successive backscatter pulses for extraction of the target parameters such as its relative distance from a CRR node, its impulse response and velocity, etc.
- We propose an original UWB-PPM-based joint communication-radar waveform design scheme.
- We provide performance analysis of the CRR network in terms of the target parameter extraction and communication BER between CRR nodes.

5.2 System Architecture

As discussed extensively in the existing literature, modern radar systems make use of pulse compression techniques such as linear frequency modulation or phase-coded waveforms employing Barker codes or Costas codes in order to improve the target

delay-Doppler resolution [138]. We adopt the idea of utilizing phase-coded waveforms for generation of orthogonal sequences required for transmission over various transmit antennas. We will consider UWB probing signals [139], though the general methodology is also applicable to any other type of excitation. The waveform comprises a sequence of UWB Gaussian monocycles in which the phase of each pulse is modulated in accordance with the orthogonal sequences corresponding to the column vectors of a specific Walsh-Hadamard matrix [138]. Each normalized Gaussian monocycle takes the following form

$$u(t) = \left[1 - 4\pi \left(\frac{t}{T}\right)^2\right] \exp\left\{-2\pi \left(\frac{t}{T}\right)^2\right\} \tag{5.1}$$

where T determines the pulse width and is assumed to be 0.2 ns, which is a typical value commonly used in UWB ranging applications [138].

5.2.1 CRR Network Setup

Fig. 5.1(a) exemplifies a typical CRR network comprising distinct CRR nodes capable of maintaining communication links between themselves, gathering data on the radar scene from sensors (suppose that the targets also induce a certain event observable at the sensors), and maintaining active probing of the target scene through the backscatter radar signals. The communication and radar functionalities occur simultaneously, where the CRR signal is used for communications between CRR nodes as well as range and target impulse response estimation. As discussed earlier, such scenarios are of particular interest in military and mission-critical applications, in which the individual radar nodes require to adopt intelligent surveillance mechanisms and have the ability to establish *ad hoc* communication links between themselves to share radar scene information. The CRR units can also gather intelligence on a specific phenomenon-of-interest like radioactivity or biohazard induced by the targets, through communicating to remote sensors. Fig. 5.1(a) represents such a setup in which this joint communication-radar operations can be realized.

5.2.2 CRR Node Transmitter Subsystem

Fig. 5.1(b) presents the internal architecture of a single CRR node. We initially construct an ensemble of orthogonal sequences of UWB Gaussian monocycles based

upon the Walsh-Hadamard codes. Each sequence corresponds to a particular column vector of the Walsh-Hadamard matrix used as illustrated in Fig. 5.2(a). Next, all the column vectors of the ensemble matrix undergo PPM in accordance with the communication data to be sent over the CRR link as shown in Fig. 5.2(a). The data link could be established between two CRR nodes or between a CRR node and a remote sensor monitoring the phenomenon-of-interest. In order to facilitate identification, the unique addresses of each pair of source and destination are embedded in the preamble of the data to be sent. An UWB-PPM signal is selected by the waveform selection module from the ensemble based on the MI minimization algorithm. This integrated signal is then sent by the transmitter to probe the radar environment and send the data to other CRR nodes. The received signal comprises either the target return or the communication data from other nodes and sensors. Subsequently, the former can be used to estimate the target parameters like range, velocity, and impulse response.

5.2.3 Target Channel Model

We now consider a CRR node with the same antenna used for both transmission and reception purposes. Let $\mathbf{x}$ represent a particular sequence of orthogonal waveforms to be used for transmission. Let $\mathbf{n}$ represent the colored noise. By colored noise we mean the combination of AWGN, backscattering from non-target scattering centers, and also the interference caused by the simultaneous operation of multiple CRR nodes. It is assumed that the length of the UWB radar pulse sequence is greater than or equal to the frame length of data to be transmitted. As shown in [140] and verified by our simulation results to be discussed later, PPM does not affect the orthogonality between various CRR waveforms. Thus we can safely design and optimize radar excitations with or without PPM.

We can express the received signal for the antenna element as

$$\mathbf{y} = \mathbf{H}\mathbf{x} + \mathbf{n}. \tag{5.2}$$

The variable $\mathbf{x} \in \mathbb{C}^{K\times 1}$ denotes the transmitted signal vector with K being the length of the UWB radar sequence, $\mathbf{y} \in \mathbb{C}^{K\times 1}$ denotes the received signal vector, $\mathbf{H} \in \mathbb{C}^{K\times K}$ denotes the target channel impulse response comprising the combined response of the transmitter-to-target, target itself, and target-to-receiver channels,

and $\mathbf{n} \in \mathbb{C}^{K\times 1}$ denotes the noise vector. $\mathbb{C}$ represents the complex number domain. We further define $E(\mathbf{H}^T\mathbf{H}) = \mathbf{R_H}$ to be the target channel covariance matrix and $E(\mathbf{n}^T\mathbf{n}) = R_\mathbf{n}$ to be the noise variance.

RCS scintillation of the target can vary slowly or rapidly depending on the target size, shape, dynamics, and its relative motion with respect to the radar. Thus, due to the wide variety of RCS scintillation sources, changes in the RCS are modeled statistically as random processes. We consider the target as a dominant scatterer amidst several clutter sources. Depending upon the motion and clutter characteristics, the radar targets have been classified into Swerling models as found in [137]. In Swerling III, the RCS samples measured by the radar are correlated throughout an entire scan but are uncorrelated from scan to scan (slow fluctuation), and the radar scene is dominated by a single powerful scatterer and many weak scatterers in its vicinity. The entries of $\mathbf{H}$ in (5.2) associated with the target response contain the RCS of the desired target and are approximated by the Swerling III variations (see also [141] and [137]):

$$f(\xi) = \frac{1}{\xi_{\text{av}}} \exp\left(-\frac{\xi}{\xi_{\text{av}}}\right) \tag{5.3}$$

where $\xi > 0$ represents the random RCS fluctuation with ξ_{av} being the average RCS. All the other entries of $\mathbf{H}$ denote the RCS of clutter sources and are assumed to be stationary. Hence, for a Swerling III model, we would expect the target echoes due to successive scans to be uncorrelated. Towards this end, we seek to use excitation sequences that will produce uncorrelated returns at two consecutive time instants.

5.2.4 CRR Node Receiver Subsystem

The reflected signal is gathered by the receive antenna and passed on to a matched filter bank as illustrated in Fig. 5.1(b), which matches the received signal to each individual transmission waveform stored in the receiver. At this stage, the radio signal that exists in the form of the UWB-PPM data is extracted by removing the excess delays between UWB pulses through demodulation. Once the radio signal is removed, the remaining waveform is treated purely as the radar backscatter. The target impulse response and parameter estimation module then attempts to discriminate the target from the surrounding clutter.

The estimated channel response and received signal characteristics such as noise

variance are forwarded to the MI minimization module. In the light of the updated radar scene, the MI minimization module selects a suitable sequence for the transmitting antenna in order to acquire the best knowledge about the target in the next time instant. This operation facilitates adaptive illumination of the radar environment and essentially leads to a cognitive dynamic system featuring the following two properties described in [87]: (i) intelligent signal processing, which builds on real-time learning through continuous interaction of the radar with the surroundings; and (ii) feedback from the receiver to the transmitter, which is a facilitator of intelligence.

In summary, the CRR waveform design approach involves the following two steps:

- Step I: Designing of the UWB-PPM waveforms in accordance with the communication data to be sent with an appropriate selection of the PPM delay; and
- Step II: Waveform selection based on the MI minimization approach to facilitate more effective target signature extraction.

5.3 Step I: UWB-PPM Waveform Design

In this section, we focus upon constructing the CRR waveforms by introducing PPM to the column vectors of the Walsh-Hadamard matrix, which is in accordance with the data to be transmitted, thus forming an ensemble $\mathbb{S}$. As to be seen from the simulation results, this introduction of excess delays into the radar pulses contained in $\mathbb{S}$ does not affect the orthogonality between various CRR waveforms. The communication source and destination identities are embedded in the preamble of the data frame. It is assumed that the data frame length is less than or equal to the length of the probing signal (i.e., length of the column vector of the Walsh-Hadamard matrix).

Fig. 5.2(a) demonstrates the proposed UWB-PPM scheme for a 16-bit data frame, where the polarity and the delay of the UWB pulses are determined by the column vector of the Walsh-Hadamard code and the PPM data, respectively. Fig. 5.2(b) represents the auto- and cross-correlation between CRR signals. The former exhibits a sharp peak at the zero delay, whereas the latter gives rise to much smaller values throughout the entire range of delay samples. This observation verifies the orthogonality between distinct CRR signals even after the PPM operation. In this

way, different CRR nodes can share the same spectral resources simultaneously as long as they use different column vectors to design their waveforms. Fig. 5.2(c) indicates the spectrum of an arbitrarily selected CRR signal $\mathbf{y}_t$ received at a reference distance of 20 m from the transmitting node operating at 4 GHz. The transmission power complies with the regulations set by the FCC mask for UWB wireless devices transmitting in outdoors and indoors, which is at -41.3 dBm/MHz in the frequency range $3.6 - 10.1$ GHz [142]. The width of each pulse in the CRR signal is assumed to be 0.2 ns.

5.3.1 PPM Delay Selection in CRR Waveforms

Performance of UWB-PPM communications in terms of the BER and the throughput has been well investigated in the literature. Some of the recent works include [42, 143, 144]. In these works, the time hopping scheme for UWB-PPM has been analyzed. UWB communications offer high data rates for communications and good immunity from multipath fading over short ranges.

We use a simple UWB-PPM scheme, where we design the PPM delay used for sending '1' or '0' such that the BER on the communication link is significantly reduced. As mentioned in [145] and [146], if the transmitted pulse is Gaussian UWB signal, then the Euclidean distance defined for the separation between two radar pulses for transmitting '1' and '0' is given by

$$d(\tau) = \sqrt{1 - \left\{ \left[1 - 4\pi \left(\frac{\tau}{T}\right)^2 + \frac{4\pi^2}{3} \left(\frac{\tau}{T}\right)^4 \right] \exp\left[-\pi \left(\frac{\tau}{T}\right)^2 \right] \right\}} \tag{5.4}$$

where τ is the PPM delay to be designed and $d(\tau)$ represents the Euclidean distance between the PPM symbols. As shown in [145], the best signal design is the one that maximizes the squared Euclidean distance. For a given choice of pulse width T, we choose the PPM delay τ that maximizes square of the Euclidean distance, $d^2(\tau)$. At the same time, we also ensure that the orthogonality between radar signals is maintained after choosing a particular τ. In other words, we seek a value for τ, which keeps the cross-correlation between the designed waveforms below a predetermined level such that the orthogonality between them is maintained.

The BER for such an UWB-PPM scheme is given as [145]

$$P_e(\tau) = \mathbb{Q}\left(\sqrt{\frac{\lambda d^2(\tau)}{2}}\right) \tag{5.5}$$

where P_e is the probability of error at a SNR of λ and $\mathbb{Q}(\cdot)$ stands for the complimentary error function or $\mathbb{Q}$ function. $\mathbb{Q}$ is defined as follows

$$\mathbb{Q}(x) = \frac{2}{\sqrt{\pi}} \int_x^{\infty} \exp(-t^2) dt.$$

Since we ensure that the orthogonality between CRR waveforms is not distorted, we can adopt an iterative design algorithm that maximizes the target scene information and at the same time is capable of maintaining active communication links between CRR nodes with an acceptable BER performance. The selection of PPM delay τ is based upon minimization of P_e, viz.,

$$\hat{\tau} = \arg\min_{\tau} P_e(\tau) = \arg\min_{\tau} \mathbb{Q}\left(\sqrt{\frac{\lambda d^2(\tau)}{2}}\right) \tag{5.6}$$

under the constraint of keeping the cross-correlation between designed waveforms below a pre-specified threshold. Once the communication data have been embedded into the orthogonal codes, we then proceed to selecting from these waveforms the best possible signal to be transmitted in the next time instant based on minimization of MI.

5.4 Step II: MI Based Waveform Selection

The basic idea behind the MI minimization approach is that, we intend to identify the best possible radar waveform for the next time instant based upon the current received backscattered signal. As the radar channel is dynamic due to the fluctuations in RCS of the target and other factors such as Doppler shift caused by relative motion of the target and the surrounding clutter, there is a need for a dynamic waveform design and selection approach in order to constantly gain information from the target scene.

5.4.1 Target Impulse Response and Parameter Estimation

The radar receiver has a complete knowledge of the transmitted waveform at all instants of time. Hence, we can use this information to extract parameters like target impulse response, target channel covariance matrix $\mathbf{R_H}$, and noise variance $R_{\mathbf{n}}$. Let $\mathbf{y}_t$ and $\mathbf{y}_{t-1}$ be the received signal vectors at two successive time instants. Using (5.2) we have,

$$E(\mathbf{y}_t^T \mathbf{y}_t) = \mathbf{x}_t^T \mathbf{R_H} \mathbf{x}_t + R_{\mathbf{n}} = \sigma_t^2 \tag{5.7}$$

$$E(\mathbf{y}_{t-1}^T \mathbf{y}_{t-1}) = \mathbf{x}_{t-1}^T \mathbf{R_H} \mathbf{x}_{t-1} + R_{\mathbf{n}} = \sigma_{t-1}^2 \tag{5.8}$$

where σ_t^2 and σ_{t-1}^2 represent the variances of the received signals at respective time instants.

Solving (5.7) and (5.8) simultaneously we can estimate the values for $\mathbf{R_H}$ and $R_{\mathbf{n}}$. These values will be used to generate the estimate for $\mathbf{y}_{t+1}$ for all values of $\mathbf{x}_{t+1} \in \mathbb{S}$ using (5.2), where $\mathbb{S}$ is the ensemble of the transmitted waveforms. We will choose $\mathbf{x}_{t+1} \in \mathbb{S}$ based on the proposed MI minimization approach.

This process of estimation of the target channel covariance matrix and the noise variance will be performed at every instance of reception of $\mathbf{y}_t$, and their values will be thus updated and used to generate new estimates for $\mathbf{y}_{t+1}$.

5.4.2 MI Minimization between Successive Target Echoes

MI between two random vectors $\mathbf{y}_i$ and $\mathbf{y}_j$, denoted as $\mathrm{MI}(\mathbf{y}_i, \mathbf{y}_j)$, is a measure of the information that $\mathbf{y}_i$ conveys about $\mathbf{y}_j$, or equivalently, the information that $\mathbf{y}_j$ conveys about $\mathbf{y}_i$. If the two random vectors are statistically dependent, then the MI between them is high. Similarly, if $\mathbf{y}_{t-1}$ and $\mathbf{y}_t$ represent two received backscatter signals at successive time intervals and they are statistically dependent (i.e., high MI), then we cannot expect any gain in information about the radar scene. We therefore, desire to obtain uncorrelated and independent target images from the radar scene in order to acquire more target scene information from scan to scan. Subsequently, we select only those waveforms for transmission that would produce less statistically dependent backscatter signals from the same radar scene. In other words, we intend to find the best transmission waveform $\mathbf{x}_t$ by selecting from the ensemble $\mathbb{S}$ a waveform that would minimize the MI between the current received target echo and the estimated echo in the next time instant.

Let $\mathbf{y}_t = \{y_{t,1}, y_{t,2}, \cdots, y_{t,K}\} \sim \mathcal{N}(\mu_t, \sigma_t^2)$ be the received signal vector, which is normally distributed over K samples with mean μ_t and variance σ_t^2. Then we can express the MI between the successive received signal vectors in subsequent time instants as

$$\mathrm{MI}(\mathbf{y}_{t-1}, \mathbf{y}_t) = H(\mathbf{y}_{t-1}|\mathbf{x}_{t-1}) + H(\mathbf{y}_t|\mathbf{x}_t) - H(\mathbf{y}_{t-1}, \mathbf{y}_t|\mathbf{x}_{t-1}, \mathbf{x}_t) \tag{5.9}$$

where the first term $H(\mathbf{y}_{t-1}|\mathbf{x}_{t-1})$ represents the average information or entropy. By classical definition of entropy it is the measure of uncertainty in the received signal at the time instant $t-1$ given the knowledge of the transmitted signal $\mathbf{x}_{t-1}$. The knowledge of the transmitted waveform is assumed to be present at all time instants. The other two terms in (5.9) are similarly defined.

Let $\mathbf{y}$ represent the sequence of the k^{th} $(k = 1, 2, \cdots, K)$ sample of N successive received signal vectors. Therefore, $\mathbf{y} = \{y_{t,k}, y_{t-1,k}, \cdots, y_{t-N+1,k}\}$ follows a multivariate normal distribution with mean vector μ and covariance matrix $\mathbf{\Sigma}$. The joint pdf of $\mathbf{y}$ is

$$f_{\mathbf{y}}(\mathbf{y}) = \frac{1}{(\sqrt{2\pi})^N |\mathbf{\Sigma}|^{\frac{1}{2}}} \exp\left[-\frac{(\mathbf{y}-\mu)^T \mathbf{\Sigma}^{-1} (\mathbf{y}-\mu)}{2}\right]. \tag{5.10}$$

Subsequently, the joint entropy can be expressed as

$$
\begin{aligned}
H(\mathbf{y}|\mathbf{x}) &= -\int f(\mathbf{y}) \left\{ -\frac{(\mathbf{y}-\mu)^T \mathbf{\Sigma}^{-1} (\mathbf{y}-\mu)}{2} - \ln \left[\left(\sqrt{2\pi} \right)^N |\mathbf{\Sigma}|^{\frac{1}{2}} \right] \right\} d\mathbf{y} \\
&= \frac{1}{2} E \left[\sum_{i,j} (y_i - \mu_i)(\mathbf{\Sigma}^{-1})_{ij} (y_j - \mu_j) \right] + \frac{1}{2} \ln \left[(2\pi)^N |\mathbf{\Sigma}| \right] \\
&= \frac{1}{2} E \left[\sum_{i,j} (y_i - \mu_i)(y_j - \mu_j)(\mathbf{\Sigma}^{-1})_{ij} \right] + \frac{1}{2} \ln \left[(2\pi)^N |\mathbf{\Sigma}| \right] \\
&= \frac{1}{2} \sum_{i,j} E[(y_j - \mu_j)(y_i - \mu_i)](\mathbf{\Sigma}^{-1})_{ij} + \frac{1}{2} \ln \left[(2\pi)^N |\mathbf{\Sigma}| \right] \\
&= \frac{1}{2} \sum_{j} \sum_{i} \mathbf{\Sigma}_{ji} (\mathbf{\Sigma}^{-1})_{ij} + \frac{1}{2} \ln \left[(2\pi)^N |\mathbf{\Sigma}| \right] \\
&= \frac{1}{2} \sum_{j} (\mathbf{\Sigma}\mathbf{\Sigma}^{-1})_{jj} + \frac{1}{2} \ln \left[(2\pi)^N |\mathbf{\Sigma}| \right] \\
&= \frac{1}{2} \sum_{j} \mathbf{I}_{jj} + \frac{1}{2} \ln \left[(2\pi)^N |\mathbf{\Sigma}| \right] \\
&= \frac{N}{2} + \frac{1}{2} \ln \left[(2\pi)^N |\mathbf{\Sigma}| \right] \\
&= \frac{1}{2} \ln \left[(2\pi e)^N |\mathbf{\Sigma}| \right] \quad \text{nats.}
\end{aligned} \tag{5.11}
$$

Following this, we can derive the joint entropy $H(\mathbf{y}_t, \mathbf{y}_{t-1}|\mathbf{x}_t, \mathbf{x}_{t-1})$ by substituting $N = 2$ in (5.11):

$$
H(\mathbf{y}_t, \mathbf{y}_{t-1}|\mathbf{x}_t, \mathbf{x}_{t-1}) = H(y_{t,k}, y_{t-1,k}|x_{t,k}, x_{t-1,k}) = \frac{1}{2} \ln \left[(2\pi e)^2 |\mathbf{\Sigma}| \right] \quad \text{nats.} \tag{5.12}
$$

Let the covariance matrix $\mathbf{\Sigma}$ be represented as (see also [103])

$$
\mathbf{\Sigma} = \begin{bmatrix} \sigma_t^2 & \rho\sigma_t\sigma_{t-1} \\ \rho\sigma_t\sigma_{t-1} & \sigma_{t-1}^2 \end{bmatrix} \tag{5.13}
$$

where ρ is the correlation coefficient. Thus,

$$
\begin{aligned}
|\mathbf{\Sigma}| &= \sigma_t^2 \sigma_{t-1}^2 - (\rho\sigma_t\sigma_{t-1})^2 \\
&= \sigma_t^2 \sigma_{t-1}^2 (1 - \rho^2).
\end{aligned} \tag{5.14}
$$

Let the univariate pdf of the received signal vector $\mathbf{y}_t$ be represented as

$$
\Psi(y) = \frac{1}{\sqrt{2\pi\sigma_t^2}} \exp \left[-\frac{(y - \mu_t)^2}{2\sigma_t^2} \right]. \tag{5.15}
$$

By definition of entropy,

$$\begin{aligned} H(\mathbf{y}_t|\mathbf{x}_t) &= -\int \Psi(y)\ln[\Psi(y)]\mathrm{d}y \\ &= -\int \Psi(y)\left[-\frac{(y-\mu_t)^2}{2\sigma_t^2} - \ln\left(\sqrt{2\pi\sigma_t^2}\right)\right]\mathrm{d}y \\ &= \frac{E\left[(y-\mu_t)^2\right]}{2\sigma_t^2} + \frac{1}{2}\ln\left(2\pi\sigma_t^2\right) \\ &= \frac{1}{2} + \frac{1}{2}\ln\left(2\pi\sigma_t^2\right) \\ &= \frac{1}{2}\ln\left(2\pi e\sigma_t^2\right) \quad \text{nats.} \end{aligned} \tag{5.16}$$

Similarly we can write

$$H(\mathbf{y}_{t-1}|\mathbf{x}_{t-1}) = \frac{1}{2}\ln\left(2\pi e\sigma_{t-1}^2\right) \quad \text{nats.} \tag{5.17}$$

Thus using (5.9), (5.11), (5.14), (5.16) and (5.17) we obtain

$$\begin{aligned} \mathrm{MI}(\mathbf{y}_{t-1},\mathbf{y}_t) &= H(\mathbf{y}_{t-1}|\mathbf{x}_{t-1}) + H(\mathbf{y}_t|\mathbf{x}_t) - H(\mathbf{y}_{t-1},\mathbf{y}_t|\mathbf{x}_{t-1},\mathbf{x}_t) \\ &= \frac{1}{2}\ln\left(2\pi e\sigma_{t-1}^2\right) + \frac{1}{2}\ln\left(2\pi e\sigma_t^2\right) - \frac{1}{2}\ln\left[(2\pi e)^2|\mathbf{\Sigma}|\right] \\ &= \frac{1}{2}\ln\left(2\pi e\sigma_{t-1}^2\right) + \frac{1}{2}\ln\left(2\pi e\sigma_t^2\right) - \frac{1}{2}\ln\left[(2\pi e)^2\sigma_t^2\sigma_{t-1}^2(1-\rho^2)\right] \\ &= -\frac{1}{2}\ln(1-\rho^2). \end{aligned} \tag{5.18}$$

We can estimate the correlation coefficient $\rho = \frac{E[\mathbf{y}_t^T\mathbf{y}_{t-1}]}{\sqrt{\sigma_t^2\sigma_{t-1}^2}}$. We can estimate the values for $\mathbf{y}_{t+1}$ over all possible values of $\mathbf{x}_{t+1} \in \mathbb{S}$ using (5.2). Thus we can also form an estimate of all values of the corresponding $\rho = \frac{E[\mathbf{y}_{t+1}^T\mathbf{y}_t]}{\sqrt{\sigma_{t+1}^2\sigma_t^2}}$ and choose the value for $\mathbf{x}_{t+1}$ that minimizes (5.18).

The MI minimization approach can be expressed as:

$$\mathrm{MI}^* = \min_{\mathbf{x}_{t+1}\in\mathbb{S}} -\frac{1}{2}\ln(1-\rho^2) \tag{5.19}$$

subject to the power constraint $E\left(\mathbf{x}_{t+1}^T\mathbf{x}_{t+1}\right) \leq P_0$, where P_0 is the power available at the transmitter.

We can summarize the CRR waveform design algorithm as follows.

1. The current $\mathbf{R_H}$ and $R_\mathbf{n}$ can be estimated through successive measurements with orthogonal UWB sequences or radar waveforms $\mathbf{x} \in \mathbb{S}$.

2. An estimate for $\mathbf{y}_{t+1}$ is obtained using (5.2) and Step 1. We then choose the PPM delay τ. and design the UWB-PPM ensemble $\mathbb{S}$. We then select $\mathbf{x}_{t+1} \in \mathbb{S}$ to be transmitted based on the MI minimization approach and (5.18).

3. The CRR waveform is transmitted carrying the communication source and destination identity information in the preamble of the data frame. The communication link can either be between two different CRR nodes or between a CRR node and a remote sensor monitoring the phenomenon-of-interest induced by the target.

4. Backscatter signal is collected and passed through a matched filter bank or a correlation receiver, which uniquely identifies the orthogonal sequence out of the ensemble $\mathbb{S}$ and demodulates the PPM signal.

5. The radar signal is used to extract the target parameters like target range, velocity, and impulse response. The estimates for $\mathbf{R_H}$ and $R_\mathbf{n}$ are updated using the current received signal and are relayed back to the MI minimization module.

6. The process is repeated iteratively.

The cognitive operation involved in the proposed strategy can thus be summarized as follows:

- The system constantly updates its estimate on the target impulse response by continual measurements of the radar environment and utilizes this information to select the best possible waveform for transmission. In this way, the waveform selection approach continuously learns from multiple interactions with the radar scene and utilizes the extracted target information in order to make the selection of the subsequent transmission waveforms. A feedback loop from the receiver to the transmitter allows the delivery of this radar scene information to the transmitter.

- The system adapts its UWB-PPM inter-pulse duration and thus adjusts its operational mode in accordance with the target parameter variation "on-the-fly".

Such architectures are similar to cognitive radars, where the systems adopt a constant learning approach as described in [87].

5.5 Simulation Results and Discussion

5.5.1 Simulation Setup

For simulation purposes, we set the PPM delay τ such that the cross-correlation coefficient between the transmission waveforms is no greater than 0.4. In this way we have an acceptable BER for communications. Furthermore, orthogonality between distinct CRR waveforms is maintained for radar waveform optimization purposes. The received signal is matched filtered in order to estimate the propagation delay. The PPM data are separately demodulated and the radar signal processing is carried out by the target impulse response and parameter estimation module. As described in the previous sections, the target channel covariance matrix is estimated and the noise variance is also determined in order to help the MI minimization module to decide upon the best UWB sequence to be used for transmission in the subsequent time interval. The center frequency of the transmission UWB pulses is 4 GHz and the sampling frequency is 10 GHz.

5.5.2 Target Range Estimation

In order to estimate the target range or equivalently the TOA of the backscatter signal, it is essential to determine the value of the pulse repetition interval (PRI) between successive Gaussian monocycles in an UWB sequence. We apply the multipath channel model as mentioned in [136] with the presence of a LOS path as the major component in the backscatter signal.

To find the target distance the CRR node will estimate the actual time delay τ_d using correlation. The transmitted signal is delayed by time τ_n and is cross-correlated with the target return as follows

$$\mathbf{R_{yx}}(\tau_d - \tau_n) = E[\mathbf{x}_t^T(\tau - \tau_n)\mathbf{y}_t(\tau - \tau_d)]. \tag{5.20}$$

In order to estimate the time delay, the maximum value of $\mathbf{R_{yx}}$ is evaluated by varying the value of τ_n at the receiver. Fig. 5.3(a) shows the range profiles of the target and the surrounding clutter. For this simulation the target and the clutter were assumed to be stationary. This profile is achieved by continually probing the stationary radar environment with CRR waveforms chosen by the MI minimization

algorithm. At each iteration we select the waveform that would produce the least correlated output. The range resolution result in Fig. 5.3(a) is obtained at the end of 10 such iterations of MI minimization. As seen from this figure, the target is located at a distance of approximately 38 m from the CRR node. Subsequently, three or more distinct CRR nodes can share the information of the target relative distance and triangulate its location over the communication links. Fig. 5.3(b) indicates the range profile of the radar scene for a duration of 4 seconds, where the target remains distinguishable from those non-target scatterers throughout the entire period.

5.5.3 MI Minimization and Target Detection Probability

Fig. 5.4(a) demonstrates the MI minimization process for different SNRs. At high SNRs, the channel covariance matrix $\mathbf{R_H}$ can be successfully estimated and therefore, the value of MI decreases as the number of iterations increases. On the other hand, the estimation of $\mathbf{R_H}$ is poor at low SNRs. Consequently, the best transmission sequence for the next time instant is not always selected and the MI does not exhibit significant decrease even with more iterations of the algorithm. Hence, there would be little gain in the information pertaining to the target scene and the waveform selection approach would fail to provide performance improvement in this case.

Fig. 5.4(b) indicates the probability of target detection in the presence of AWGN and clutter interference. We use the performance measure of SCNR in order to evaluate the detection probability. This measure can be expressed as shown in [1, Chapter 6]

$$\text{SCNR} = \frac{1}{\frac{1}{\text{SNR}} + \frac{1}{\text{SCR}}} \tag{5.21}$$

where SCR is signal to clutter ratio and can be evaluated as shown in [147, Eq. (19)]. For a particular CRR waveform and a stationary radar scene, 1000 simulations were run for each SCNR and the probability of successful target detection was plotted based on the hypothesis testing method employing the optimal Neyman-Pearson detector algorithm in [138] for a fixed false positive rate of 10^{-5}. Then the next CRR waveform was chosen according to the MI minimization algorithm and the process was repeated for 50 iterations. As seen from Fig. 5.4(b), the MI minimization algorithm converges after 50 iterations, yielding a detection probability of 0.9 at SCNR = 8 dB as compared to SCNR = 17 dB at the first iteration. However, as we

increase the number of iterations, the probability of detection does not show further improvement after 50 iterations.

In Fig. 5.4(c), we compare the probability of target detection for varying waveforms selected by the MI minimization algorithm to the probability for an arbitrary static waveform used to estimate the target parameters over multiple snapshots. As the proposed approach always chooses distinct waveforms, which would produce received signals which have low correlation over time, the system adapts its probing signal better to the fluctuating target RCS. The static waveform on the other hand, in spite of multiple iterations, is unable to match the time-varying target response. Hence, the probability of target detection is suboptimal in this case.

5.5.4 Communication BER and Throughput Performance

Fig. 5.5(a) shows the performance of the CRR waveform design for a single CRR node from a communications perspective. The plot indicates the BER for different systems based on simulation results obtained with both Matlab and Simulink operating platforms, which have been investigated in the literature for joint communication-radar networks. The proposed CRR waveform solution can be modified by incorporating additional modulation levels for PPM, e.g., 16- or 4-ary PPM. However, as we go on increasing the delay between the radar pulses in order to send larger constellation of signals, the orthogonality of the UWB sequences is affected. As we increase the delay between radar pulses in order to send the larger constellation of signals, the auto-correlation of the radar waveform is significantly affected. We observe that as the inter-pulse delay is increased the side lobes in the auto-correlation plot become more dominant. This affects the orthogonality of the UWB-PPM waveform and in turn affects the performance of the radar receiver subsystem. Consequently, choosing the appropriate Euclidean distance or the delay for PPM results in a trade-off between communication and radar signal design requirements. As seen from the plot and also described in [24, 25, 28], UWB-OFDM signals offer better bit error performance when we adopt data redundancy bits for error control. However, the proposed UWB-PPM design performs comparably to UWB-OFDM schemes when no redundant bit is added. In simulating UWB-OFDM joint communication-radar waveforms the sub-carrier spacing used was 20 MHz and no cyclic prefixes were used. Transmit/receive antenna gain is assumed to be 15 dB, transmit power is assumed

to be 2 Watts. The minimum usable power at the receive antenna is assumed to be -100 dBm. For the UWB-OFDM system we utilize the CRC bits for coding and error control.

Fig. 5.5(b) shows the throughput analysis for the CRR waveform as compared to other UWB-OFDM signal designs. UWB communications in general achieve high data rate over short distances. As the distance between the communicating nodes increases the throughput falls. The proposed design offers a data rate of just about 200 Mbps at a distance of 20 m, which is better than that offered by the 4-carrier uncoded UWB-OFDM. The throughput for the UWB case has been estimated based on [148].

5.5.5 Mobile Target Scene Simulation

Fig. 5.6(a) shows the target and clutter range profile for a dynamic radar environment, in which the target and clutter sources are in relative motion with respect to the observing CRR node. The simulation was carried out with a relative velocity of 3.5 m/s. By choosing CRR waveforms based on the estimated target impulse response and ensuring that at each instance of reception the received signals are uncorrelated from each other, the proposed MI minimization algorithm is able to achieve resolvable target and clutter returns at the 10^{th} iteration as shown in Fig. 5.6(a). In Fig. 5.6(b) we observe that the target and the surrounding clutter are distinctly resolved into different range bins even if the radar scene is dynamic. The MI minimization algorithm is self-corrective since it updates the estimated value of the target channel covariance matrix and also the noise variance at each step. This result demonstrates the effectiveness of the proposed MI minimization algorithm for dynamic radar scenes with mobile targets and clutter.

5.5.6 Impact of Multipath Channel on System Performance

In this section, we study the effect of multipath propagation on the performance of the proposed system. Fig. 5.7(a) displays the average power delay profile of the UWB channel model mentioned in [136], which is used throughout the simulations. The excess delay is measured relative to the first arrival, and the vertical axis denotes the energy level of each delay bin. On average, over 92% of the total energy is confined within 100 ns. This means that a PRI greater than 100 ns would experience

very little inter symbol interference (ISI). In addition, over 99% of the total energy arrives within 160 ns. We set the value of PRI to be above 200 ns for our system to avoid ISI.

As described previously, we intend to estimate the delay τ that maximizes $\mathbf{R_{yx}}$. We therefore perform the peak detection on $\mathbf{R_{yx}}$ to obtain an estimate for the TOA and hence the distance of the target. In Fig. 5.7(b), we compare the ranging performance based on the mean TOA from the received signal and the TOA determined via the peak detection of $\mathbf{R_{yx}}$. Apparently, this result indicates the ranging error with respect to the TOA variation caused by the multipath dispersion. As seen from the figure, at low SCNRs the error using TOA obtained from the peak detection of $\mathbf{R_{yx}}$ is smaller than the one using the mean TOA. We also compare this result with the Cramer-Rao Lower Bound (CRLB) for the TOA estimation method in [149]. It can be found that the proposed scheme achieves errors close to CRLB at high SCNRs.

Fig. 5.7(c) represents the effect of PRI on the ranging performance. As seen from this figure, the ranging error sharply increases as we decrease the PRI below 200 ns. This complies with the previous analysis on the delay interval within which the incoming signal power is confined. Finally, the proposed technique outperforms the method based on the mean TOA throughout the entire range of PRI.

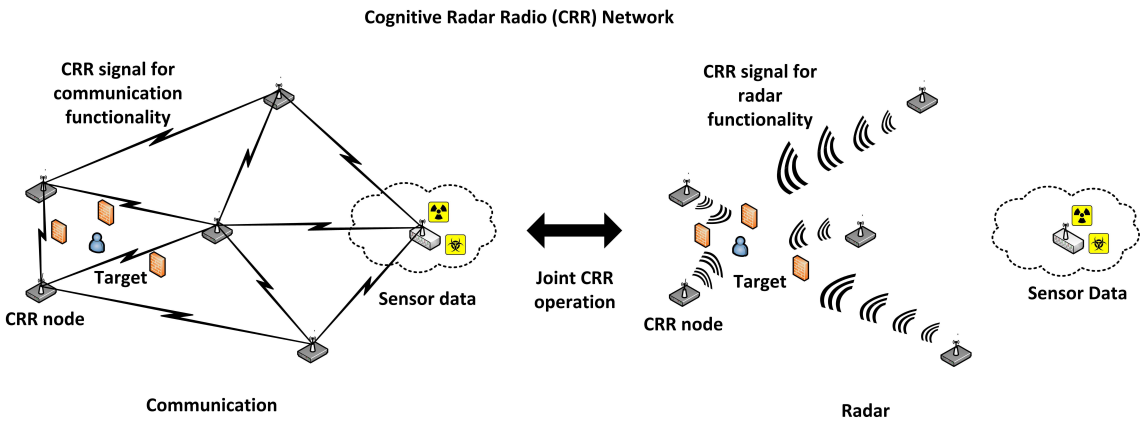

(a)

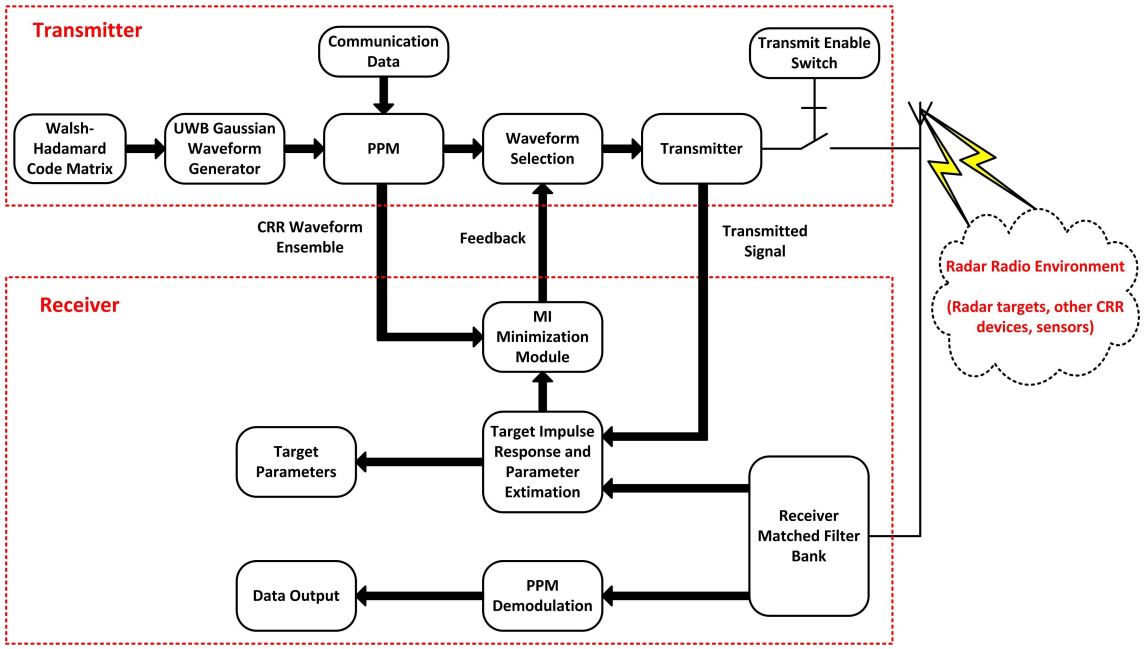

(b)

Figure 5.1: (a) Coexistence of communication and radar functionalities in a CRR network, and (b) CRR node architecture.

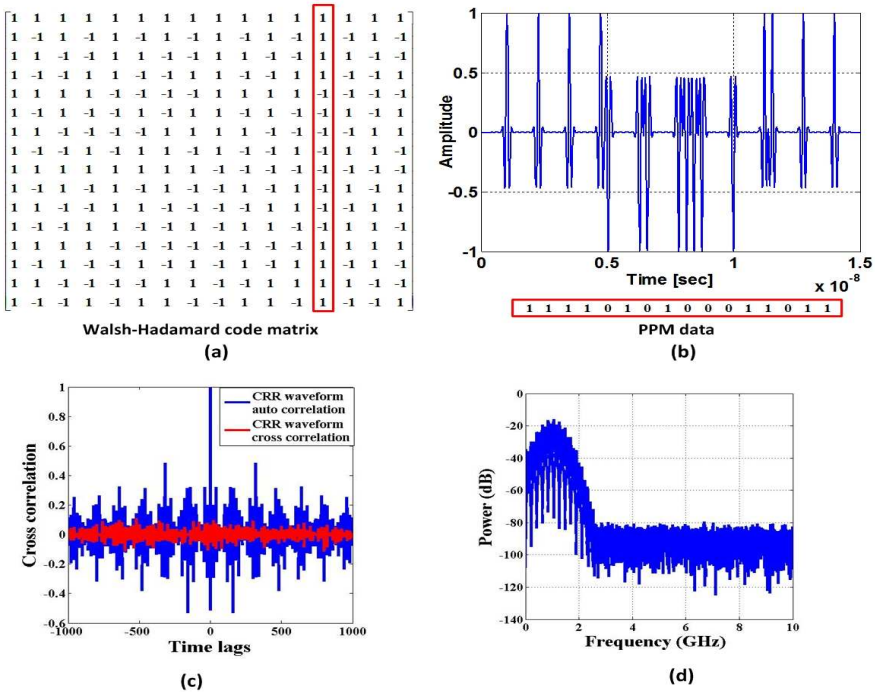

Figure 5.2: (a)column vector of the Walsh-Hadamard code matrix, (b) 16-bit CRR transmission waveform, (b) orthogonality of CRR waveforms, and (c) spectrum of the received CRR signal at a reference distance of 20 m at 4 GHz center frequency.

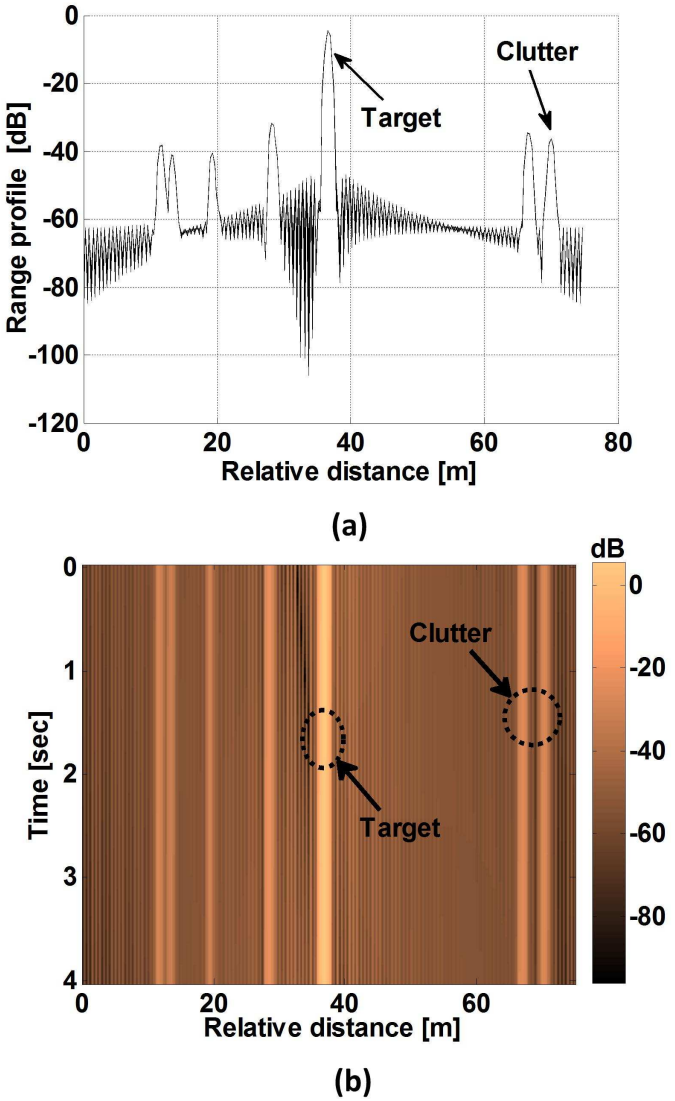

Figure 5.3: (a) Static target and non-target (clutter) scatterers resolved after 10 iterations of MI minimization at a CRR node, and (b) target and clutter returns after 10 iterations of MI minimization.

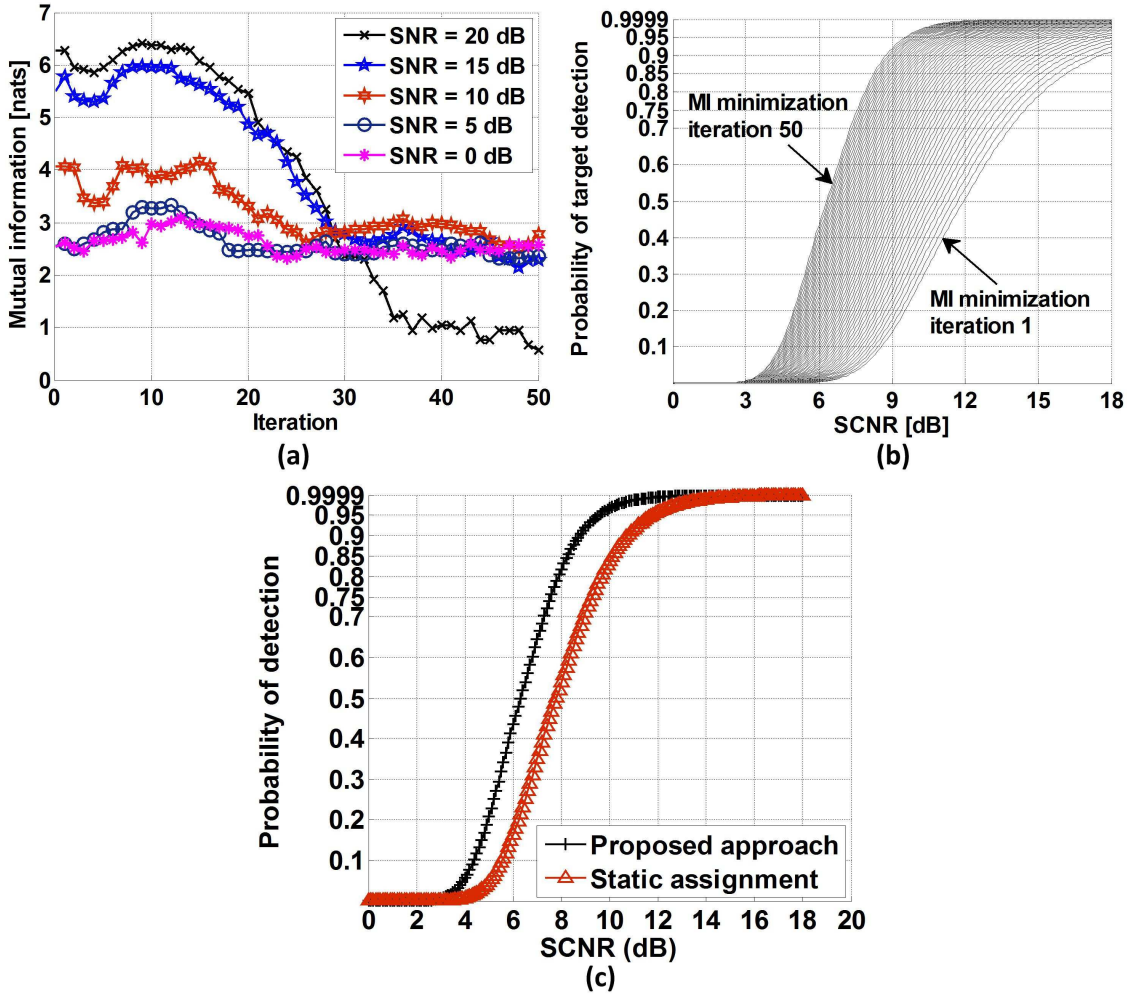

Figure 5.4: (a) Minimization of MI algorithm at different SNRs, (b) probability of target detection against SCNR for various iterations of the MI minimization algorithm, and (c) probability of detection for waveform selection based on MI minimization and static waveform assignment.

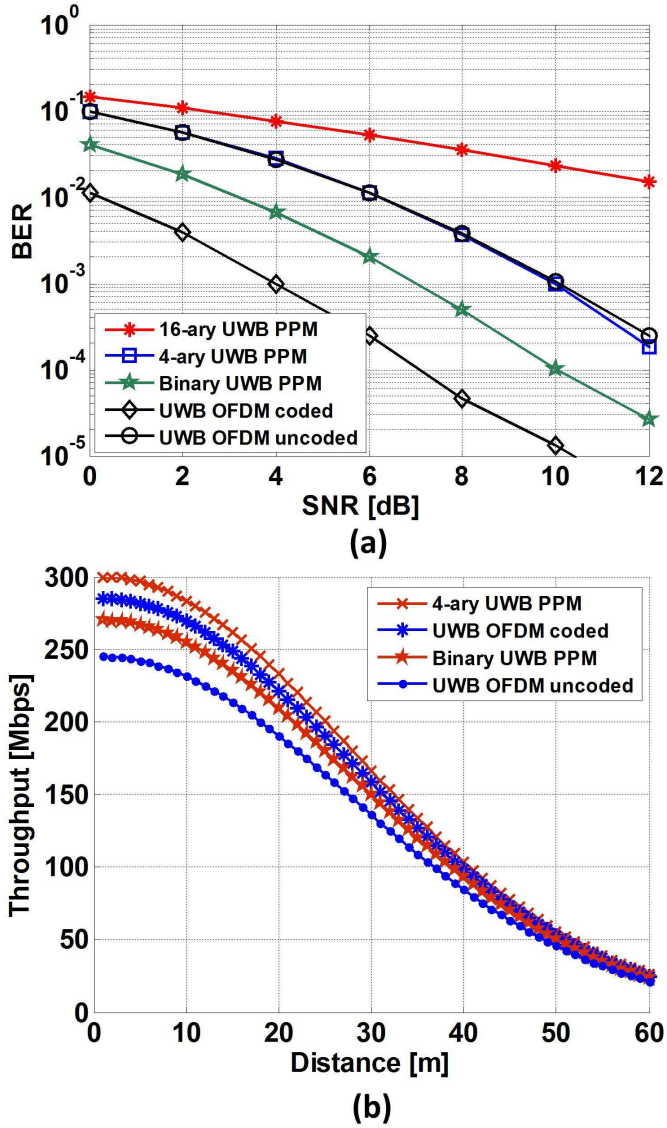

Figure 5.5: (a) BER of different joint communication-radar waveform designs, and (b) throughput performance against distance from a particular CRR node.

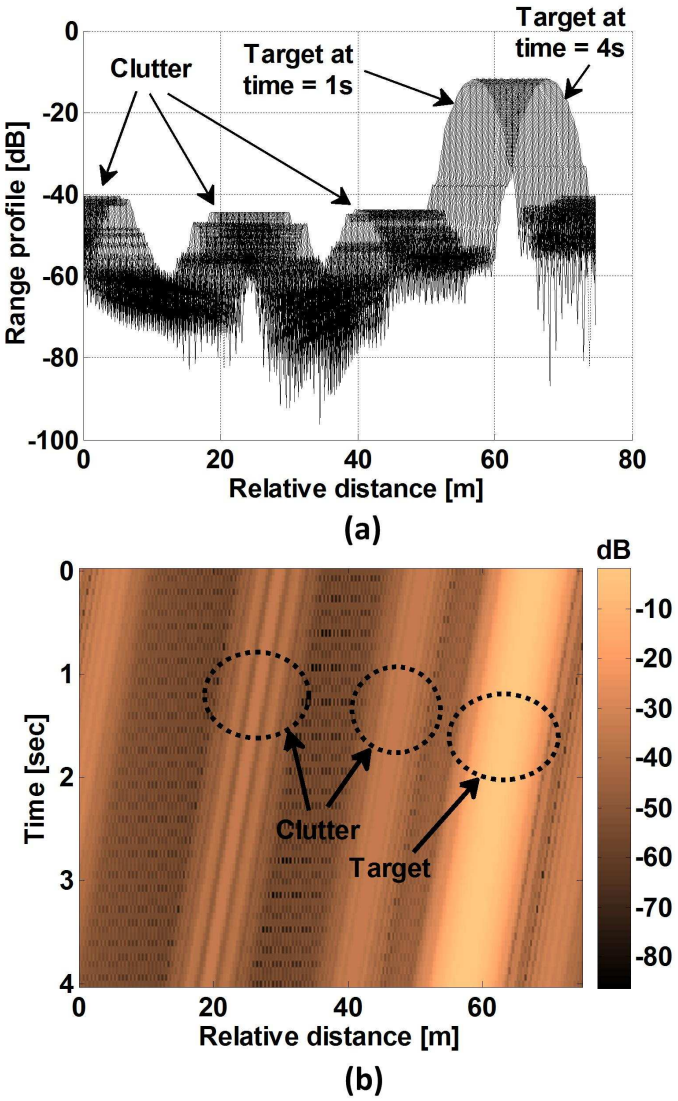

Figure 5.6: (a) Target range profile for a target velocity = 3.5 m/s for 4 s time duration after 10 iterations of MI minimization, and (b) target and clutter returns after 10 iterations of MI minimization.

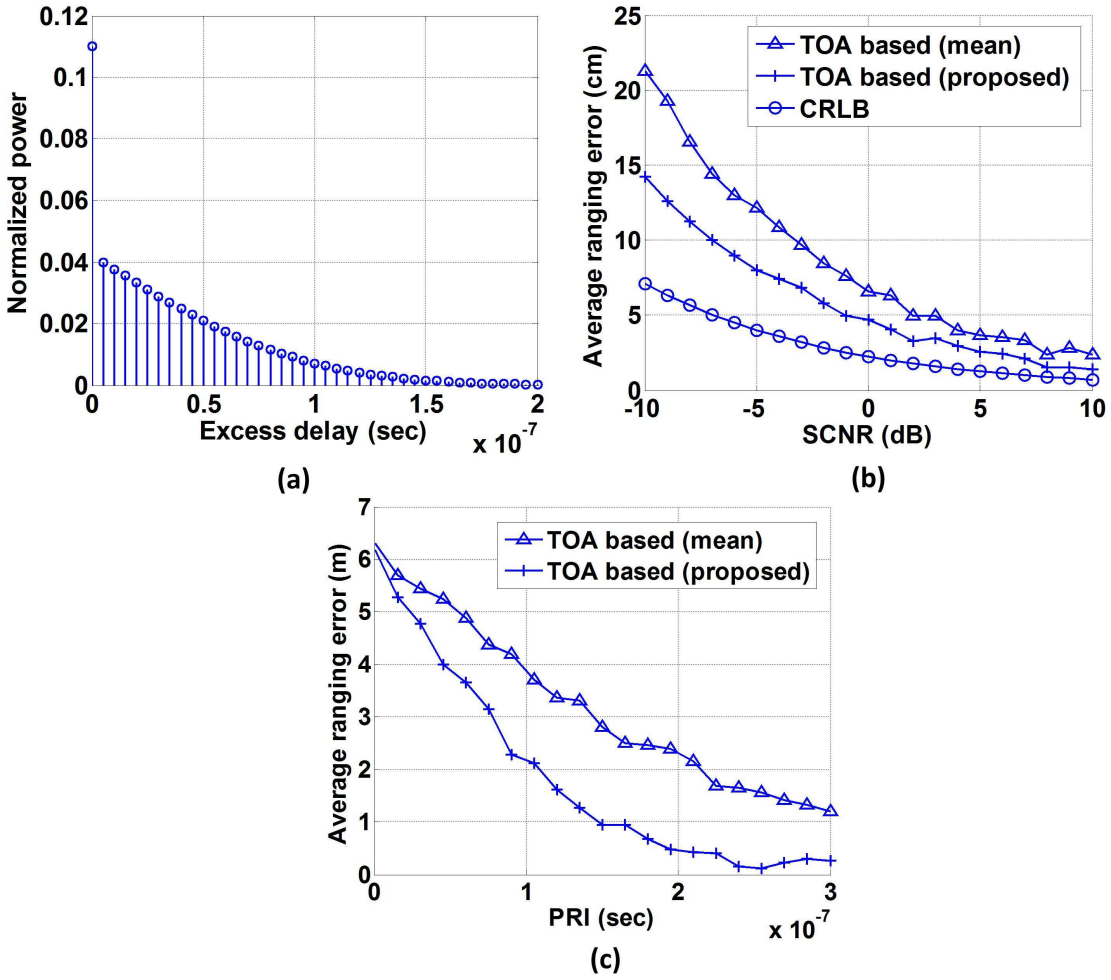

Figure 5.7: (a) UWB channel model, (b) average ranging error based on TOA estimation in the multipath UWB channel, and (c) average ranging error against PRI in the multipath UWB channel.

5.6 Chapter Summary

In this chapter, a joint communication-radar waveform design solution for the CRR network is developed. As indicated by the simulation results, the CRR waveform optimization approach promises better target impulse response extraction and range resolution. From a communications perspective, the proposed CRR waveform design also promises high data rate performance over short ranges. The radar and communication signals share the same spectral and temporal domains using the current design strategy. This approach was based upon constant learning of the target environment and adapting the transmission waveform characteristics to suit the dynamic target scene. Such a cognitive approach ensures maximum information extraction from the radar scene and better target discrimination capability. The

proposed unified system would constitute a unique cost-efficient platform for future intelligent surveillance applications, for which both environment sensing along with the allocation of *ad hoc* communication links are essential. Such systems can be used in mission-critical and military applications for addressing the remote surveillance and communication issues simultaneously. It is envisaged that the future personal communication and tracking devices will have comprehensive radar-like function, such as spectrum sensing and localization, in addition to multi-mode and multi-band communication capability.

Chapter 6

Location Aware Spectrum and Power Allocation Algorithm for Cognitive Wireless Systems

In this chapter, a novel approach to spectrum and power allocation is proposed for joint cognitive communication-radar networks, which aim at integrating cognitive radio and cognitive radar paradigms to achieve intelligent utilization of spectrum resources in wireless networks. The CRR nodes discussed in chapter 5 are mobile radar units capable of extracting target parameters in the radar environment and are able to simultaneously exchange communication data over the CRR network. The communication functionality was an added feature to the CRR node design. On the other hand, the CRR units, proposed in this chapter are wireless devices which have the main purpose of exchanging data over the network. Although they will benefit from the physical location information provided by the cognitive radar aspect of the CRR design, exchange of data over the network is the primary function served by the CRR nodes in the network. For example, the CRR network presented in chapter 5 could be applied to a battlefield scenario in which the soldiers could carry hand-held wireless devices or CRR units, capable to track down a mobile target and at the same time exchange vital radar scene information through the communication link. Whereas in this chapter, the CRR nodes represent the wireless devices like routers and hubs, which have a sole purpose of exchanging data over the network and are empowered with location information on other devices and users through the cognitive radar component in their design. Thus CRR nodes described in this

chapter are primarily radio units and the CRR nodes mentioned in chapter 5 are mainly radar units.

This approach exploits the location information offered by cognitive radar combined with spectrum sensing capability of cognitive radio to aid spectrum and power allocation by minimizing harmful interference among neighboring devices. Such systems require both *coexistence* and *sharing of perception* of radio environment and radar scene. To offer better spectrum resource utilization, entropy of the received signal is employed in order to detect spectrum holes over the network topology. This entropy-based technique also demonstrates superior performance as compared to the conventional method based on energy detection. Simulation results indicate both throughput improvement and interference reduction among neighboring devices.

After designing the approach to spectrum and power allocation for the CRR network, the second aspect of this chapter is to investigate the inclusion of a cognitive mechanism in predicting the spectral holes over the CRR network, by adopting a HMM learning approach. Such a cognitive mechanism would enhance the overall throughput of the entire network, since the wireless devices operating with the CRR nodes would now be able to utilize the white spaces in the spectrum. To realize opportunistic spectrum access, spectrum sensing is applied to detect the presence of spectrum holes. If SUs randomly or sequentially sense the channels until a spectrum hole is detected, significant amount of the scarce spectrum resource will be wasted, since SUs transmit only after a decision has been made. On the other hand, with the use of an intelligent predictive method, SUs can learn from the past activities of PUs on each channel to predict the next channel state. By prioritizing the order in which channels are sensed according to the channel availability likelihoods, the probability that an SU gets a channel upon its first attempt significantly increases, thus reducing the possible waste. Simulation results indicate improvement in throughput and reduction in interference between neighboring wireless devices.

This inclusion of the cognitive mechanism for opportunistic spectrum access over the CRR network facilitates the fusion of the cognitive radar and cognitive radio paradigms. Such a fusion could achieve efficient power and spectrum resource allocation in a wireless network.

6.1 Introduction

6.1.1 Location Aware Spectrum and Power Allocation

Dynamic spectrum access allows frequency bands to be assigned based on the needs of radios without causing significant interference and degradation to the overall throughput. The concept of system cognition proves to be an effective way for intelligent spectrum management in wireless networks [87, 150]. The design and implementation of cognitive radios that constantly adapt their operational modes according to the changing radio environment are therefore necessary to utilize the spectrum more efficiently [151]. In terms of cognitive radio, PUs of spectrum resources are referred to as the authorized users of the radio channels and SUs compete for the channels when PUs are inactive [87, 150]. Hence, one of the most important challenges of cognitive radio is spectrum hole detection, which is to acquire awareness of the frequency usage and existence of PUs in neighboring bands. On the other hand, when SUs are using the vacant channels, cognitive radio can also be aware of initialization of any primary communication activities in their vicinity. The detection of PUs is very important, not only to prevent interference but also to detect any opportunity of communication for SUs as shown in [87].

Location information of cognitive radio can prove to be beneficial in identifying spectrum holes over the network, which can be used to assist in spectrum allocation in order to avoid interference among users in close vicinity. This information can be obtained from a dedicated cognitive radar network as discussed in [37, 88] and chapters 3 and 4. This motivates the design of a novel CRR system presented in the current work. Essentially, we combine the functionalities of cognitive radio and cognitive radar to facilitate localization as well as intelligent spectrum and power allocation. Specifically, in the CRR network studied in this chapter, *radar targets are primarily radio users*, which results in coexistence of radio environment and radar scene. Furthermore, the knowledge about the location and identification of a specific radar target, which uses certain radio channels for communications, can be fed into the cognitive radio network to assist in decision making about spectrum assignment strategies. Similarly, the cognitive radio network can also localize and identify the radio users by analyzing the received signal. This information can be fed into the cognitive radar network to assist in radar waveform design and selection,

target state estimation, and power allocation [37, 88–90]. This leads to sharing of perception of radio and radar scenes under surveillance.

Location information of CRUs can prove to be beneficial in identifying spectral holes over the network. This location information can be used to assist spectrum allocation in order to avoid interference between users in close vicinity. This would allow the design and implementation of this innovative concept of CRR network for various applications like remote detection, sensing, localization, tracking, monitoring, transfer of information between wireless devices or between co-operative sensor nodes.

IEEE 802.11b standard divides the spectrum into 14 overlapping, staggered channels whose center frequencies are 5 MHz apart. Given the separation between channels 1, 6, and 11, the signal on any channel could be sufficiently attenuated to minimally interfere with a transmitter on any other channel located in the vicinity. In this Chapter, we utilize these three channels for spectrum allocation between the CRU.

The proposed CRR network is illustrated in Fig. 6.1. The system consists of cognitive base stations (CBSs) at fixed locations and cognitive mobile stations (CMSs) sharing 3 non-overlapping channels 1, 6 and 11 under IEEE 802.11b. A CBS comprises a joint communication and radar platform (see e.g., the system concepts proposed in [152, 153]). On the other hand, a CMS is a radio user as well as a radar target. For example, a RFID tag could be attached to a CMS for enhanced and recognizable RCS [37]. Subsequently, the radar components in CBSs transmit probing waveforms, which are reflected by CMSs. The relevant information for positioning such as RSS, TOA, and AOA is recorded at CBSs and forwarded to a cognitive engine (CE) through wired links, which is the centralize decision-making entity as shown in Fig. 6.1. The CE then works out the locations of CMSs by triangulation [2]. It is worth emphasizing that, cognitive operations based on the experience gained from the recognized radar-returns from CMSs could be implemented following the cognitive radar concepts developed in [37, 88] and the previous chapters, which include: (i) adaptive and continuous allocation of limited transmit power among the activated CBSs; (ii) intelligent illumination of the environment through antenna beamsteering at CBSs; and (iii) adjusting the set of activated CBSs to achieve the optimized CMS detection and localization.

Subsequently, the spectrum holes are identified by using an information-theoretic

measure known as entropy of the received signal. Conventional spectrum sensing methods include energy detection [154], matched filtering [155], and cyclostationarity-based detection. Owing to its low computational complexity, the energy detection algorithm is commonly used. This method requires knowledge of noise and signal power. Nevertheless, the noise may not be stationary and its variance may not be known *a priori*. On the other hand, matched filtering is the optimum method for spectrum hole detection. However, it demands full knowledge of the signaling features such as bandwidth, operating frequency, modulation type and order, pulse shaping, etc. As a result, this method is not suitable for practical usage.

The entropy-based spectrum sensing can distinguish signals from noises because it is known that a stochastic signal with Gaussian pdf has the maximum entropy [156]. This detection method has been proposed recently [157] and has been proved to be intrinsically robust against noise uncertainty. The existence of radio users over a channel is established when the entropy of the received signal is smaller than a prescribed threshold. Each CMS constantly performs spectrum sensing over the three available channels and notifies the availability of a particular channel to the CE through the radio links with the CBSs as depicted in Fig. 6.1. The CE then decides upon the optimal spectrum allocation strategy and determines the corresponding operational parameters like transmission power for each CMS by utilizing the location information in order to minimize interference and enhance overall system throughput. Eventually, this enables an interference-suppressed secondary radio link between each pair of CMS and its neighboring SU as shown in Fig. 6.1. For simplicity, we will assume that the SU is not a CMS (i.e., it is a radio user but not a radar target).

The key contributions of this Chapter are:

1. Developing an algorithm based upon entropy of the received signal to detect the radio user activity over a channel.

2. Fusing together cognitive radar and cognitive radio paradigms to achieve dynamic spectrum and power allocation over the wireless network.

3. Evaluation of network throughput and comparison of the proposed method with conventional energy based detection.

4. Developing a cognitive spectrum access scheme for CRR units to facilitate

detection of spectral holes over the wireless network.

6.2 CRR Network Model

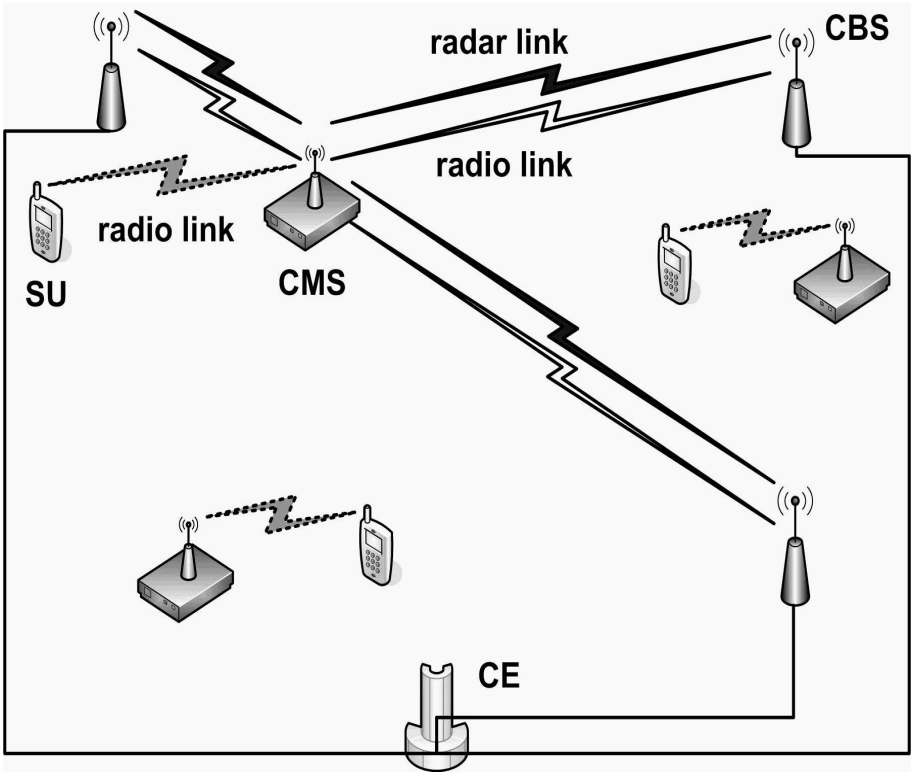

Figure 6.1: CRR network architecture.

We now present the analysis of the entropy-based spectrum sensing undertaken by CMSs. This method establishes the presence or absence of a user over a radio channel based upon hypothesis testing as follows

$$\begin{aligned} H_0 &: y(n) = \eta(n), \qquad\quad n = 0, 1, ..., K-1 \\ H_1 &: y(n) = x(n) + \eta(n), \quad n = 0, 1, ..., K-1 \end{aligned} \tag{6.1}$$

where H_0 and H_1 denote the absence and presence of the user, respectively. $y(n)$ is the received signal, $x(n)$ indicates the transmitted signal from the user, $\eta(n)$ is the AWGN, and K denotes the number of samples over the observation period. Therefore, the distribution of $y(n)$ follows the Gaussian pdf as

$$\begin{aligned} H_0 &: y(n) \sim \mathcal{N}(0, \sigma_\eta^2) \\ H_1 &: y(n) \sim \mathcal{N}(\mu, \sigma_x^2 + \sigma_\eta^2) \end{aligned} \tag{6.2}$$

where $\mathcal{N}(\cdot,\cdot)$ denotes the normal distribution, σ_η^2 is the noise variance, and μ and σ_x^2 are the mean and variance of the signal, respectively.

Applying discrete Fourier transform to (6.1) and (6.2), we obtain

$$\begin{aligned} H_0 &: \mathbf{Y}(k) = \eta(k), \qquad\qquad k = 0, 1, ..., K-1 \\ H_1 &: \mathbf{Y}(k) = \mathbf{X}(k) + \eta(k), \quad k = 0, 1, ..., K-1 \end{aligned} \tag{6.3}$$

where $\mathbf{Y}(k)$, $\mathbf{X}(k)$, and $\eta(k)$ represent the complex vectors of received signal, transmitted signal, and noise, respectively. Alternatively, $\mathbf{Y}(k)$ can also be written as

$$\mathbf{Y}(k) = \frac{1}{K} \sum_{n=0}^{K-1} x(n) \exp\left(-j \frac{2\pi}{K} kn\right) \tag{6.4}$$

The detection strategy involves testing of the information entropy $\mathcal{H}(\mathbf{Y})$, which is a measure of uncertainty associated with the random signal $\mathbf{Y}$, defined as

$$\mathcal{H}(\mathbf{Y}) = -\sum_{i=1}^{I} p(Y_i) \log_2 p(Y_i) \tag{6.5}$$

In the preceding equation, I is the total number of countable states, often referred to as the dimension of the probability space. $p(Y_i)$ denotes the probability of observation of a received signal level, Y_i, such that $\sum_{i=1}^{I} p(Y_i) = 1$. We use the histogram method for entropy estimation as suggested in [157]. Let o be the number of occurrences of received signal strength falling in the ith bin, Hence, $p(Y_i) \approx o_i/O$ with O being the total number of occurrences. The bin width δ can be defined as

$$\delta = \frac{Y_{\max} - Y_{\min}}{I} \tag{6.6}$$

where $Y_{\max}$ and $Y_{\min}$ are the maximum and minimum values of the received signal strength. Following (6.3) and (6.5), the estimated entropy (or the test statistic) is given by

$$\lambda(\mathbf{Y}) = \mathcal{H}(\mathbf{Y}) = -\sum_{i=1}^{I} \frac{o_i}{K} \log_2 \frac{o_i}{K} \tag{6.7}$$

Subsequently, we utilize the above test statistic to evaluate the two hypotheses

for spectrum user detection

$$\begin{aligned} H_0 &: \lambda(\mathbf{Y}) > \lambda_0 \\ H_1 &: \lambda(\mathbf{Y}) \leq \lambda_0 \end{aligned} \tag{6.8}$$

where λ_0 is the threshold determined by the probability of false alarm. The value of λ will decrease according to the convex property of information entropy as the channel changes its state from "free" to "busy". In the next section we will describe the algorithm for adapting transmission parameters of CMSs once spectral holes are identified.

6.3 Spectrum and Power Allocation Algorithm

As described earlier, all the CMSs perform entropy-based spectrum sensing on the three available radio channels and notify the CE about spectrum holes detected in their neighboring regions. The CE takes into consideration the physical locations of all the CMSs acquired through the radar units of the CBSs, and allots the available frequencies with an intention of minimizing interference among neighboring CMSs. It instructs each CMS to occupy a vacant channel and decides upon the transmission power for each CMS with an objective of enhancing the overall system throughput. The capacity of the radio link between two radio users can be expressed as [158, 159]

$$C(\rho, \eta) = B \log_2 \left(1 + \frac{\rho}{1+\eta}\right) \tag{6.9}$$

where $C(\rho, \eta)$ denotes the capacity of the radio link as a function of the SNR ρ, the interference-to-noise ratio (INR) η, and the channel bandwidth B. Therefore, the total capacity (or throughput) of the CRR network can be calculated as

$$\begin{aligned} \bar{C} &= \sum_{l=1}^{3} \sum_{m=1}^{M} C\left(\frac{\alpha_{mm}(l) P_m(l)}{\sigma_\eta^2}, \frac{\sum_{n \neq m} \alpha_{mn}(l) P_n(l)}{\sigma_\eta^2}\right) \\ &= \sum_{l=1}^{3} \sum_{m=1}^{M} C\left(\rho_m(l), \eta_m(l)\right), \qquad n \in \{1, 2, \cdots, M\}. \end{aligned} \tag{6.10}$$

In the preceding equation, $l \in \{1, 2, 3\}$ is the index of the available channel, M is the total number of point-to-point communication links using a particular channel, $\alpha_{mm}(l)$ represents the channel gain of link m using channel l, $\alpha_{mn}(l)$ represents

the channel gain between the transmitter of link n and the receiver of link m, $P_m(l)$ and $P_n(l)$ are the transmission powers for link m and link n, respectively. $\rho_m(l) = \alpha_{mm}(l)P_m(l)/\sigma_\eta^2$ and $\eta_m(l) = \sum_{n\neq m} \alpha_{mn}(l)P_n(l)/\sigma_\eta^2$ are the SNR and INR of link m occupying channel l, respectively. Note that the same wireless link may utilize multiple channels for data communications.

Next, the transmission power of each link is subject to the following constraint

$$\sum_{l=1}^{3} P_m(l) \leq P_0, \quad \forall m. \tag{6.11}$$

We adopt the Lagrange multiplier method in order to derive the power allocation strategy. The stationary point on $\bar{C}$ is found using

$$\frac{\partial \bar{C}}{\partial P_m(l)} = \sum_{l=1}^{3}\sum_{m=1}^{M} \frac{\partial C\left(\rho_m(l), \eta_m(l)\right)}{\partial P_m(l)} = 0. \tag{6.12}$$

Furthermore, following (6.11) and (6.12), we have $\partial C/\partial P_m(l) = \gamma$ (a constant for a particular link). Subsequently, applying the capacity function in (6.10) yields

$$\begin{aligned}
&\frac{\partial C\left(\rho_m(l), \eta_m(l)\right)}{\partial P_m(l)} \\
&= \frac{\partial}{\partial P_m(l)} \left\{ B \ln \left[1 + \frac{\rho_m(l)}{1+\eta_m(l)} \right] \right\} \\
&= \frac{B}{1 + \frac{\rho_m(l)}{1+\eta_m(l)}} \times \left[\frac{1}{1+\eta_m(l)} \frac{\partial \rho_m(l)}{\partial P_m(l)} - \frac{\rho_m(l)}{\left[1+\eta_m(l)\right]^2} \frac{\partial \eta_m(l)}{\partial P_m(l)} \right].
\end{aligned} \tag{6.13}$$

As the INR $\eta_m(l)$ is not a function of the transmission power $P_m(l)$, the above equation can be further simplified by substituting the expressions of $\rho_m(l)$ and $\eta_m(l)$:

$$\frac{B\alpha_{mm}(l)}{\sigma_\eta^2 + \sum_{n\neq m} \alpha_{mn}(l)P_n(l) + \alpha_{mm}(l)P_m(l)} = \gamma. \tag{6.14}$$

Rearranging the above equation yields

$$P_m(l) = \frac{B}{\gamma} - \frac{\sigma_\eta^2 + \sum_{n\neq m} \alpha_{mn}(l)P_n(l)}{\alpha_{mm}(l)}. \tag{6.15}$$

This is similar to the water-filling approach. We then solve (6.15) iteratively in order to find the profile of $P_m(l)$ across all the available channels ($l = 1, 2, 3$) for link m.

The algorithm can be summarized as follows (see also Fig. 6.1).

1. All the CMSs in the CRR network maintain active radar links with the CBSs.

2. The CBSs extract the propagation parameters relevant to positioning by analyzing the backscatter signals from the CMSs, and forward the information to the CE in order to perform centralized CMS localization.

3. The CMSs also inform the CE about the availability of vacant channels using (6.8) in their neighboring regions. This message is sent through the radio links between the CMSs and CBSs.

4. The CE calculates the optimum spectrum and transmission power allocation strategies for each CMS, which are forwarded to all the CMSs via the radio links between the CBSs and CMSs.

5. Each CMS then establishes an interference-suppressed radio link with the SU within its exclusive coverage area.

6. As the CMSs are mobile, the preceding steps are repeated to dynamically update the transmission parameters of each CMS.

6.4 Cognitive Mechanism for Opportunistic Spectrum Access for Cognitive Radios

Coming to the second aspect of this research which is utilizing the cognitive mechanism for devising a predictive opportunistic spectrum access method, one of the early works in applying HMM is [160], in which the authors modeled each channel as a Poisson distribution, and used an HMM to predict the availability of a channel. The HMM was trained with the Baum-Welsh algorithm (BWA) [161] predicting the presence of PUs to avoid transmission collision. An SU would occupy an idle channel until a PU was predicted to become active, and then it will switch to another predicted idle channel. Simulation results showed that the probability of collision can be reduced compared to the random selection case. The authors in [162] applied a prediction method to reduce the number of channel sensing needed to perform. They proposed a novel artificial neural network (ANN) to predict the channel state in order to reduce the sensing energy. The accuracy of the ANN algorithm was compared with the accuracy of HMM in [162]. An entropy based prediction method

was introduced in [163]. Authors looked for the correlated channels to optimize the sensing strategy. In [164], the authors applied maximum likelihood to predict the length of idle period of each channel. By selecting the channel with the longest predicted idle time, they achieved a reduction in the number of channel switching needed.

To realize opportunistic spectrum access, spectrum sensing is applied to detect the presence of spectrum holes. If SUs randomly or sequentially sense the channels until a spectrum hole is detected, significant amount of the scarce spectrum resource will be wasted, since SUs transmit only after a decision has been made. On the other hand, with the use of an intelligent predictive method, SUs can learn from the past activities of each channel to predict the next channel state. By prioritizing the order in which channels are sensed according to the channel availability likelihoods, the probability that an SU gets a channel upon its first attempt significantly increases, thus reducing the possible waste. This research introduces a learning-based HMM to predict the channel activities. Simulation results show that the proposed HMM can predict the channel activities with high accuracy after sufficient training. This algorithm predicts the availability of the channels by only making use of the current state of the spectrum. Furthermore, by incorporating the outcome of the actual channel sense, the algorithm is able to make self-regulation before next decision, so that errors will not propagate.

We present a novel HMM-based learning method to learn the behavior of PUs on a channel and predict their activity in the next time slot. The number of states in the proposed HMM is not fixed and grows as the training proceeds. We demonstrate that this model can avoid propagation of error if an error occurs. The accuracy of the proposed method is studied through simulation. We use a four-channel system to illustrate the average number of channel sensing to be performed by an SU to obtain a spectrum hole within a given probability of success.

6.4.1 Hidden Markov processes

In this study, the spectrum under consideration is divided into K channels and each PU that transmits will occupy one of the channels. The presence of PUs on a channel is represented with a "1" and the absence of PUs is shown with "0". Some simplifications are made in this learning model. We assume that channel sensings

are performed periodically (which is known as the time stamp) and the channel sensing is ideal, i.e., the effects of noise, missed detection and false alarm errors are negligible. An SU uses an HMM-based approach to learn about the PU usage pattern of each channel through observing the outcomes of the channel sensing. Using the trained HMM, SUs predict the availability of the channels for possible usage in the next time slot through the algorithm to be introduced shortly.

A Hidden Markov Process is a doubly stochastic process with hidden states that generate observations [118]. It is denoted mathematically as $\{X_t, Y_t; t \in \mathbf{N}\}$, where t denotes the time stamp index which takes an integer number. $X(t)$ is the N-state hidden stochastic process, and $X(t) \in \mathcal{Y}$ where $\mathcal{Y}$ is the N possible states whose transition probabilities are described by the $N \times N$ transition matrix $\mathbf{A}$. $Y(t)$ is the stochastic process of the observations, and $Y(t) \in \mathcal{O}$ where $\mathcal{O}$ is the finite set of possible observations with M possible outcomes. The distribution of the observation outcomes at each state is described by the respective column vector of the $N \times M$ emission matrix $\mathbf{B}$. The mathematical model that can generate a hidden Markov process is called HMM. Similar to the HMM defined in chapter 4, this HMM model can be described as $\lambda = \{\mathbf{A}, \mathbf{B}, \pi\}$. One of the main challenges in HMM is how to adjust the model parameters ($\lambda = \{\mathbf{A}, \mathbf{B}, \pi\}$), to maximize $\Pr(O|\lambda)$, where $\Pr(\cdot)$ represents probability.

In the following, we shall differentiate this approach with the conventional BWA-based HMM approach.

6.4.2 Conventional BWA-based HMM

BWA [161] is the most commonly used method to estimate the maximum likelihood of λ. To be able to predict, we have to gather some information from the channel activities over the past time slots. Suppose that we observe the channel for T time slots; having the HMM (λ), the channel state for the next time slot can be predicted by the following rule

$$\hat{Y}(t+1) = \begin{cases} 1 & \Pr(\zeta, 1|\lambda) \geq \Pr(\zeta, 0|\lambda) \\ 0 & \Pr(\zeta, 1|\lambda) < \Pr(\zeta, 0|\lambda), \end{cases} \tag{6.16}$$

where $\zeta = \{Y(t-T+1), ..., Y(t)\}$ denotes the past T observations.

In order to apply BWA, first the number of states (N) needs to be defined.

Since there is no information about the current state and previous states at the time when parameters are estimated [161], hereafter we shall refer it as unknown-state sequence HMM (USS-HMM). Since this approach needs to perform parameter estimation in real-time for every prediction, the computation complexity is high, as will be discussed later. Other challenges for this approach include defining the optimum number of states (N) and the observation sequence length (T) for an accurate estimation.

6.4.3 Proposed HMM

Under the assumption that the statistics of the channel activities remain unchanged, which means that the Doppler spread of the signal remains less than the signal bandwidth, the prediction will be performed much faster through training. This means that we consider a wide sense stationary channel activity instead of a time-varying channel. The functional block diagram of the proposed method is shown in Fig. 6.2. As shown in the figure, the HMM is trained with a certain number of observations until a satisfactory convergence of the HMM parameters is achieved. After training, the HMM predictor only needs the current observation to predict the next channel state. This is unlike USS-HMM, where there is a need to use a sequence of observations to iteratively compute every prediction. In this algorithm, re-train is needed only if the channel statistics have changed. In order to prevent the propagation of the error in predictions, the HMM model is retrained if the channel statistics change.

The channel state at the next time slot will be predicted by

$$\hat{Y}(t+1) = \begin{cases} 1 & \Pr(S(t), 1|\lambda) \geq \Pr(S(t), 0|\lambda) \\ 0 & \Pr(S(t), 1|\lambda) < \Pr(S(t), 0|\lambda), \end{cases} \tag{6.17}$$

where $S(t)$ is the HMM state at time slot t. In this approach, since the proposed HMM knows the state sequence as well as the observation sequence, to distinguish from USS-HMM, the proposed HMM is referred to as the known-state sequence HMM (KSS-HMM).

We now provide more details about the HMM model as shown in Fig. 6.3. The number of states (i.e. N) in this model grows dynamically as learning proceeds. zero represents the initial state. The negative and positive states represent unused

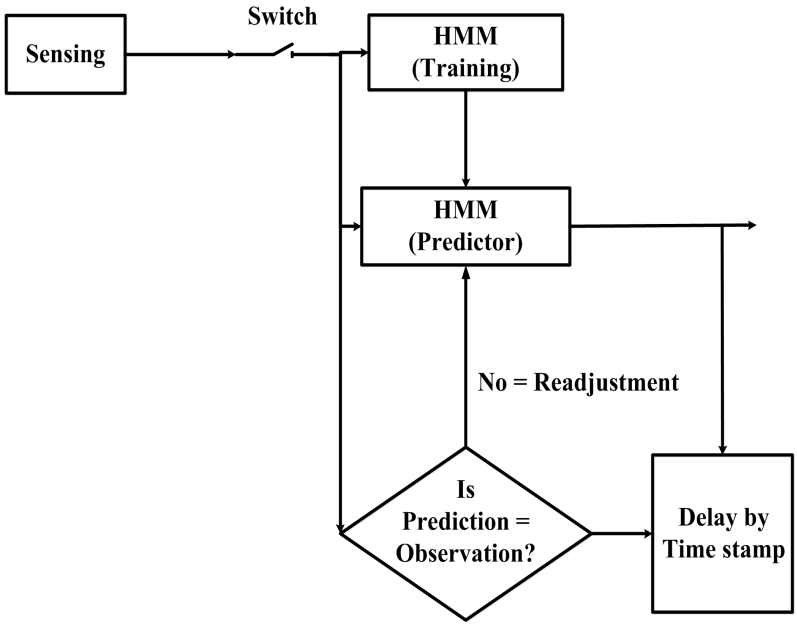

Figure 6.2: Proposed training-based HMM system model

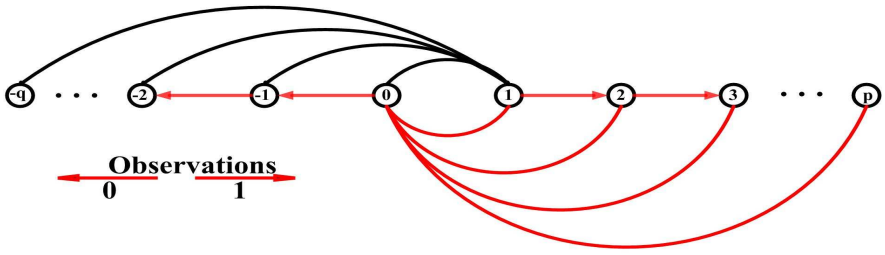

Figure 6.3: Proposed HMM state transition

and in-use channels, respectively. Being at a positive state, by observing a one, the run length increases and the system moves to the next state, and we go back to the state zero after observing a zero. On the other hand, the system will sequentially move to a more negative state by observing a zero, and will jump forward to the state one immediately after observing a one while we are at a non-positive state. If there is insufficient positive or negative states corresponding to higher run length, the system will expand itself on its move by adding in new states.

We use sufficient number of observations during the training phase to estimate λ [161]. In KSS-HMM, $\pi(0) = \pi(1) = \frac{1}{2}$ and for all other states π is zero. Moreover, $N = q+p+1$ (q and p are defined in Fig. 6.3) and $M = 2$. When all of the paths are

known, then it is possible to count the number of times each particular transition or output observation is applied in a set of training data. It has been proven in [161] that counting functions, say $\Phi_{mn}(x(t))$ for the state transitions and $\Phi_{kn}(y(t))$ for the output observations provide the maximum likelihood estimates for the desired model parameters, such that

$$\hat{a}_{mn} = \frac{\Phi_{mn}(x(t))}{\sum_{n} \Phi_{mn}(x(t))}, \tag{6.18}$$

$$\hat{b}_{kn} = \frac{\Phi_{kn}(y(t))}{\sum_{n} \Phi_{kn}(y(t))}. \tag{6.19}$$

$\Phi_{mn}(x(t))$ represent the number of state transitions from state m to state n and $\Phi_{kn}(y(t))$ represents the number of k observations while in state n. Thus $\hat{a}_{mn}$ and $\hat{b}_{kn}$ represent the relative frequency of state and observation instances as mentioned in [118]. The basis of the proposed HMM is therefore to account the probabilities of occurrence of different run lengths of ones (or zeros). Clearly, the number of states (N) depends on how long the algorithm is trained, and hence it also affects the accuracy of the training. Although a disadvantage of the algorithm is that we have to deal with a situation where the number of states dynamically grows during the training, there is a nice property about $\mathbf{A}$ and $\mathbf{B}$ in this model. Since the HMM adopted in the algorithm has only two possible transitions from one state, therefore the transition matrix $\mathbf{A}$, is a sparse matrix. It is not difficult to figure out that the non-zero elements in $\mathbf{A}$ is actually identical to the elements in the emission matrix. In the following, we shall see that this simplifies the prediction process and enables a corrective action to be taken if a prediction is in error.

The transition probability between any two states is denoted by

$$a_{ij} = \Pr(x(t) = s_i | x(t-1) = s_j), \tag{6.20}$$

where s_i and s_j are the states at time t and $t-1$, respectively, and a_{ij} denotes the transition probability presented in the (i, j) element of the matrix $\mathbf{A}$.

During the learning or training process, the transition and emission probability over T observations can be easily calculated by (6.18) and (6.19). As there are only two possible observation states, HMM is designed in a way that only two states

are reachable from the current state. Moreover the probability of transition from current state to either of the two states is equal to the probability of observing either a zero or a one. Thus having the emission matrix ($\mathbf{B}$), means having the probability of next state as well as the distribution of observations.

$$\begin{cases} b_{1,i} = a_{i,i+1}, b_{0,i} = a_{i,0} & i > 0 \\ b_{0,i} = a_{i,i-1}, b_{1,i} = a_{i,1} & i \leq 0 \end{cases} \tag{6.21}$$

This property makes the states sequence trackable. With this property, the proposed method is not required to compute the maximum likelihood over a long sequence of observations for each prediction. Retraining the KSS-HMM is only needed when the behavior of PUs on the channel is changing.

A minimum separation factor ($0 \leq \delta < 1$) can be added to the decision criterion, so it will look like:

$$\Pr(S(t), 0|\lambda) - \Pr(S(t), 1|\lambda) > \delta. \tag{6.22}$$

The purpose of prediction is to prioritize which channel to be sensed in the next time instant. If (6.22) is satisfied, SU will sense the channel and transmit over the channel only if the prediction is correct. On the other hand, if (6.22) is not satisfied, SU will decide that the channel is occupied on $t+1$. It is obvious that if $\delta = 0$, (6.22) is equivalent to (6.17). In case of an inaccurate prediction, the system will notice the prediction error after the sensing. Since $S(t+1)$ only depends on observation outcome rather than predicted result, the system will move to the correct state and errors will not propagate.

6.5 Simulation Results

6.5.1 Simulation Results for Location Aware Spectrum and Power Allocation

For the purpose of simulation, we assume a square grid of 10×10 CMSs sharing the three available channels under IEEE 802.11b. Fig. 6.4 indicates the initial random channel assignment over the CMSs. Each CMS occupies a square footprint and communicates with an SU within this exclusive coverage area. Each color (blue, red, or yellow) represents one of the three available channels (1, 6 and 11). The

transmission power for each CMS is uniformly distributed between 0 and P_0 for the first-stage power allocation. The area of dark circle at the center of each square footprint represents the transmission power of the corresponding CMS. Apparently, the initial channel assignment is susceptible to severe interference as can be seen from Fig. 6.4, where a large number of neighboring cells utilize the same radio channel for communications.

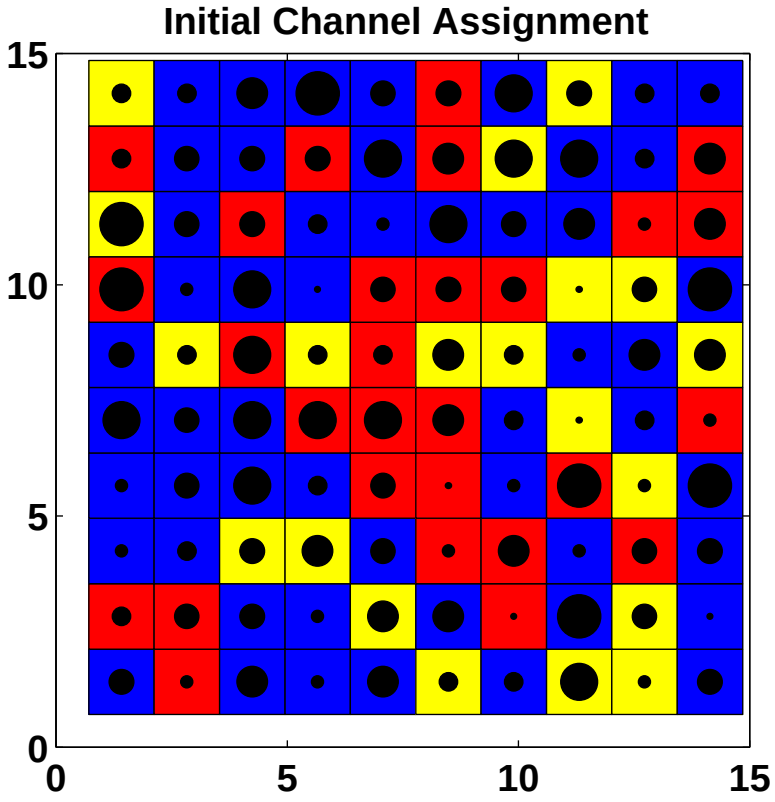

Figure 6.4: Initial random channel assignment.

Next, each CMS constantly maintains radar links with the CBSs. The propagation parameters such as received signal strength, time-of-arrival, and angle-of-arrival obtained at more than three non-collocated CBSs can be used to localize the CMSs. For simplicity, it is assumed that the CMS locations have been successfully estimated (e.g., by following the methodologies proposed in [37, 88]). Once the location of each CMS is established, the CE decides upon the spectrum allocation strategy based on the knowledge of spectrum holes or vacant channels around each CMS, which is imparted to the CE via the radio links between CMS and CBS.

Subsequently, the transmission power of each CMS is adjusted iteratively as per the power allocation algorithm. We consider a simplified interference scenario,

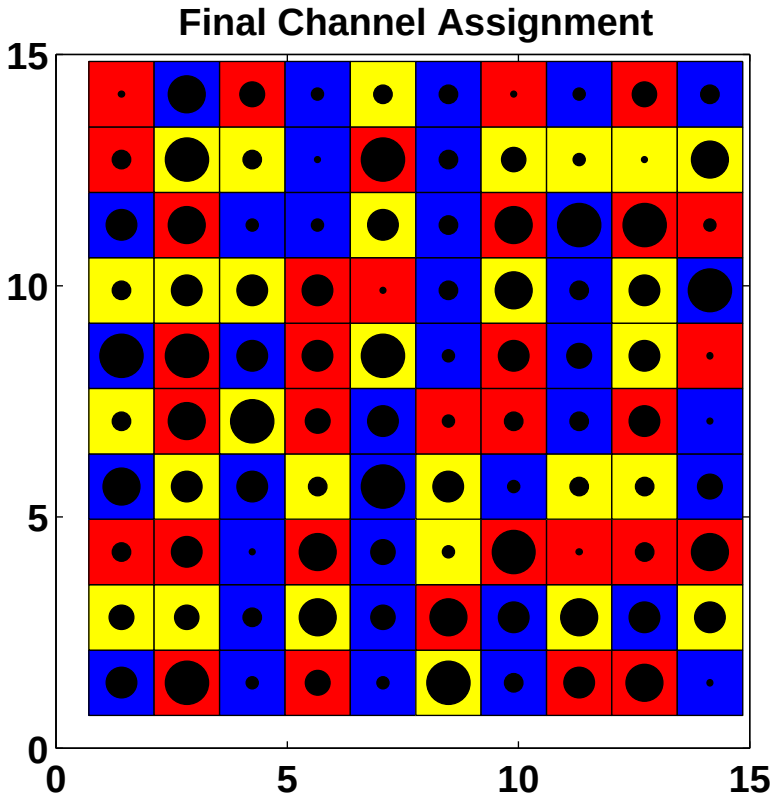

Figure 6.5: Final location-aware channel assignment.

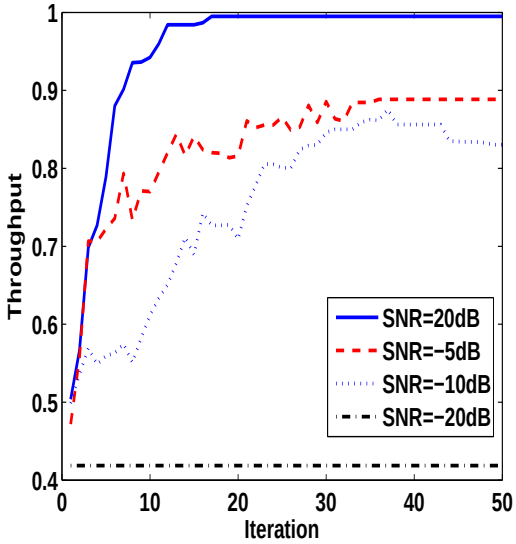

Figure 6.6: CRR network throughput.

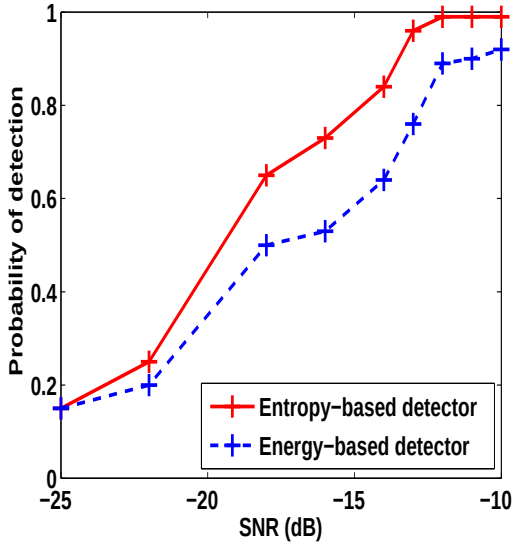

Figure 6.7: Performance of spectrum user detection.

where the two channel gains α_{mm} and α_{mn} in (6.10) are assumed to be two fixed constants. Furthermore, only the first-tier interferers (i.e., for each CMS under consideration, its immediate 8 neighboring cells) are taken into account for power allocation using (6.15). The main intention of this spectrum and power allocation algorithm is to avoid clustering of CMSs using the same channel, and to distribute transmission power according to the water-filling approach in order to enhance the overall throughput. Fig. 6.5 indicates the final channel assignment. In this case, we observe lower number of neighboring CMSs sharing the same channel. This indicates reduction of interference among CMSs.

Fig. 6.6 illustrates the throughput of the overall system. Each characteristics curve in this plot represents a throughput at a particular value of SNR. It can be seen that the throughput converges after a certain number of iterations for each SNR. In general, faster convergence is achieved for higher SNRs. Nevertheless, in the case of very low SNR (SNR $= -20$ dB), more iterations fail to result in improved throughput.

Finally, Fig. 6.7 demonstrates the performance of the entropy-based detector as compared against the energy-based detector. These results have been generated by averaging over 100 simulations at different SNRs. The probability of false alarm has been fixed at 0.15 for evaluating the value of the threshold λ_0 in (6.8). As discussed previously, the entropy-based detector does not require any previous knowledge about transmission parameters of the signal or noise characteristics. It is

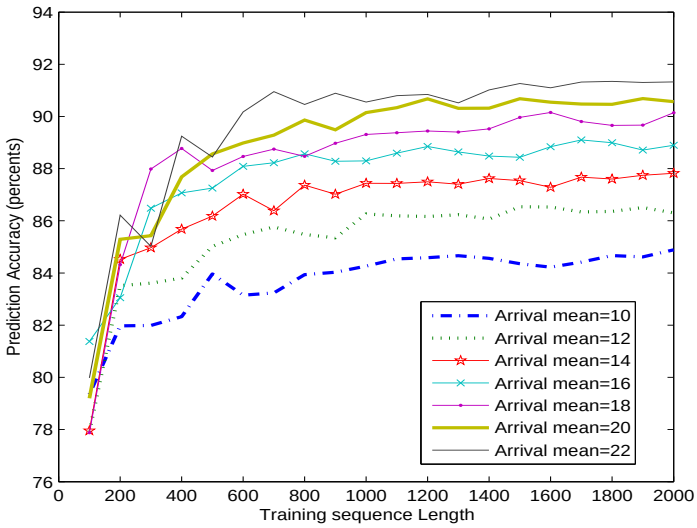

Figure 6.8: KSS-HMM prediction accuracy on test data set

also quite robust and insensitive to noise uncertainty. Thus its performance is superior as compared to the energy-based detection in terms of probability of spectrum user detection even at lower SNRs as can be seen from Fig. 6.7.

6.5.2 Simulation Results on Cognitive Mechanism for Opportunistic Spectrum Access

This section presents some simulation results of KSS-HMM and USS-HMM. To evaluate the prediction accuracy, the statistics of PU activities on each channel are assumed to remain unchanged over the simulation period. It is assumed that the average traffic intensity (γ) calculated by (6.23) is equal to 0.5, which means that the mean of ON and OFF periods are considered equal.

$$\gamma = \frac{\text{Mean ON time}}{\text{Mean Arrival Time}} \tag{6.23}$$

Moreover, we set $\delta = 0$ for the current simulations. Channel activities are generated as training and test datasets for various mean arrival times, from 10 to 20 time slots between arrivals. Fig. 6.8 shows the KSS-HMM prediction accuracy for different mean arrival (poisson) values. As expected the prediction accuracy improves by increasing the length of the training sequence. Clearly using 1000 samples is sufficiently good to generate stable training results.

In Fig. 6.9, the total error probability, and error probabilities in prediction of the

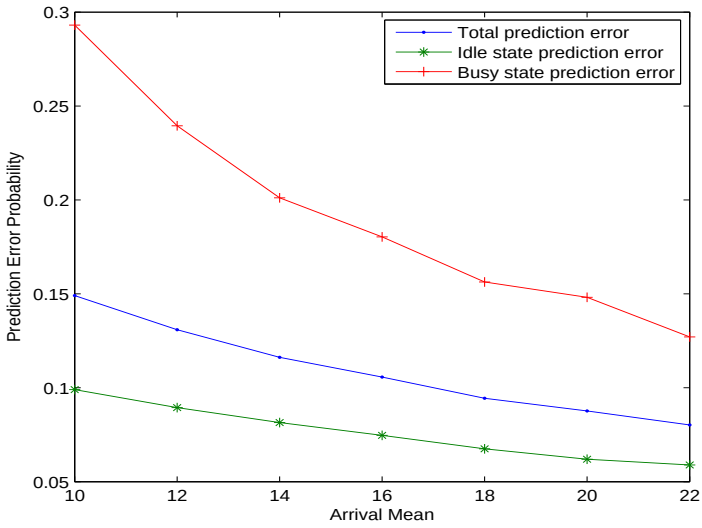

Figure 6.9: Prediction accuracy for a channel

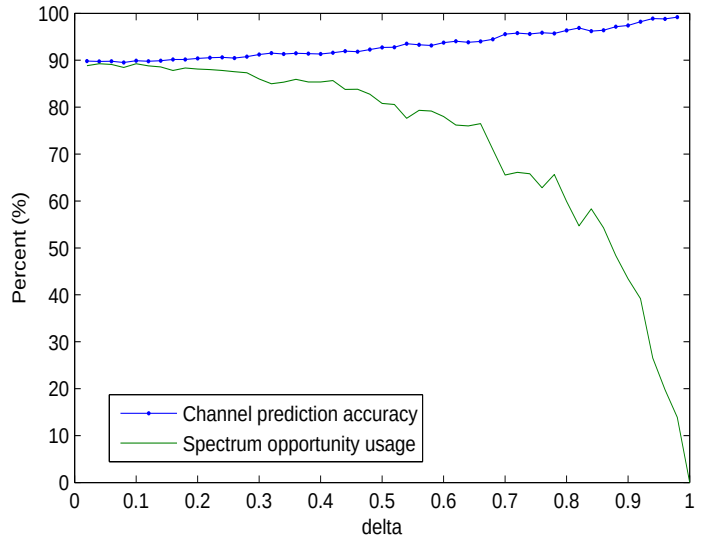

Figure 6.10: Effect of δ value on channel prediction accuracy and spectrum opportunity usage

idle and busy states, are illustrated for several arrival means. P_e (busy) represents the probability that the channel is busy, but the HMM mistakenly predicts as an idle state. On the other hand, P_e(Idle) shows the probability that a busy state is predicted, but the channel is actually idle. It is observed that by increasing the arrival mean, the accuracy increases. This is due to the fact that if more transitions are observed, the accuracy in estimating the transition probabilities is improved. In the simulation, the KSS-HMM is trained with 1000 samples, and tested on the binary sequence of $30,000$ samples.

In [160], the authors tested their developed HMM in looking for spectrum opportunity among four channels. PU activities on each channel followed Poisson

Table 6.1: ON/OFF period means for different channels

Channel	1	2	3	4
ON period mean	5	7	4	8
OFF period mean	5	7	4	8

Table 6.2: Comparison of KSS-HMM and USS-HMM prediction accuracy

HMM type	Arrival mean						
	10	12	14	16	18	20	22
KSS-HMM	0.8388	0.8524	0.8830	0.8936	0.9016	0.9088	0.9192
USS-HMM	0.8478	0.8588	0.8858	0.8918	0.9076	0.9124	0.9184

distribution with equal mean for the ON and OFF durations. A similar approach is used to test the performance of the proposed HMM. In this scenario, we trained a KSS-HMM for each channel with 1000 samples and tested for $30,000$ samples. The effect of different values of δ on the channel prediction accuracy and the percentage that spectrum holes are properly made use of, are shown in Fig. 6.10. In this simulation, a channel prediction is said to be accurate if we successfully predict an empty channel for transmission among the four channels. As can be seen, the increase of δ leads to increase in the accuracy, but reduces the number of opportunities that are caught by the SU. Another issue which must be discussed is the acceptable accuracy of predicting an idle channel in a time slot. Table 6.1 shows the mean of Poisson distribution for both ON and OFF periods. Fig. 6.11 compares the learning based and random channel selection approaches for the aforementioned scenario. As it could be expected the random selection succeeds only about 50% of time, while the learning based approach caches the available channel on its first attempt in over 90% of its attempts. In learning based approach, only less than 0.02% of attempts were not successful until checking the last channel, while about 7% of random channel selection attempts were unsuccessful till the last check. Compared to KSS-HMM, the complexity of USS-HMM is much higher. The training complexity for KSS-HMM is $2(T+1)\times N$, where T is the training sequence length and N is the number of states. Furthermore, KSS-HMM training is done only once and after that whenever it is required. Therefore the actual training calculations required for each KSS-HMM prediction is $(2(T+1)\times N)/\tau$, where τ is the number of predictions made without the need for retraining. Moreover, each KSS-HMM decision lays only on a hyperplane test. On the other hand, USS-HMM has N^2T calculations after the

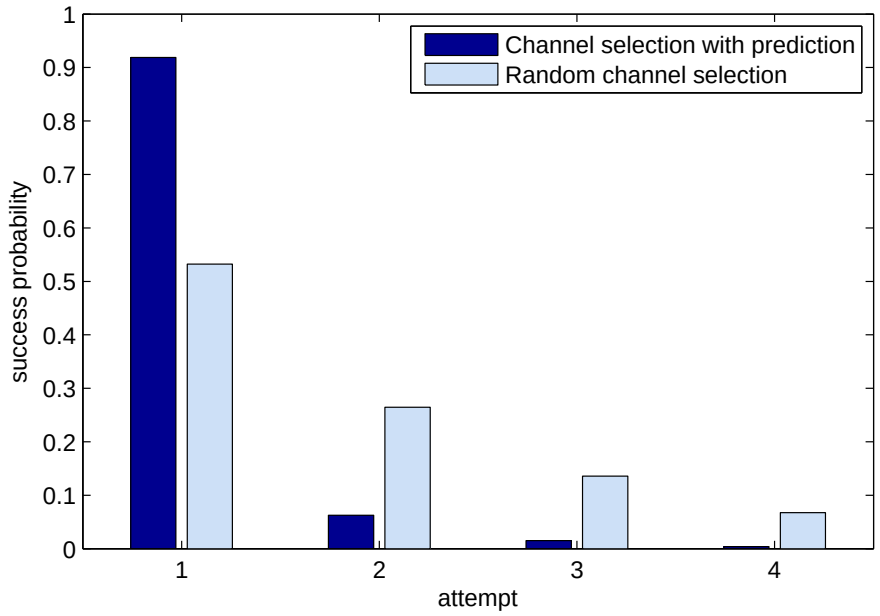

Figure 6.11: Comparison of channel selection with prediction and random channel selection

training [162], and it must be retrained after each prediction, while each iteration of training needs MN^2T calculations and it usually requires minimum 100 iterations to converge [161]. M is the number of observation symbols (here M=2).

The prediction accuracy of KSS-HMM and USS-HMM, over 5000 time slots, is presented in Table 6.2. The KSS-HMM is trained once over 1000 time slots, while the three-state USS-HMM is trained with 150 time slots for each prediction. The results show that USS-HMM works slightly better on average, but there are situations where KSS-HMM has slightly better accuracy.

6.5.3 Chapter Summary

In this chapter, we presented the integration of cognitive radio and radar concepts in order to facilitate efficient spectral resource allocation among the wireless devices. Simulation results demonstrate superior performance of the proposed algorithm in terms of interference minimization and enhancement in throughput. The innovation of CRR devices capable of dynamically adapting their operational modes in accordance with the changing environments and the needs of the wireless devices seems to offer increased productivity and adaptability as compared to the traditional radars and radio systems. Also the integration of these two concepts opens up new possibilities for implementation of improved sensing, detection, co-operative communication and intelligent signal processing algorithms for wireless applications.

The second part of this chapter focused on HMM-based cognitive algorithm which can be used for channel activity prediction of the CRR devices. As investigated in the second part, the CRR nodes can detect spectral holes over the network through the predictive opportunistic spectrum access algorithm. This enhances the overall throughput of the CRR network. The algorithm is simple in principle and predictions can be made without the need to perform sophisticated optimization. Using the fact that channel sensing is still necessary before SU transmission even prediction is made, the algorithm can make use of this observation later to self-correct any prediction error occurs. The performance of the prediction algorithm is examined through simulation and compared with the random channel access method. This study also has shown that the proposed HMM model can achieve nearly the same performance as the conventional USS-HMM model in the channel selection problem.

Chapter 7

Conclusion and Future Work

In this thesis, we have investigated various cognitive architectures for designing radar systems. The striking difference between traditional and cognitive radar system designs is the ability of the radar receiver to offer a cognitive feedback to the transmitter, which enables it to implement intelligent illumination of the radar scene. The major advantage of such a system design is the ability of the radar system to adapt to the dynamically varying radar environment. The radar system can adapt its operational parameters by constantly interacting with the radar environment and gaining updated target parameter information. Such an architecture enables the intelligent target illumination strategies like adaptive waveform design and intelligent selection of radar units for a network scenario.

The motivation behind this research was to explore various cognitive mechanisms, which would enable the design of intelligent radar systems capable of adapting its operational modes in accordance with target dynamics. In Chapter 3, a cognitive waveform optimization approach was investigated for MIMO radar systems. In this approach we adopted a two-step procedure based on MI optimization to design the MIMO radar waveforms. The objective behind such a waveform optimization approach was to gain the information on target parameters through the proposed iterative optimization approach. The first of this two step procedure comprised of waveform design based on maximization of MI between estimated target impulse and received radar signal with an objective to "match" the transmitted waveform with the target impulse response. This step was based on recent works on information theory based waveform design methods. The second step was developed in order to minimize the MI between the successive received radar echoes in order to

ensure that the subsequent received signals remain statistically independent over the temporal domain in a bid to gain updated target impulse response estimate. Both these approaches work in tandem to produce significant performance gains in terms of detection probability and target parameter extraction capability of the radar system. In Chapter 4, we investigated the HMM based tracking application wherein the HMM based model estimated the target dynamics by learning the trajectory. This tracking approach was utilized to predict the nearest set of radar units in the vicinity of the target in the next time instant. This enabled significant power savings and also made possible the realization of the track-before-detect mechanism. As demonstrated by the simulation results the tracking capability of the proposed approach was comparable to the standard benchmark methods for target tracking even though only a limited set of radar units were required to perform the cognitive detection of the target. This approach was also found to be suitable to track fast moving targets since the HMM tracking model allowed continual learning on the target dynamics. The algorithm was not only found to have comparable execution times with the standard benchmark methods but also provided better localization performance with respect to the step size of the target. In Chapter 5, we investigated the joint communication-radar waveform design method based on cognitive principles. This approach allowed the distinct wireless nodes to exchange radar scene information between themselves using the same waveform used for performing radar operations. The motivation of this joint cognitive radar radio (CRR) waveform design method was in mission critical and military applications. In such applications, there is a need to exchange communications data as well as perform radar operations using a smart waveform design approach. Simulation results have demonstrated that performance of such a waveform design in terms of BER and throughput is comparable to the joint communication-radar design mechanisms mentioned in the literature. The radar performance in terms of target detection and parameter extraction is greatly enhanced by utilizing cognitive approach for waveform selection. In Chapter 5 the CRR nodes are mobile radar units with a communication capability. Whereas in Chapter 6 the CRR units are radio users equipped with location information of other neighboring CRR units provided through a radar module. The possible integration of cognitive radio and cognitive radar paradigms is investigated in this chapter. By achieving such a fusion of paradigms efficient resource utilization in terms of transmission power and spectral resources could be achieved over a wireless network.

This work focused on the location aware spectrum and power allocation for wireless network. The location information on wireless devices gained through utilization of cognitive radar units was coupled with the spectrum sensing ability of the cognitive radio mechanism to realize this intelligent resource allocation algorithm. In this chapter we also investigated the cognitive opportunistic spectrum access mechanism in order to efficiently sense the wireless environment to gain information over possible spectral holes. This information could be exploited by SUs for communication thus enhancing the overall throughput of the wireless network.

Future works in this research field could involve extending this idea of cognitive radar network system, which incorporates several radars working together in a cooperative manner with the goal of realizing a remote-sensing capability far in excess of what the radar components are capable of achieving individually. In the extended target recognition application, the cognitive radar network can provide more robust detection performance, more accurate position estimation, and more reliable target aspect angle for each radar. By utilizing a cognitive architecture for MIMO radars, the issue of target-aspect sensitivity can be solved even for maneuvering targets by adapting the radar transmission parameters like the waveform shape, power and frequency. In this way, cognitive mechanisms could be applied for the development of more complex radar architectures like on-board radars in remote air-surveillance. Cognitive radar system design could be extended to implement waveform design solutions for hostile indoor and outdoor channel environments where the radar channels are highly time variant and the target responses are suppressed by strong clutter or non-target sources in applications like tracking movement of human subjects in an indoor environment. Cognitive radars could also be designed for bio-medical applications like synthesis of body area networks for remotely observing and monitoring the physiological and physical conditions of patients.

Another interesting avenue for research is the fusion of cognitive radar and cognitive radio paradigms which can result in the development of cognitive dynamic systems for wireless applications. Both of these models strive to impart intelligence to traditional wireless systems which utilize a static framework for resource management and hence are not able to cope up with the ever increasing demands of wireless devices being deployed. From a technological perspective, the innovation of CRR devices presented in this thesis, which are capable of dynamically adapting their operational modes in accordance with the changing environments and the needs of the

wireless devices, seems to offer increased productivity and adaptability as compared to the traditional radars and radio systems. The CRR system design and results presented in this thesis could be extended to flexible mobile sensor network applications such as new ambient intelligence applications in environment monitoring, robotics, intelligent cars and traffic systems, smart homes, health monitoring and industrial automation. The results presented in this thesis open up new possibilities for implementation of improved sensing, decentralized detection, development of cooperative radar systems and intelligent signal processing algorithms for wireless and radar applications.

References

[1] B. R. Mahafza and A. Z. Elsherbeni, *Matlab Simulations for Radar Systems Design.* 1^{st} Ed., CRC Press,Chapman and Hall, 2005.

[2] M. L. Skolnik, *Introduction to Radar systems,* 3^{rd} *Ed.* McGraw-Hill Publications, New York, 2001.

[3] M. Bell, "Information theory and radar waveform design," *IEEE Trans. Inform. Theory*, vol. 39, no. 12, pp. 1578–1597, 1993.

[4] J. R. Guerci, *Space-Time Adaptive Processing.* Artech House, Norwood, MA, 2003.

[5] J. Guerci and E. Baranoski, "Knowledge-aided adaptive radar at DARPA: an overview," *IEEE Signal Process. Mag.*, vol. 23, no. 1, pp. 41–50, Jan. 2006.

[6] P. Stoica, J. Li, X. Zhu, and J. Guerci, "On using a priori knowledge in space-time adaptive processing," *IEEE Trans. Signal Process.*, vol. 56, no. 6, pp. 2598–2602, June 2008.

[7] R. Romero and N. Goodman, "Information-theoretic matched waveform in signal dependent interference," in *Proc. IEEE Radar Conference*, May 2008, pp. 1–6.

[8] D. Garren, M. Osborn, A. Odom, J. Goldstein, S. Pillai, and J. Guerci, "Enhanced target detection and identification via optimised radar transmission pulse shape," *IEE Proceedings Radar, Sonar and Navigation*, vol. 148, no. 3, pp. 130–138, June 2001.

[9] N. Goodman, P. Venkata, and M. Neifeld, "Adaptive waveform design and sequential hypothesis testing for target recognition with active sensors," *IEEE J. Sel. Topics Signal Process.*, vol. 1, no. 1, pp. 105–113, June 2007.

[10] Y. Wei, H. Meng, Y. Liu, and X. Wang, "Radar phase-coded waveform design for extended target recognition under detection constraints," in *Proc. IEEE Radar Conference (RADAR)*, May 2011, pp. 1074–1079.

[11] E. Fishler, A. Haimovich, R. Blum, D. Chizhik, L. Cimini, and R. Valenzuela, "MIMO radar: an idea whose time has come," in *Proc. the IEEE Radar Conference.*, April 2004, pp. 71–78.

[12] D. Rabideau and P. Parker, "Ubiquitous MIMO multifunction digital array radar," in *Proc. Thirty-Seventh Asilomar Conference on Signals, Systems and Computers.*, vol. 1, Nov. 2003, pp. 1057–1064.

[13] J. Zhang, H. Wang, and X. Zhu, "Adaptive waveform design for separated transmit/receive ULA-MIMO radar," *IEEE Trans. Signal Process.*, vol. 58, no. 9, pp. 4936–4942, Sept. 2010.

[14] T. Barnard and D. Weiner, "Non-Gaussian clutter modeling with generalized spherically invariant random vectors," *IEEE Transactions on Signal Processing*, vol. 44, no. 10, pp. 2384–2390, Oct 1996.

[15] L. Brennan and L. Reed, "Theory of Adaptive Radar," *IEEE Transactions on Aerospace and Electronic Systems*, vol. AES-9, no. 2, pp. 237–252, March 1973.

[16] D. Zhang, F. Xia, Z. Yang, L. Yao, and W. Zhao, "Localization technologies for indoor human tracking," in *Proc.* 5^{th} *International Conference on Future Information Technology (FutureTech)*, May 2010, pp. 1–6.

[17] P. Dutta, A. Arora, and S. Bibyk, "Towards radar-enabled sensor networks," in *Proc. The Fifth International Conference on Information Processing in Sensor Networks (IPSN)*, 2006, pp. 467–474.

[18] R. Thoma, O. Hirsch, J. Sachs, and R. Zetik, "UWB sensor networks for position location and imaging of objects and environments," in *Proc. The Second European Conference on Antennas and Propagation (EuCAP)*, Nov. 2007, pp. 1–9.

[19] J. Choliz, M. Eguizabal, A. Hernandez-Solana, and A. Valdovinos, "Comparison of algorithms for UWB indoor location and tracking systems," in *Proc.*

IEEE 73^{rd} *Vehicular Technology Conference (VTC Spring)*, May 2011, pp. 1–5.

[20] S. Gezici, Z. Tian, G. Giannakis, H. Kobayashi, A. Molisch, H. Poor, and Z. Sahinoglu, "Localization via ultra-wideband radios: a look at positioning aspects for future sensor networks," *IEEE Signal Process. Mag.*, vol. 22, no. 4, pp. 70–84, July 2005.

[21] F. Cao and D. Wang, "Accurate wireless location and tracking technique for indoor UWB non-linear/non-gaussian systems," in *Proc. Third International Conference on Communications and Mobile Computing (CMC)*, April 2011, pp. 449–452.

[22] M. Najar, J. Huerta, J. Vidal, and J. Castro, "Mobile location with bias tracking in non-line-of-sight," in *Proc. IEEE International Conference on Acoustics, Speech, and Signal Process. (ICASSP)*, vol. 3, May 2004.

[23] D. Garmatyuk, J. Schuerger, Y. Morton, K. Binns, M. Durbin, and J. Kimani, "Feasibility study of a multi-carrier dual-use imaging radar and communication system," in *Proc. European Radar Conference (EuRAD).*, Oct. 2007, pp. 194–197.

[24] S. C. Surender and R. M. Narayanan, "UWB noise-OFDM netted radar: Physical layer design and analysis," *IEEE Trans. Aerosp. Electron. Syst.*, vol. 47, no. 2, pp. 1380–1400, Apr. 2011.

[25] D. Garmatyuk, J. Schuerger, Y. Morton, K. Binns, M. Durbin, and J. Kimani, "Feasibility study of a multi-carrier dual-use imaging radar and communication system," *Proc. European Radar Conference (EuRAD)*, pp. 194–197, 2007.

[26] D. Garmatyuk and J. Schuerger, "Conceptual design of a dual-use radar/communication system based on OFDM," in *Proc. IEEE Military Communications Conference (MILCOM)*, Nov. 2008, pp. 1–7.

[27] D. Garmatyuk, J. Schuerger, and K. Kauffman, "Multifunctional software-defined radar sensor and data communication system," *IEEE Sensors Journal*, vol. 11, no. 1, pp. 99–106, Jan. 2011.

[28] C. Sturm, T. Zwick, and W. Wiesbeck, "An OFDM system concept for joint radar and communications operations," *Proc. IEEE* 69^{th} *Veh. Technol. Conf. (VTC Spring)*, pp. 1–5, 2009.

[29] D. Garmatyuk and K. Kauffman, "Radar and data communication fusion with UWB-OFDM software-defined system," in *Proc. IEEE International Conference on Ultra-Wideband (ICUWB)*, Sept. 2009, pp. 454–458.

[30] S. Blunt, M. Cook, and J. Stiles, "Embedding information into radar emissions via waveform implementation," in *Proc. International Waveform Diversity and Design Conference (WDD)*, Aug. 2010, pp. 195–199.

[31] G. Lellouch and H. Nikookar, "On the capability of a radar network to support communications," in *Proc.* 14^{th} *IEEE Symposium on Communications and Vehicular Technology*, Nov. 2007, pp. 1–5.

[32] S. Surender, R. Narayanan, and C. Das, "Performance analysis of communications and radar coexistence in a covert UWB OSA system," in *Proc. IEEE Global Telecommunications Conference (GLOBECOM)*, Dec. 2010, pp. 1–5.

[33] L. Wang, J. McGeehan, C. Williams, and A. Doufexi, "Application of cooperative sensing in radar-communications coexistence," *IET Communications*, vol. 2, no. 6, pp. 856–868, July 2008.

[34] S. Haykin, "Cognitive radar networks," in *Proc. IEEE International Workshop on Computational Advances in Multi-Sensor Adaptive Processing*, Dec. 2005, pp. 1–3.

[35] ——, "Cognitive radar: A way of the future," *IEEE Signal Process. Mag.*, vol. 23, no. 1, pp. 30–40, Jan. 2006.

[36] N. A. Goodman, P. R. Venkata, and M. A. Neifeld, "Adaptive waveform design and sequential hypothesis testing for target recognition with active sensors," *IEEE J. Sel. Topics Signal Process.*, vol. 1, no. 1, pp. 105–113, 2007.

[37] Y. Chen and P. Rapajic, "Ultra-wideband cognitive interrogator network: adaptive illumination with active sensors for target localisation," *IET Communications*, vol. 4, no. 5, pp. 573–584, 2010.

[38] S. Haykin, "Cognitive radar networks," in *Proc. Fourth IEEE Workshop on Sensor Array and Multichannel Processing*, July 2006, pp. 1–24.

[39] P. Chavali and A. Nehorai, "Cognitive radar for target tracking in multipath scenarios," in *Proc. International Waveform Diversity and Design Conference (WDD)*, Aug. 2010, pp. 110–114.

[40] S. Haykin, A. Zia, I. Arasaratnam, and Y. Xue, "Cognitive tracking radar," in *Proc. IEEE Radar Conference*, May 2010, pp. 1467–1470.

[41] Y. Liu, D. Wang, X. Wang, and H. Meng, "Fusion-based target tracker for sector scan radar," in *Proc.* 8^{th} *International Conference on Signal Process.*, vol. 4, 16-20 2006.

[42] Y. Wei, H. Meng, and X. Wang, "Adaptive single-tone waveform design for target recognition in cognitive radar," in *Proc. IET International Radar Conference*, April 2009, pp. 1–4.

[43] L. Fan, J. Wang, B. Wang, and D. Shu, "Time resources allocation in cognitive radar system," in *Proc. International Conference on Networking, Sensing and Control (ICNSC)*, April 2010, pp. 727–730.

[44] M. Inggs, "Passive coherent location as cognitive radar," in *Proc. International Waveform Diversity and Design Conference*, Feb. 2009, pp. 229–233.

[45] B. Chakraborty, Y. Li, J. Zhang, T. Trueblood, A. Papandreou-Suppappola, and D. Morrell, "Multipath exploitationwith adaptivewaveform design for tracking in urban terrain," in *Proc. IEEE International Conference on Acoustics Speech and Signal Process. (ICASSP)*, March 2010, pp. 3894–3897.

[46] H. Godrich, A. Petropulu, and H. Poor, "Sensor selection in distributed multiple-radar architectures for localization: A knapsack problem formulation," *IEEE Trans. Signal Process.*, vol. 60, no. 1, pp. 247–260, Jan. 2012.

[47] R. Tharmarasa, T. Kirubarajan, M. Hernandez, and A. Sinha, "Pcrlb-based multisensor array management for multitarget tracking," *IEEE Trans. Aerosp. and Electron. Syst.*, vol. 43, no. 2, pp. 539–555, April 2007.

[48] P. Chavali and A. Nehorai, "Scheduling and power allocation in a cognitive radar network for multiple-target tracking," *IEEE Trans. Signal Process.*, vol. 60, no. 2, pp. 715–729, Feb. 2012.

[49] Y. Yang and R. S. Blum, "Radar waveform design using minimum meansquare error and mutual information," in *Proc. IEEE Workshop on Sensor Array and Multichannel Process (SAM), Waltham, MA, USA*, Sep. 2006, pp. 234–238.

[50] I. Bekkerman and J. Tabrikian, "Spatially coded signal model for active arrays," in *Proc. IEEE International Conference on Acoustics, Speech, and Signal Processing (ICASSP)*, vol. 2, May 2004.

[51] ——, "Target detection and localization using MIMO radars and sonars," *IEEE Trans. Signal Process.*, vol. 54, no. 10, pp. 3873–3883, Oct. 2006.

[52] E. Fishler, A. Haimovich, R. Blum, R. Cimini, D. Chizhik, and R. Valenzuela, "Performance of MIMO radar systems: advantages of angular diversity," in *Proc. Thirty-Eighth Asilomar Conference on Signals, Systems and Computers.*, vol. 1, Nov. 2004, pp. 305–309.

[53] E. Fishler, A. Haimovich, R. Blum, J. Cimini, L.J., D. Chizhik, and R. Valenzuela, "Spatial diversity in radars-models and detection performance," *IEEE Trans. Signal Process.*, vol. 54, no. 3, pp. 823–838, March 2006.

[54] P. Stoica, J. Li, and Y. Xie, "On probing signal design for MIMO radar," *IEEE Trans. Signal Process.*, vol. 55, no. 8, pp. 4151–4161, Aug. 2007.

[55] L. Xu and J. Li, "Iterative generalized-likelihood ratio test for MIMO radar," *IEEE Trans. Signal Process.*, vol. 55, no. 6, pp. 2375–2385, June 2007.

[56] D. Bliss and K. Forsythe, "Multiple-input multiple-output (MIMO) radar and imaging: degrees of freedom and resolution," in *Proc. Thirty-Seventh Asilomar Conference on Signals, Systems and Computers*, vol. 1, Nov. 2003, pp. 54–59.

[57] K. Forsythe, D. Bliss, and G. Fawcett, "Multiple-input multiple-output (MIMO) radar: performance issues," in *Proc. Thirty-Eighth Asilomar Conference on Signals, Systems and Computers*, vol. 1, Nov. 2004, pp. 310–315.

[58] J. Li and P. Stoica, "MIMO radar with colocated antennas," *IEEE Signal Process. Mag.*, vol. 24, no. 5, pp. 106–114, Sept. 2007.

[59] L. Xu, J. Li, and P. Stoica, "Target detection and parameter estimation for MIMO radar systems," *IEEE Trans. Aerosp. Electron. Syst.*, vol. 44, no. 3, pp. 927–939, July 2008.

[60] J. Li, L. Xu, P. Stoica, K. Forsythe, and D. Bliss, "Range compression and waveform optimization for MIMO radar: A Cramer-Rao Bound based study," *IEEE Trans. Signal Process.*, vol. 56, no. 1, pp. 218–232, Jan. 2008.

[61] W. Melvin and J. Guerci, "Knowledge-aided signal processing: a new paradigm for radar and other advanced sensors," *IEEE Trans. Aerosp. Electron. Syst.*, vol. 42, no. 3, pp. 983–996, July 2006.

[62] V. Mecca, D. Ramakrishnan, and J. Krolik, "MIMO radar space-time adaptive processing for multipath clutter mitigation," in *Proc. Fourth IEEE Workshop on Sensor Array and Multichannel Processing*, July 2006, pp. 249–253.

[63] M. Arik and O. Akan, "Collaborative mobile target imaging in UWB wireless radar sensor networks," *IEEE J. Sel. Areas in Commun.*, vol. 28, no. 6, pp. 950–961, Aug. 2010.

[64] C. Chang and A. Sahai, "Object tracking in a 2d UWB sensor network," in *Proc. Thirty-Eighth Asilomar Conference on Signals, Systems and Computers*, vol. 1, Nov. 2004, pp. 1252–1256.

[65] P. Dutta, A. Arora, and S. Bibyk, "Towards radar-enabled sensor networks," in *Proc. The Fifth International Conference on Information Processing in Sensor Networks (IPSN)*, 2006, pp. 467–474.

[66] M. Chiani, A. Giorgetti, M. Mazzotti, R. Minutolo, and E. Paolini, "Target detection metrics and tracking for UWB radar sensor networks," in *Proc. IEEE International Conference on Ultra-Wideband (ICUWB)*, Sept. 2009, pp. 469–474.

[67] R. Thoma, O. Hirsch, J. Sachs, and R. Zetik, "UWB sensor networks for position location and imaging of objects and environments," in *Proc. The Second European Conference on Antennas and Propagation (EuCAP)*, Nov. 2007, pp. 1–9.

[68] J. Choliz, M. Eguizabal, A. Hernandez-Solana, and A. Valdovinos, "Comparison of algorithms for UWB indoor location and tracking systems," in *Proc. IEEE 73rd Vehicular Technology Conference (VTC Spring)*, May 2011, pp. 1–5.

[69] S. Gezici, Z. Tian, G. B. Giannakis, H. Kobayashi, A. F. Molisch, H. V. Poor, and Z. Sahinoglu, "Localization via ultra-wideband radios: A look at positioning aspects of future sensor networks," *IEEE Signal Process. Mag.*, vol. 22, no. 4, pp. 70–84, July 2005.

[70] D. Macagnano and G. de Abreu, "Tracking multiple dynamic targets in los-nlos condition with multidimensional scaling," in *Proc. 5th Workshop on Positioning, Navigation and Communication (WPNC)*, March 2008, pp. 251–257.

[71] G. Destino and G. de Abreu, "Improving source localization in nlos conditions via ranging contraction," in *Proc. 7th Workshop on Positioning Navigation and Communication (WPNC)*, March 2010, pp. 56–61.

[72] F. Daum, "Nonlinear filters: beyond the kalman filter," *IEEE Trans. Aerosp. Electron. Syst. Mag.*, vol. 20, no. 8, pp. 57–69, Aug. 2005.

[73] F. Gustafsson, F. Gunnarsson, N. Bergman, U. Forssell, J. Jansson, R. Karlsson, and P.-J. Nordlund, "Particle filters for positioning, navigation, and tracking," *IEEE Trans. Signal Process.*, vol. 50, no. 2, pp. 425–437, Feb 2002.

[74] P. van Genderen, "A communication waveform for radar," in *Proc. 8th International Conference on Communications (COMM)*, June 2010, pp. 289–292.

[75] S. Sen and A. Nehorai, "Sparsity-based multi-target tracking using OFDM radar," *IEEE Trans. Signal Process.*, vol. 59, no. 4, pp. 1902–1906, April 2011.

[76] ——, "Target detection in clutter using adaptive OFDM radar," *IEEE Signal Process. Letters*, vol. 16, no. 7, pp. 592–595, July 2009.

[77] ——, "OFDM MIMO radar with mutual-information waveform design for low-grazing angle tracking," *IEEE Trans. Signal Process.*, vol. 58, no. 6, pp. 3152–3162, June 2010.

[78] C. Sturm, T. Zwick, and W. Wiesbeck, "An OFDM system concept for joint radar and communications operations," in *Proc. IEEE* 69^{th} *Vehicular Technology Conference (VTC Spring)*, April 2009, pp. 1–5.

[79] M. Braun, C. Sturm, A. Niethammer, and F. Jondral, "Parametrization of joint OFDM-based radar and communication systems for vehicular applications," in *Proc. IEEE* 20^{th} *International Symposium on Personal, Indoor and Mobile Radio Communications*, Sept. 2009, pp. 3020–3024.

[80] C. Sturm, M. Braun, and W. Wiesbeck, "Deterministic propagation modeling for joint radar and communication systems," in *Proc. URSI International Symposium on Electromagnetic Theory (EMTS)*, Aug. 2010, pp. 942–945.

[81] Y. Sit, C. Sturm, and T. Zwick, "Doppler estimation in an OFDM joint radar and communication system," in *Proc. German Microwave Conference (GeMIC)*, March 2011, pp. 1–4.

[82] Y. Sit, L. Reichardt, C. Sturm, and T. Zwick, "Extension of the OFDM joint radar-communication system for a multipath, multiuser scenario," in *Proc. IEEE Radar Conference (RADAR)*, May 2011, pp. 718–723.

[83] S. J. Xu, Y. Chen, and P. Zhang, "Integrated radar and communication based on DS-UWB," in *Proc. The Third International Conference Ultrawideband and Ultrashort Impulse Signals*, Sept. 2006, pp. 142–144.

[84] Z. Lin and P. Wei, "Pulse amplitude modulation direct sequence ultra wideband sharing signal for communication and radar systems," in *Proc.* 7^{th} *International Symposium on Antennas, Propagation EM Theory (ISAPE)*, Oct. 2006, pp. 1–5.

[85] M. Jamil, H.-J. Zepernick, and M. Pettersson, "On integrated radar and communication systems using oppermann sequences," in *Proc. IEEE Military Communications Conference (MILCOM).*, Nov. 2008, pp. 1–6.

[86] C.-X. Wang, X. Hong, H.-H. Chen, and J. Thompson, "On capacity of cognitive radio networks with average interference power constraints," *IEEE Transactions on Wireless Communications*, vol. 8, no. 4, pp. 1620–1625, April 2009.

[87] S. Haykin, "Cognitive radar: a way of the future," *IEEE Signal Process. Mag.*, vol. 23, no. 1, pp. 30–40, Jan. 2006.

[88] Y. Nijsure, Y. Chen, C. Litchfield, and P. Rapajic, "Hidden Markov model for target tracking with UWB radar systems," in *Proc. IEEE* 20^{th} *Personal, Indoor and Mobile Radio Communications (PIMRC)*, Sep. 2009, pp. 2065–2069.

[89] S. Haykin, "Next generation of radar systems enabled with cognition," in *Proc. IEEE Radar Conference*, May 2010, pp. 1–1.

[90] H. Celebi, I. Guvenc, S. Gezici, and H. Arslan, "Cognitive-radio systems for spectrum, location, and environmental awareness," *IEEE Antennas Propag. Mag.*, vol. 52, no. 4, pp. 41–61, 2010.

[91] R. Romero and N. Goodman, "Adaptive beamsteering for search-and-track application with cognitive radar network," in *Proc. IEEE Radar Conference (RADAR)*, May 2011, pp. 1091–1095.

[92] ——, "Waveform design in signal-dependent interference and application to target recognition with multiple transmissions," *IET Radar, Sonar Navigation*, vol. 3, no. 4, pp. 328–340, August 2009.

[93] J. Li and P. Stoica, "MIMO radar with colocated antennas," *IEEE Signal Process. Mag.*, vol. 24, no. 5, pp. 106–114, Sep. 2007.

[94] A. M. Haimovich, R. S. Blum, and L. J. Cinimi, "MIMO radar with widely separated antennas," *IEEE Signal Process. Mag.*, vol. 25, no. 1, pp. 116–129, Jan. 2008.

[95] G. H. Jajamovich, M. Lops, and X. Wang, "Space-time coding for MIMO radar detection and ranging," *IEEE Trans. Signal Process.*, vol. 58, no. 12, pp. 6195–6206, Dec. 2010.

[96] Y. Yang, R. S. Blum, Z. S. He, and D. R. Fuhrmann, "MIMO radar waveform design via alternating projection," *IEEE Trans. Signal Process.*, vol. 58, no. 3, pp. 1440–1445, Mar. 2010.

[97] X. Song, S. Zhou, and P. Willett, "Reducing the waveform cross correlation of MIMO radar with space-time coding," *IEEE Trans. Signal Process.*, vol. 58, no. 8, pp. 4213–4224, Aug. 2010.

[98] B. Tang, J. Tang, and Y. Peng, "MIMO radar waveform design in colored noise based on information theory," *IEEE Trans. Signal Process.*, vol. 58, no. 9, pp. 4684–4697, Sep. 2010.

[99] Y. Nijsure, Y. Chen, P. Rapajic, C. Yuen, Y. H. Chew, and T. F. Qin, "Information-theoretic algorithm for waveform optimization within ultra wideband cognitive radar network," in *Proc. IEEE International Conference on Ultra-Wideband (ICUWB)*, Sep. 2010, pp. 1–4.

[100] P. Stoica, J. Li, and Y. Xie, "On probing signal design for MIMO radar," *IEEE Trans. Signal Process.*, vol. 55, no. 8, pp. 4151–4161, Aug. 2007.

[101] I. Y. Immoreev, S. Samkov, and T. H. Tao, "Short-distance ultra wideband radars," *IEEE Aerosp. Electron. Syst. Mag.*, vol. 20, pp. 9–14, June 2005.

[102] A. Rihaczek, *Principles of High-Resolution Radar.* Mark Resources, Marina del Rey, CA, 1977.

[103] T. M. Cover and J. A. Thomas, *Elements of Information Theory.* Wiley-Interscience, 2006.

[104] S. Sira, D. Cochran, A. Papandreou-Suppappola, D. Morrell, W. Moran, S. Howard, and R. Calderbank, "Adaptive waveform design for improved detection of low-RCS targets in heavy sea clutter," *IEEE J. Select. Topics Signal Process.*, vol. 1, no. 1, pp. 56–66, June 2007.

[105] T.-T. Cao, J. Palmer, and P. Berry, "False alarm control of CFAR algorithms with experimental bistatic radar data," in *Proc. IEEE Radar Conference 2010*, May 2010, pp. 156–161.

[106] C. Morelli, M. Nicoli, V. Rampa, and U. Spagnolini, "Hidden Markov models for radio localization in mixed LOS/NLOS conditions," *IEEE Trans. Signal Process.*, vol. 55, no. 4, pp. 1525–1542, Apr. 2007.

[107] F. Gustafsson and F. Gunnarsson, "Mobile positioning using wireless networks," *IEEE Signal Process. Mag.*, vol. 22, no. 4, pp. 41–53, 2005.

[108] J. J. J. Caffery, *Wireless Location in CDMA Cellular Radio Systems*. Kluwer Academic Publishers, 2000.

[109] L. Cong and W. Zhuang, "Hybrid TDOA/AOA mobile user location for wideband CDMA cellular systems," *IEEE Trans. Wireless Commun.*, vol. 1, pp. 439–447, July 2002.

[110] J. Y. Lee and R. A. Scholtz, "Ranging in a dense multipath environment using an UWB radio link," *IEEE J. Select. Areas Commun.*, vol. 20, no. 9, pp. 1677–1683, 2002.

[111] M. Z. Win and R. A. Scholtz, "Ultra-wide bandwidth time-hopping spread-spectrum impluse radio for wireless multiple-access communications," *IEEE Trans. Commun.*, vol. 48, no. 4, pp. 679–689, 2000.

[112] F. Ramirez-Mireles, "Performance of ultrawideband SSMA using time hopping and M-ary PPM," *IEEE J. Select. Areas Commun.*, vol. 19, no. 6, pp. 1186–1196, 2001.

[113] R. Cardinali, L. D. Nardis, M. D. Benedetto, and P. Lombardo, "UWB ranging accuracy in high- and low-data-rate applications," *IEEE Trans. Microw. Theory Tech.*, vol. 54, no. 4, pp. 1865–1875, 2006.

[114] B. Chen and P. Willett, "Superimposed hmm transient detection via target tracking ideas," *IEEE Trans. Aerosp. and Electron. Syst.*, vol. 37, no. 3, pp. 946–956, Jul 2001.

[115] D. Schulz, W. Burgard, D. Fox, and A. Cremers, "Tracking multiple moving targets with a mobile robot using particle filters and statistical data association," in *Proc. IEEE International Conference on Robotics and Automation, (ICRA).*, vol. 2, 2001, pp. 1665–1670.

[116] L. J. Greenstein, V. Erceg, Y. S. Yeh, and M. V. Clark, "A new path-gain/delay-spread propagation model for digital cellular channels," *IEEE Trans. Veh. Technol.*, vol. 46, no. 2, pp. 477–485, 1997.

[117] M. Najar and J. Vidal, "Kalman tracking for mobile location in NLOS situations," in *Proc. 2003 IEEE International Symposium on Personal, Indoor and Mobile Radio Communications (PIMRC)*, Sep. 2003, pp. 2203–2207.

[118] L. R. Rabiner, "A tutorial on hidden markov models and selected applications in speech recognition," *Proc. IEEE*, vol. 77, no. 2, pp. 257–286, 1989.

[119] Y. Song and H. Yu, "A new hybrid TOA/RSS location tracking algorithm for wireless sensor network," in *Proc.* 9^{th} *International Conference on Signal Process. (ICSP)*, 2008, pp. 2645–2648.

[120] D. Kim, M. A. Ingram, and W. W. S. Jr., "Measurements of small-scale fading and path loss for long range RF tags," *IEEE Trans. Antennas Propag.*, vol. 51, no. 8, pp. 1740–1749, 2003.

[121] J. D. Griffin and G. D. Durgin, "Complete link budgets for backscatter-radio and RFID systems," *IEEE Antennas Propag. Mag.*, vol. 51, no. 2, pp. 11–25, 2009.

[122] ——, "Gains for RF tags using multiple antennas," *IEEE Trans. Antennas Propag.*, vol. 56, no. 2, pp. 563–570, 2008.

[123] S. Mazuelas, F. Lago, D. Gonzalez, A. Bahillo, J. Blas, P. Fernandez, R. Lorenzo, and E. Abril, "Dynamic estimation of optimum path loss model in a RSS positioning system," in *IEEE/ION Position, Location and Navigation Symposium*, May 2008, pp. 679–684.

[124] N. Patwari, A. O. Hero, M. Perkins, N. S. Correal, and R. J. O'Dea, "Relative location estimation in wireless sensor networks," *IEEE Trans. Signal Process.*, vol. 51, no. 8, pp. 2137–2148, Aug. 2003.

[125] A. Catovic and Z. Sahinoglu, "The Cramer-Rao bounds of hybrid TOA/RSS and TDOA/RSS location estimation schemes," *IEEE Commun. Lett.*, vol. 8, no. 10, pp. 626–628, Oct. 2004.

[126] G. McLachlan and T. Krishnan, *The EM Algorithm and Extension.* John Wiley & Sons, New York, 1996.

[127] R. Zhan and J. Wan, "Iterated unscented Kalman filter for passive target tracking," *IEEE Trans. Aerosp. Electron. Syst.*, vol. 43, no. 3, pp. 1155–1163, July 2007.

[128] X. Kuang and H. Shao, "Maximum likelihood localization algorithm using wireless sensor networks," in *Proc. First International Conference on Innovative Computing, Information and Control (ICICIC)*, vol. 3, 2006, pp. 263–266.

[129] H. Cho and S. W. Kim, "Mobile robot localization using biased chirp-spread-spectrum ranging," *IEEE Trans. Ind. Electron.*, vol. 57, no. 8, pp. 2826–2835, Aug. 2010.

[130] A. Shareef and Y. Zhu, "Localization using extended Kalman filters in wireless sensor networks," *Kalman Filter: Recent Advances and Applications, Edited by V. M. Moreno and A. Pigazo, Chapter 13*, Apr. 2009, InTech, Vienna, Austria.

[131] S. Mazuelas, F. Lago, D. Gonzalez, A. Bahillo, J. Blas, P. Fernandez, R. Lorenzo, and E. Abril, "Dynamic estimation of optimum path loss model in a RSS positioning system," in *Proc. IEEE/ION Position, Location and Navigation Symposium*, May 2008, pp. 679–684.

[132] Y. Nijsure, Y. Chen, P. Rapajic, C. Yuen, Y. Chew, and T. Qin, "Information-theoretic algorithm for waveform optimization within ultra wideband cognitive radar network," in *Proc. IEEE International Conference on Ultra-Wideband (ICUWB)*, vol. 2, Sept. 2010, pp. 1–4.

[133] R. Challamel, P. Tome, D. Harmer, and S. Beauregard, "Performance assessment of indoor location technologies," in *Proc. IEEE/ION Position, Location and Navigation Symposium*, May 2008, pp. 624–632.

[134] Y. Yang and R. S. Blum, "Radar waveform design using minimum mean-square error and mutual information," *in Proc.* 4^{th} *IEEE Workshop on Sensor Array and Multichannel Proc. (SAM), Waltham, MA, USA*, pp. 234–238, 2006.

[135] Y. Yang, R. S. Blum, Z. S. He, and D. R. Fuhrmann, "MIMO radar waveform design via alternating projection," *IEEE Trans. Signal Process.*, vol. 58, no. 3, pp. 1440–1445, Mar. 2010.

[136] D. Cassioli, M. Z. Win, and A. F. Molisch, "The ultra-wide bandwidth indoor channel: from statistical model to simulations," *IEEE J. Sel. Areas Commun.*, vol. 20, pp. 1247–1257, Aug 2002.

[137] A. Rihaczek, *Principles of High-Resolution Radar.* Mark Resources, Marina del Rey, CA, 1977.

[138] M. L. Skolnik, *Introduction to Radar Systems,* 3^{rd} *Ed.* McGraw-Hill, New York, 2001.

[139] Y. Chen and P. Rapajic, "Ultra-wideband cognitive interrogator network: adaptive illumination with active sensors for target localisation," *IET Commun.*, vol. 4, no. 5, pp. 573–584, 2010.

[140] H. Zhang and T. A. Gulliver, "Biorthogonal pulse position modulation for time-hopping multiple access UWB communications," *IEEE Trans. Wireless Commun.*, vol. 4, no. 3, pp. 1154–1162, May 2005.

[141] N. A. Goodman, P. R. Venkata, and M. A. Neifeld, "Adaptive waveform design and sequential hypothesis testing for target recognition with active sensors," *IEEE J. Sel. Topics Signal Process.*, vol. 1, no. 1, pp. 105–113, 2007.

[142] FCC, "Federal communications commission: Revision of part 15 of the commission's rule regarding ultra-wideband transmission systems, first report and order," *ET Docket* $98-153$, pp. 1–118, 2002.

[143] Y. S. Shen, F. B. Ueng, J. D. Chen, and S. T. Huang, "A performance analysis of the high-capacity TH multiple access UWB system using PPM," in *Proc. IEEE* 20^{th} *International Symposium on Personal, Indoor and Mobile Radio Communications (PIMRC)*, Sep. 2009, pp. 2454–2458.

[144] N. V. Kokkalis, P. T. Mathiopoulos, G. K. Karagiannidis, and C. S. Koukourlis, "Performance analysis of M-ary PPM TH-UWB systems in the presence of MUI and timing jitter," *IEEE J. Sel. Areas Commun.*, vol. 24, no. 4, pp. 822–828, Apr. 2006.

[145] F. Ramirez-Mireles, "Signal design for ultra wideband PPM communications," in *Proc. IEEE MILCOM 2002*, vol. 2, Oct. 2002, pp. 1085–1088.

[146] ——, "On the capacity of UWB over multipath channels," *IEEE Commun. Lett.*, vol. 9, no. 6, pp. 523–525, June 2005.

[147] R. McMillan and I. Kohlberg, "A probabilistic model of the radar signal-to-clutter and noise ratio for weibull-distributed clutter," in *Proc. IEEE Radar Conference*, May 2010, pp. 882–886.

[148] K. Shujaee, A. Ebaid, R. George, and M. Sazegarnejad, "Channel modeling and range extension for uwb communications using directional antenna in los and nlos path loss models," in *Automation Congress, 2008. WAC 2008. World*, 28 2008-oct. 2 2008, pp. 1 –6.

[149] J.-Y. Lee and S. Yoo, "Large error performance of UWB ranging in multipath and multiuser environments," *IEEE Trans. Microw. Theory Tech.*, vol. 54, pp. 1887–1895, June 2006.

[150] Federal Communications Commission Spectrum Efficiency Working Group, "Spectrum Policy Task Force Report," *FCC Report*, Nov. 2002.

[151] J. Mitola and G. Q. Maguire, "Cognitive radio: making software radios more personal," *IEEE Personal Communications*, vol. 6, no. 4, pp. 13–18, 1999.

[152] D. Garmatyuk, J. Schuerger, Y. Morton, K. Binns, M. Durbin, and J. Kimani, "Feasibility study of a multi-carrier dual-use imaging radar and communication system," in *Proc. European Radar Conference (EuRAD)*, Oct. 2007, pp. 194–197.

[153] C. Sturm, T. Zwick, and W. Wiesbeck, "An OFDM system concept for joint radar and communications operations," in *Proc. IEEE* 69^{th} *Veh. Technol. Conf. (VTC Spring)*, Apr. 2009, pp. 1–5.

[154] H. Urkowitz, "Energy detection of unknown deterministic signals," *in Proc. IEEE*, vol. 55, no. 4, pp. 523–531, 1967.

[155] F. F. Digham, M.-S. Alouini, and M. K. Simon, "On the energy detection of unknown signals over fading channels," *IEEE Trans. Communications*, vol. 55, no. 1, pp. 21–24, Jan. 2007.

[156] X. Chen and S. Nagaraj, "Entropy based spectrum sensing in cognitive radio," in *Proc. Wireless Telecommunications Symposium (WTS)*, Apr. 2008, pp. 57–61.

[157] Y. L. Zhang, Q. Y. Zhang, and T. Melodi, "A frequency-domain entropy-based detector for robust spectrum sensing in cognitive radio networks," *IEEE Commun. Lett.*, vol. 14, no. 6, pp. 533–535, June 2010.

[158] C. E. Shannon, "Communication in the presence of noise," *Proc. of the IRE*, vol. 37, no. 1, pp. 10–21, 1949.

[159] A. G. Burr, "Capacity of cognitive channel and power allocation," in *Proc. Information Theory Workshop (ITW)*, Oct. 2009, pp. 510–514.

[160] I. Akbar and W. Tranter, "Dynamic spectrum allocation in cognitive radio using hidden markov models: Poisson distributed case," in *Proc.IEEE SoutheastCon.*, March 2007, pp. 196–201.

[161] J. Candy, *Introduction to Radar Systems*. Wiley-Interscience, 2009.

[162] V. Tumuluru, P. Wang, and D. Niyato, "A neural network based spectrum prediction scheme for cognitive radio," in *Proc. IEEE International Conference on Communications (ICC)*, May 2010, pp. 1–5.

[163] S. Yin, D. Chen, Q. Zhang, and S. Li, "Prediction-based throughput optimization for dynamic spectrum access," *IEEE Trans. Vehicular Technology*, vol. 60, no. 3, pp. 1284–1289, March 2011.

[164] M. Hoyhtya, S. Pollin, and A. Mammela, "Classification-based predictive channel selection for cognitive radios," in *Proc. IEEE International Conference on Communications (ICC)*, May 2010, pp. 1–6.